Development of a Vegetation Fluorescence Canopy Model

ESTEC Contract No. 16365/02/NL/FF

Final Report
April 2005

Contractor
York University, 4700 Keele Street, Toronto, Ontario CANADA M3J 1P3
Project Manager: Dr. J. R. Miller, Tel: +1(416)736-2100 Ext 77757 Fax: +1(416)736-5817
e-mail: jrmiller@yorku.ca
Contracts Officer: Mr. David Phipps, Tel: +1(416)736-2100 Ext 55813
email: dphipps@yorku.ca

ESA
Technical Representative: Dr. M. Berger (EOP-FSL)
Contracts Officer: Mrs. F. de la Feld (IMT-CAO)

CONTRIBUTORS:
J. Miller (York University, Canada)
M. Berger (ESTEC, The Netherlands)
Y. Goulas (University of Paris/LURE, France)
S. Jacquemoud (University of Paris, France)
J. Louis (University of Paris/LURE, France)
G. Mohammed (P&M Technologies, Canada)
N. Moise (University of Paris/LURE, France)
J. Moreno (University of Valencia, Spain)
I. Moya (University of Paris/LURE, France)
R. Pedrós (University of Paris, France)
W. Verhoef (NLR, The Netherlands)
P. Zarco-Tejada (CSIC, Spain)

ABSTRACT

The FluorMOD project undertook to develop an integrated leaf-canopy model to simulate solar-induced chlorophyll fluorescence in vegetation. Two new models were developed following a review and adaptation of existing relevant models: *FluorSAIL* for the canopy, and *FluorMODleaf* for leaf-level fluorescence. These models are linked by *FluorMODgui*, a graphic user interface which permits the leaf and canopy models to be run either individually or as an integrated unit. Outputs available in the 400-1000 nm spectral range are the apparent leaf spectral reflectance and transmittance, and the canopy apparent reflectance, with and without fluorescence effects. The integrated model has undergone initial testing and validation which indicates that it is able to reproduce the shape of fluorescence emission in the red and far-red spectral regions. The beta version of the model is now available for further validation by the scientific community. The current models and documentation can be accessed from a dedicated web page at **http://www.ias.csic.es/fluormod**

TABLE OF CONTENTS

EXECUTIVE SUMMARY

Further information related to the study can be obtained, subject to intellectual property restrictions, from the Technical Documentation and Information Centre (TIDC) at ESTEC.

EXECUTIVE SUMMARY

Purpose of the FluorMOD project

The FluorMOD project was initiated in 2002 by the European Space Agency to advance the science of vegetation fluorescence simulation through the development and integration of leaf and canopy fluorescence models based on physical methods. Its primary objective was to simulate the effects of solar-induced fluorescence on unstressed vegetation. A beta version of the model is now completed, initial testing and validation has been done, and the product, *FluorMODgui,* is available for further testing and validation by the scientific community.

The project contributes to the science necessary to gauge the technical feasibility of a space mission aimed at measuring the solar-induced fluorescence signal. This is perceived to be a challenging task for two reasons: the technical difficulties inherent in developing a new canopy model that simulates canopy spectral reflectance and fluorescence, and the present dearth of suitable field data with which to validate and assess such a model.

Chlorophyll Fluorescence

Terrestrial vegetation systems and biosphere processes & interactions are so complex that detailed characterization and description of the system is needed. Such model development demands a precise physics basis. Consequently, remote sensing requires accurate quantitative approaches that exploit all types of information in the optical signal. As regards biosphere dynamics, notably at short time scales, spectral reflectance and directionality of radiance alone cannot provide comprehensive information since these responses are not strictly connected to fundamental processes of plant physiology.

The connection is found in vegetation fluorescence, known to convey very specific information on the efficiency of light energy usage by plants, thereby relating to plant vitality and the potential for biomass production. Chlorophyll *a* fluorescence from light-excited vegetation emanates in specific red and far-red spectral regions, and is produced by Photosystems I and II (PSI and PSII) which are pigment-protein complexes involved in the initial stages of photosynthesis. Steady-state chlorophyll fluorescence is known to be highly responsive to changes in environmental conditions and is a widely used indicator of plant photosynthetic function. Passive measurements of natural sunlight-induced fluorescence would open new ways for global monitoring of vegetation, with improved estimates of vegetation photosynthetic potential and direct implications for surface carbon flux estimation.

Project Approach

The FluorMOD project merges scientific expertise from the fields of plant physiology, fluorescence instrumentation development, leaf & canopy biophysical modelling, and hyperspectral remote sensing & modelling, in a uniquely synergistic endeavour.

The project was subdivided into five main tasks.

- *Task 1* – A review of leaf and canopy models which include fluorescence, and selection of appropriate models for further development.
- *Task 2* – Development of the leaf model to incorporate fluorescence, and testing of the new leaf model with controlled experiments.
- *Task 3* – Development of the canopy model, involving scaling-up of the leaf model through the canopy according to canopy structure variables, and simulation tests of whether the above-canopy fluorescence signals – superimposed on the much stronger reflected radiance signatures – could be discerned.

- *Task 4* – Preliminary validation of the combined leaf-canopy model.
- *Task 5* – Delivery of the leaf-canopy fluorescence model and reporting.

***FluorMOD* Model Overview**

The *FluorMOD* integrated model, newly developed as a result of this project, simulates the effects of chlorophyll fluorescence at leaf and canopy levels using atmospheric inputs and inputs from two newly developed sub-component models – *FluorMODleaf* and the canopy model, *FluorSAIL*. Both models have been conveniently linked through a menu-driven graphic user interface *FluorMODgui*, which permits the leaf and canopy models to be run either individually or as an integrated unit. The integrated model is applicable to broad-leaf species.

The up-to-date models, graphic interface version, and documentation can be obtained by interested collaborators from a dedicated web page at **http://www.ias.csic.es/fluormod**

***FluorMODleaf* Leaf Model**

The *FluorMODleaf* model simulates chlorophyll fluorescence effects on leaf reflectance and transmittance, based on the widely used and validated PROSPECT leaf optical properties model.

Inputs for *FluorMODleaf* are: the number of leaf layers, chlorophyll a+b content, water equivalent thickness, dry matter content, fluorescence quantum efficiency, temperature, species type, and PSII:PSI stoichiometry. In addition, within-canopy irradiance profiles are taken into account, including two PAR-dependent parameters denoting electron transport resistance and a heat dissipation constant. The main drivers of chlorophyll fluorescence (CF) are summarized below, with an asterisk (*) indicating key inputs to the *FluorMODleaf* model.

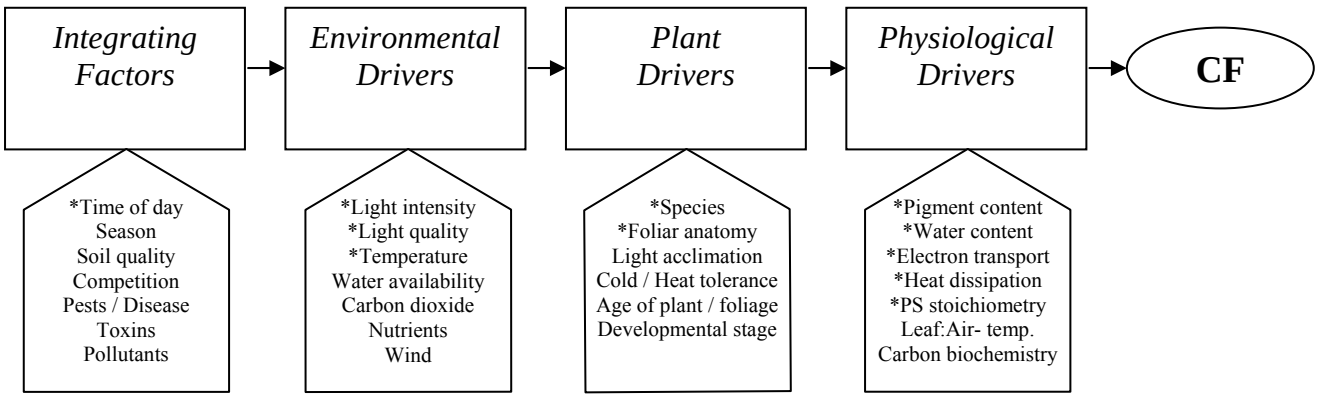

The core of the new model is the fluorescence emission elementary spectrum, a combination of PSI and PSII fluorescence spectra. Outputs of the model have been compared to actual fluorescence measurements obtained in a laboratory study completed for the project. We are able to predict the shape of the fluorescence spectrum but not necessarily its magnitude. Possibly, a scaling factor may be needed, or further analysis might be necessary to exclude the possible confounding effects of non-fluorescing pigments (such as carotenoids) which absorb light but do not produce fluorescence in the red and far-red spectral regions.

FluorSAIL Canopy Model

The *FluorSAIL* canopy model simulates chlorophyll fluorescence effects on canopy reflectance using inputs from *FluorMODleaf*. *FluorSAIL* is based on the SAIL model, a basic canopy radiative transfer standard. The excitation-fluorescence matrix computed by *FluorMODleaf*, along with the internal radiation profiles simulated for direct-solar and diffuse fluxes, are used to calculate the radiance of each leaf. Numerical integration is used to predict the top-of-canopy radiance caused by contributions due to scattering and fluorescence. A PAR light-level fluorescence dependence is applied to individual leaves depending on their depth and orientation with respect to the sun. In addition, distinction is made between sunlit and shaded leaves by employing the gap probability function of SAIL. The output of *FluorSAIL* can be used to obtain top-of-canopy as well as top-of-atmosphere radiance contributions associated with solar-induced fluorescence.

Inputs for *FluorSAIL* are: a 6-parameter spectra derived from MODTRAN-4 or measured direct horizontal irradiance and diffuse irradiance spectra, a soil reflectance spectrum, leaf reflectance & transmittance spectra and an excitation-fluorescence response matrix in upward and downward directions (all from *FluorMODleaf*), two PAR-dependent coefficients as mentioned for the leaf model, solar zenith angle and relative azimuth angles, canopy leaf area index, leaf inclination distribution function, and a hot spot parameter.

Based on simulation trials, it can be concluded that the new canopy fluorescence model allows the investigation of quite subtle interactions between atmospheric absorption on the one hand and directional fluorescence and BRDF effects on the other. This is necessary for a correct interpretation of *in-situ* measurements and airborne or spaceborne hyperspectral radiance data obtained under passive illumination conditions.

FluorMODgui Graphic User Interface

The *FluorMODgui* V3.0 Graphic User Interface provides a seamless link between inputs and outputs required for running both *FluorMODleaf* and *FluorSAIL* models, facilitating consistent user interaction and enabling the setup of multiple runs to simulate diurnal effects under different viewing geometries. The interface enables the simulation of leaf and canopy reflectance with the effects of chlorophyll fluorescence, running the leaf and canopy models *FluorMODleaf* and *FluorSAIL* independently or through a coupling scheme.

Outputs available in the 400-1000 nm spectral range from *FluorMODgui* are the leaf spectral reflectance and transmittance, and the canopy reflectance with and without fluorescence effects. In addition, solar and sky irradiance above the canopy, radiance with and without fluorescence above the canopy, and top-of-atmosphere radiances for bare soil and surroundings same as target are also produced.

Potential Applications of *FluorMOD* Model

The graphic user interface *FluorMODgui* will facilitate the testing of various remote sensing detection scenarios for future airborne and spaceborne fluorescence missions, and will support entry into several potential applications. Such applications include:

- **Quality control of satellite sensors**. Predicted values of fluorescence may be compared to apparent values obtained by new instruments in order to test, calibrate, and improve instrument accuracy.
- **Early identification of physiological strain**. Measured fluorescence values that diverge significantly from those predicted for normal, unstressed vegetation may be indicative of

early stress. The situation could be used to trigger more frequent or fine-scale monitoring of target vegetation.

- **Vegetation management.** Management practices that alter physical or physiological attributes of forest, agricultural, horticultural, savanna, or other vegetative systems may be evaluated for their relative efficacy over time, based on their effects on photosystem viability.
- **Photosynthesis modelling.** Fluorescence inputs to photosynthesis models would help to build and refine gross primary productivity models for non-stress scenarios, and in this way, supply photosynthetic benchmarks for healthy vegetation over time.
- **Algorithm development.** Knowledge of the expected values for fluorescence can be used to improve the accuracy of algorithms for hyperspectral data processing, notably those that derive variable estimates from measurements in the red to near-infrared spectral region.
- **Airborne sensing of chlorophyll fluorescence**. Information obtained from airborne sensors would help validate FluorMOD predictions and support model improvements.

Model Validation

Initial testing of the new *FluorMOD* models has revealed that it is able to simulate the shape of the fluorescence signature in the red and far-red spectrum. Sensitivity analyses will determine the degree of accuracy of the amplitude simulations.

A canopy validation study conducted in the project investigated whether diurnal variations in actual measured fluorescence in olive trees agreed with changes in reflectance at 760 nm, and also with the simulation of the model for the 760-nm-band over the course of the day. These aspects were in agreement, although sun geometry also affected the peak. Therefore, caution is needed to carefully account for the influence of sun angle in future studies. It is also noted that if a scaling factor is to be used to amplify fluorescence signals for comparative analysis between simulations and field observations, it should be applied with awareness of a realistic fluorescence quantum efficiency (considered as a maximum of 0.1 here); accordingly, resultant amplitudes for fluorescence may be relatively small, which will be an important consideration for future spaceborne applications.

Recommendations

Validation of the sub-component and integrated models has been addressed in initial studies achievable within the timeframe of this project. A comprehensive validation effort will entail a much broader range of studies from interested members of the scientific research community. Some suggested guidelines for these future studies are:

- ***Identification of potential sources of error***

Given that many factors can influence the fluorescence signal, it is essential that efforts in testing and validation incorporate stringent attention to experimental factors, to ensure that they are standardized, accurate, and well-documented. These will help to identify potential sources of disagreement between ground-truthing results and model predictions, and to locate possible errors in the individual models or the integrated leaf-canopy model. These ongoing validation studies will supply important information for future improvements in *FluorMODleaf*, *FluorSAIL* and *FluorMODgui*.

- ***Who should conduct testing and validation***

The need for stringent monitoring and control of experimental factors suggests that validation activities will need to be conducted in an orderly rollout, first to the scientific research community, then to more applied investigators, and finally, to operational users such as specialists in resource inventory monitoring, agriculture, and horticulture. It is also anticipated that members of the FluorMOD development team will serve as collaborators and resource personnel in validation project planning and execution.

- ***Validation formats***

An array of datasets can be used to test the accuracy and limits of the leaf and canopy models. These include existing datasets and those from new studies. Existing datasets that contain both ground-based and remote (e.g., from towers or airborne sensors) measures of two-band chlorophyll fluorescence will be needed, along with hyperspectral signatures acquired in temporal synchrony. A key aspect of existing and new datasets is that they should be able to address respective leaf-level and canopy-level accuracies of models. The recent LURE passive multidetector providing measurements at two wavelengths (687 and 760 nm), and analysis of hyperspectral signatures at sufficient spectral resolution, are examples of fluorescence extraction approaches that might be appropriate for these activities. Selection of species for studies will necessarily be constrained to those with broad-leaf foliar structure, including many tree, shrub, and temperate crop species.

- ***Provision of a feedback mechanism***

Feedback of validation results to the FluorMOD development team will expectedly occur through the usual scientific mechanisms of publications, conference presentations, and professional interactions. In addition, the project website can serve as a venue for contact and information exchange, from which inquiries may be fielded to the appropriate model design team member(s).

In conclusion, the FluorMOD project provides a solid foundation for a broad range of further studies in chlorophyll fluorescence remote sensing, and contributes much-needed science to the vision of eventually monitoring fluorescence from space.

1. INTRODUCTION

It is now recognized that terrestrial vegetation systems and biosphere processes & interactions are so complex that detailed characterization and description of the system is needed. Further, model development demands a precise physics basis. Consequently, remote sensing requires accurate quantitative approaches that exploit all types of information in the optical signal. As regards biosphere dynamics, notably at short time scales, spectral reflectance and directionality of radiance alone cannot provide comprehensive information since these responses are not strictly connected to fundamental processes of plant physiology.

The connection is found in vegetation fluorescence, known to convey very specific information on the efficiency of light energy usage by plants, thereby relating to plant vitality and the potential for biomass production.

For remote sensing purposes, laser-induced fluorescence or other small scale and short-range methods are not practical at this time, and only natural sunlight-induced fluorescence can be considered. Passive measurements of solar-induced fluorescence would provide a new way for global monitoring of vegetation, with improved estimates of vegetation photosynthetic potential and direct implications for surface carbon flux estimation.

Although another study, the FLEX-Instrument definition pre-study, has been completed under ESA contract, there are still many unknowns regarding the measurement, analysis and exploitation of natural fluorescence, which necessitate the development of appropriate models and campaigns to assess, using ground-based measurements, outstanding technical, instrumental, and basic scientific fluorescence issues.

1.1. FluorMOD project objectives

The FluorMOD project was launched in 2002 by the European Space Agency to advance the science of vegetation fluorescence simulation. The main objective was the development and integration of leaf and canopy fluorescence models based on physical methods. The development of a linked leaf-canopy model to simulate the effects of natural solar-induced fluorescence on canopy-level fluorescence signal contributes to the assessment of fluorescence detection potential using near-contact, airborne and satellite-level remote sensing sensors. This project is expected to further advance the underlying science of a possible future vegetation fluorescence space mission by addressing the modelling aspects.

1.2. Project tasks

Task 1. Review of existing vegetation fluorescence models, and selection of appropriate models. A comprehensive review of passive fluorescence science, leaf fluorescence models, and canopy fluorescence approaches, which forms the basis for shaping the proposed leaf-canopy fluorescence modelling approach.

Task 2. Analysis of the leaf fluorescence model: model advancement. Development and coding of the leaf fluorescence model (software development); development of measurement protocols for leaf reflectance, transmittance, fluorescence, controlling variables for fluorescence emission,

and experiments to assess leaf fluorescence model performance; and reporting on the adequacy of the leaf fluorescence model, in relation to pigment content and controlling variables.

Task 3. Development of an integrated leaf-canopy fluorescence model. Development and coding of the fluorescence radiative transfer model, with the coupled leaf fluorescence model (software development); coupling of high resolution atmospheric model with the fluorescence RT model; and performance of simulations for specific scenarios on the model.

Task 4. Model validation using campaign data and comparison with indirect retrieval methods. Validation of the model, addressing its performance in controlled field experiments and with appropriate existing hyperspectral datasets, focusing on the success of fluorescence retrievals with such datasets.

Task 5. Project conclusion, recommendations, reporting, delivery of model(s). Findings and achievements of the project, herein reported.

1.3. Challenges in modelling chlorophyll fluorescence

The chlorophyll fluorescence signal is very small, constituting only about 3-5% of absorbed light on average. Discriminating this signal is a challenge, in view of the considerable amount of extraneous noise present in a spectral signal. Also, there are many environmental, plant, and physiological factors that influence fluorescence, and their effects are not fully understood quantitatively for a broad range of plant species and situations. The occurrence of non-photochemical quenching – a physiological dissipation mechanism that serves to harmlessly rid plant tissues of excess light energy under conditions of stress – complicates efforts to model fluorescence in a straightforward manner.

Given the confounding influence of stress, and the inherent complexity of the various drivers of chlorophyll fluorescence, the choice was made to focus on non-stress fluorescence behaviour to simplify modelling and focus on the behaviour of vegetation under favourable environmental conditions.

1.4. Benefits expected: Potential applications of FluorMOD

An array of possible applications are envisaged for the model. These include:

- **Quality control of satellite sensors**. Predicted values of fluorescence may be compared to apparent values obtained by new instruments, in order to test, calibrate, and improve instrument accuracy.
- **Early identification of physiological strain**. Measured fluorescence values that diverge significantly from those predicted for normal, unstressed vegetation may be indicative of early stress; the situation could trigger more frequent or fine-scale monitoring of target vegetation. (Assumption: sensors are already calibrated for accuracy, so that measured fluorescence values are known to be correct.)
- **Vegetation management.** Management practices that alter physical or physiological attributes of forest, agricultural, horticultural, savanna, or other vegetative systems may be evaluated for their relative efficacy over time, based on their effects on photosystem viability.

- **Photosynthesis modelling.** Fluorescence inputs to photosynthesis models would help to build and refine gross primary productivity models for non-stress scenarios, and in this way, supply photosynthetic benchmarks for healthy vegetation over the course of a rotation.
- **Algorithm development.** Knowledge of the expected values for fluorescence can be used to improve the accuracy of algorithms for hyperspectral data processing, notably those that derive variable estimates from measurements in the red to near-infrared spectral region.
- **Airborne sensing of chlorophyll fluorescence**. Information obtained from airborne sensors, e.g., AIRFLEX, would help validate FluorMOD predictions and support model improvements.

2. REVIEW OF EXISTING VEGETATION FLUORESCENCE MODELS: SELECTION OF APPROPRIATE MODELS

2.1. Review of passive fluorescence science

In the past 30 years, Earth observation from space has demonstrated that it is possible to monitor global changes at a large scale. A key component involved in global changes is the biosphere, in which vegetation plays a major role. Information provided by sun-induced fluorescence from vegetation is one possible way to improve our knowledge about the terrestrial carbon cycle, owing to the modulation of chlorophyll fluorescence by photosynthetic efficiency. As active remote sensing of fluorescence by satellite is far beyond current technical possibilities (Ounis, 2001), passive remote sensing seems to be the only possible way to make use of this feature.

Chlorophyll *a* fluorescence from light-excited vegetation emanates in specific red and far-red spectral regions, and is produced by Photosystems I and II (PSI and PSII) which are pigment-protein complexes involved in the initial stages of photosynthesis (see Table 2.1.1). In a general way, chlorophyll fluorescence production is inversely related to photosynthesis, except when non-photochemical quenching of fluorescence occurs. Under stress or under moderate to high irradiance, plant tissues increase heat production to dissipate excess energy. This tends to decrease fluorescence emission, at least in the initial and intermediate stages of stress. Therefore, the relative balance between the three major dissipation mechanisms – photosynthesis, heat production, and chlorophyll fluorescence emission – ultimately determines the actual pattern of response observed for fluorescence (for reviews of theory and photosynthetic applications, see Papageorgiou, 1975; Krause and Weis, 1984; Lichtenthaler and Rinderle, 1988; Schreiber et al., 1994; Govindjee, 1995).

Table 2.1.1. Chlorophyll *a* fluorescence bands in oxygenic thylakoids of chloroplasts, at room temperature (modified from Govindjee, 1995).

Emission range – Peak or shoulder (nm)	**Name**	**Possible origin of Chl a**	**Comments**
683-687	F685	PSII core	Major band
693-698	F695	PSII core	Minor shoulder
705-712	F710	PSI core or antenna	Minor
720-760	F740	PSII + PSI	Broad vibrational satellite bands

PSI contributions to total chlorophyll fluorescence have been estimated at up to 6% or 12% in C_3 or C_4 plants, respectively (Pfündel, 1998). However, only PSII produces variable chlorophyll fluorescence, which reflects changes in photochemistry and which is most responsive to physiological perturbation.

Passive methods are the focus of much current interest as they are the logical interface with future remote sensing platforms. Passive methods provide information about the steady-state fluorescence F_T (or a quasi-steady state often referred to as F_S) induced by sunlight. Measurement in at least two wavebands is most useful because it allows one band to be normalized against the other, or a ratio of useful bands to be obtained.

A wide array of natural and artificial factors influence chlorophyll fluorescence (see Figure 2.1.1), and a considerable degree of normal and stress-induced fluctuation exists (Mohammed et al., 1995; DeEll and Toivonen, 2003; Mohammed et al., 2003). Of all these factors, light intensity is probably the most fundamental correlate with fluorescence. Chlorophyll fluorescence increases with increasing light, unless carbon dioxide is limiting (e.g., from stomatal closure). For example, the effect of different light intensities on the relative level of steady state fluorescence F_S of *Ficus* sp., *Nerium oleander* and *Pisum sativum* was monitored simultaneously at 690 and 730 nm (Srivastava et al., 1995). They found that steady-state fluorescence was clearly higher at moderate light intensities than at the low or the high light intensities in all three plants at both 690 and 730 nm. The optimum level of F_S differed among the species, and was higher at 690 than at 730 nm; at low and high light intensities F_S at both wavelengths was similar. In practical terms, these findings are consistent with the diurnal cycle. Chlorophyll fluorescence on a sunny day is known to increase in the early hours of the morning with increasing light, but to decrease around midday (with concomitant stomatal closure and increase in non-photochemical quenching of fluorescence), then recover toward evening or night as PAR diminishes.

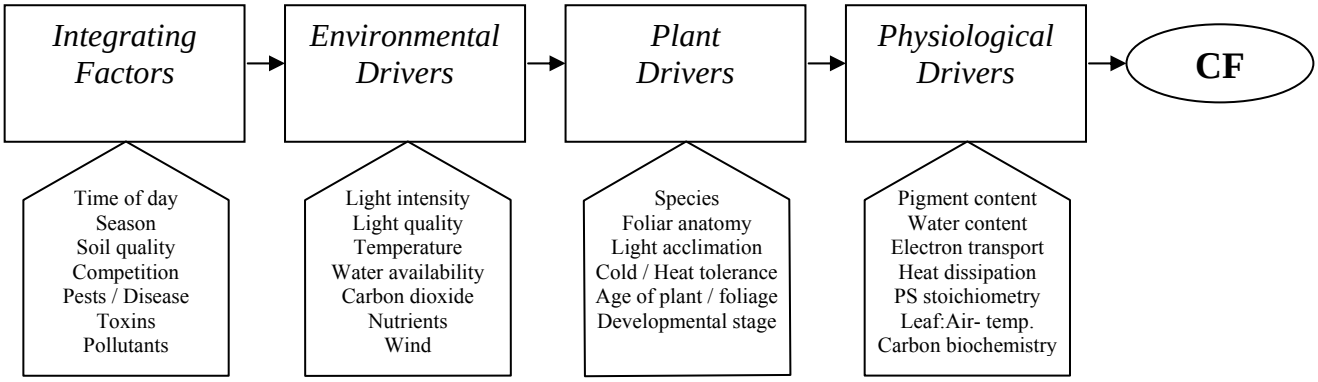

Figure 2.1.1. Drivers of leaf chlorophyll fluorescence.

One of the most powerful applications of chlorophyll fluorescence is in the early, previsual detection of physiological strain. Early detection may facilitate remedial actions before survival, growth and productivity are constrained, and may help to forecast long term resource quality. However, since many factors affect chlorophyll fluorescence in a similar way, the technique cannot be used to identify the presence of a particular stressor, but only to indicate apparent physiological strain. In passive measurement of fluorescence, such early detection may be possible, assuming these measurements provide consistent information beyond chlorophyll content. Cerovic et al. (1999) reported that the ratio F690/F740 is largely affected by changes in chlorophyll content at values lower than 250 mg m^{-2} (pale leaves) but is quite insensitive to changes in chlorophyll content higher than 300 mg m^{-2}.

Ratios involving the red and far-red wavebands are responsive to various factors. For example, F690/F730 has been shown to decrease with increasing carbon dioxide uptake rate in *Fagus sylvatica*, increase under water deficit in *Populus alba* and *Pseudotsuga menziesii* (Lichtenthaler and Rinderle, 1988; Valentini et al., 1994); and increase in DCMU-treated foliage of several coniferous species (Lichtenthaler and Rinderle, 1988). The ratio was also responsive to ozone exposure in *Pinus strobus* (Theisen et al., 1994). Autumnal senescence in broad-leaf species, which is initiated by shorter day lengths and cooler temperatures and which signifies a seasonal cessation of regular photosynthetic processes, is a seasonally-

induced water stress that induces a dramatic increase in the F690/F735 ratio (Lichtenthaler, 1987; Lang and Lichtenthaler, 1991; D'Ambrosio et al., 1992; Mineucchi et al., 1999).

2.1.1. Methods for measurement of passive fluorescence

The aim of introducing fluorescence into a radiative transfer canopy model is to separate fluorescence yield variations from other variations induced by changes in the type of illumination (direct or diffuse) and for bi-directional effects. An instrument allowing measurements with variable viewing directions and having a footprint sufficiently large to integrate the structure of the plants will be required. This instrumentation will generate high quality data to feed canopy fluorescence models.

The method commonly envisaged to extract the fluorescence signal from the reflected radiance is the use of the Fraunhofer Line in-filling approach. Fraunhofer lines are dark lines in the solar spectrum resulting from absorption by constituents. Hence, light detectable in a Fraunhofer region can signify fluorescence, which may be measurable by sufficiently sensitive instruments (Moya et al., 1992; Carter et al., 1990, 1996; Kebabian et al., 1999). Several Fraunhofer lines exist in the red and far-red solar spectrum which may be useful for remote sensing of chlorophyll fluorescence. Figure 2.1.1 shows the position of the main Fraunhofer lines in relation with the chlorophyll fluorescence emission and reflectance spectrum. The output parameters are the reflectance and the fluorescence contribution. This method was first applied to passive fluorescence remote sensing by Plascyk (1975) using solar atmosphere absorption lines (Hα).

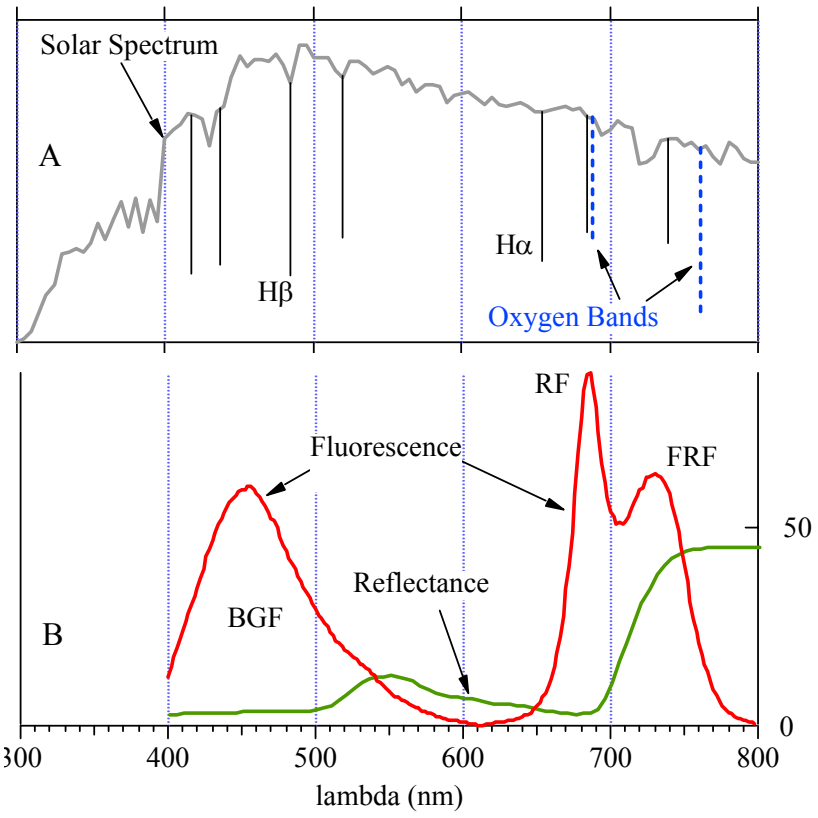

Figure 2.1.1. **(A)** Solar spectrum at sea level. Vertical lines represent the position and the intensity of main absorption bands. Dashed lines: oxygen absorption bands due to terrestrial atmosphere. Continuous line: absorption bands due to the solar atmosphere. **(B)** Continuous line: fluorescence emission spectrum of a grapevine leaf excited at 355 nm. Dashed line: reflectance spectrum of the same leaf. BGF: Blue Green fluorescence, RF: Red Fluorescence, FRF: Far Red Fluorescence.

Solar irradiance exhibits three main absorption bands in the red and near infra-red part of the spectrum. Compared to the Hα line, the oxygen absorption bands are larger and better situated with respect to the chlorophyll fluorescence emission spectrum of leaves.

2.1.2. Available instruments

In order to supply data to feed fluorescence models, and to validate new models, reliable instrumentation and methods for passive fluorescence detection is a prerequisite.

Two immediately available approaches to acquiring passive fluorescence data include use of a passive multi-detector providing measurements at two wavelengths (687 and 760 nm), and analysis of hyperspectral signatures. A possible concern is that analytical methods may need further refinement for extraction of fluorescence information from the hyperspectral signatures, but this is a promising approach that warrants further testing and development. The two-band detector may be a reliable instrument to generate good quality chlorophyll fluorescence data in the short term.

Based on the atmospheric oxygen absorption bands, a single-channel instrument measuring at 760 nm and a multi-channel instrument measuring at 760 and 687 nm have been developed (Moya et al., 1998; Evain et al., 2001). Both instruments are operational and have been tested in several campaigns (Evain et al., 2002). Based on a Fabry-Perot interferometer, a second system measuring in the Hα line (656 nm) has been constructed and is still being tested.

Passive fluorescence measurements using atmospheric oxygen absorption bands are based on commercially-available narrow-band interference filters. They are reasonably simple and accurate. The high rate of data acquisition allows measurements under naturally changing light conditions. In addition, the fluorescence information is available simultaneously in two channels: 687 and 760 nm, giving access to the F687/F760 ratio. Also, the radiance of the target is obtained at these wavelengths. However they have had some drawbacks; for example, variability is introduced when light encounters air-mass interference on its way through the atmosphere. As the atmosphere path-length changes with the sun zenith angle, the depth of the absorption bands exhibits large variations during the diurnal cycle, with a minimum around solar noon. Until now, a reference panel in the vicinity of the target was required to determine the actual depth of the oxygen band in the irradiance signal (Moya et al., 1998). Recent progress on the modelling of the air mass absorption (Evain, 2002) together with the use of a complementary channel in the infra-red part of the spectrum made the continuous use of a reference panel unnecessary.

Another approach using oxygen for passive fluorescence sensing includes that from an American company, Aerodyne, whose patented instrument, the Plant Fluorescence Sensor, uses a completely different method, based on the luminescence of oxygen (Kebabian et al., 1999; Freedman et al., 2002). The light from fluorescing plants is passed through a low-pressure cell containing oxygen; the oxygen absorbs the energy and then re-emits photons which are then detected by a photomultiplier tube. The instrument measures at 688 and 762 nm (and calculates an R/FR ratio). It is being refined for airborne applications. A potential

drawback of the sensor is its integration time of 600 s, which seems too slow to follow sun-induced fluorescence variations.

It is also possible to extract fluorescence information from the derivative of the red edge of hyperspectral reflectance signatures, specifically at about 690 nm and 750 nm, using fibre spectrometers and the Compact Airborne Spectrographic Imager (CASI), as shown under both laboratory and natural illumination conditions at leaf and canopy levels (Zarco-Tejada et al., 2000 a & b; 2003). Further, it was possible to model these effects at the leaf level using a leaf radiative transfer model, the Fluorescence-Reflectance-Transmittance (FRT) model based on the Kubelka-Munk theory. Efforts to scale up to airborne platforms using CASI at 450 m have had preliminary success in tracking diurnal steady-state fluorescence (Zarco-Tejada et al., 2001). However, any efforts to extract fluorescence information from passive spectral reflectance must account for the influence of chlorophyll content. If chlorophyll content is relatively stable, fluorescence information may address the functionality of the chlorophyll that is present (Lichtenthaler and Rinderle, 1988; Schreiber et al., 1994).

2.2. Review of leaf fluorescence models

Canopy fluorescence models require, among other input parameters, the leaf reflectance, transmittance, and fluorescence spectra. Because of the importance of photosynthetic function, leaf optical properties have been the subject of hundreds of studies since the middle of the last century. Most papers focused on the spectral properties of leaves (hemispherical reflectance and transmittance) which were used to estimate their biochemical content (chlorophyll, water, dry matter, etc.) and their anatomical structure (http://www.multimania.com/opticleaf/). For instance, when foliage changes through phenological aging or when plants undergo environmental stresses, leaf chlorophyll content is observed to decline: this results in an increase in the reflectance and transmittance over the visible spectrum. These relationships were usually established empirically or directly estimated, using a physical model. Leaf chlorophyll fluorescence in the red and far-red regions has also been the subject of many papers detailing theory, measurement methods, and interpretation (relationship with photosynthesis and plant physiological status) but historically, the two scientific communities have grown in parallel with only few interactions. The historical use of artificial light sources for fluorescence excitation (difficult to implement on spaceborne remote sensing platforms), and also the complexity of the artificially-induced fluorescence signal, may help to explain that situation. The study of solar-induced fluorescence, which occurs under natural conditions and which is superimposed on leaf reflectance and transmittance, has built bridges between communities.

One cannot separate fluorescence from reflectance and transmittance in a leaf optical properties model. For that reason, it is necessary first to review the existing models which successfully account for absorption and scattering phenomena within a plant leaf.

2.2.1. Leaf reflectance and transmittance models

While experimental measurements of leaf optical properties were progressing, deterministic approaches based on diverse representations of light interactions with plant leaves were also developed. These models are distinguished by the underlying physics and by the complexity of the leaf. The simplest ones consider the blade as a single scattering and absorbing layer. In the most complicated ones, all the cells are described in detail (shape, size, position, and biochemical content). Whatever the approach, these models have improved our understanding

of the interactions of light with plant leaves. Ustin et al. (2004) and Jacquemoud (2004) extensively reviewed computer-based leaf models which, from the late sixties to the present, have improved our understanding of the interaction of light with plant leaves. They can be categorized into different classes, arranged in order of increasing complexity:

- **Plate models** (Figure 2.2.1a): The first plate model was introduced by Allen et al. (1969) who represented a leaf as an absorbing plate with rough surfaces giving rise to Lambertian diffusion. Parameters here are an index of refraction and an absorption coefficient. This model was successful in reproducing the reflectance spectrum of a compact corn leaf characterized by few air-cell wall interfaces. The same authors rapidly extended the model to non-compact leaves by regarding them as piles of N plates separated by N−1 air spaces (Allen et al., 1970). The solution of such a system, provided in the last century by Stokes (1862), has been extended to N being a real number: this is the so-called generalized plate model. This additional parameter N actually describes the leaf internal structure and plays a role similar to that of the scattering coefficients in the Kubelka-Munk model. Now in widespread use in the remote sensing community, the PROSPECT model (*Leaf Optical Properties Spectra*) has been designed this way (Jacquemoud and Baret, 1990). It was among the first radiative transfer codes to accurately simulate the hemispherical reflectance and transmittance of various plant leaves (monocots, dicots or senescent leaves) over the solar spectrum from 400 nm to 2500 nm. Several versions have been made widely available in the community (Fourty et al., 1996; Jacquemoud et al., 1996; Baret and Fourty, 1997; Fourty and Baret, 1998; Jacquemoud et al., 2000) and validated on different datasets.

- **N-flux models** (Figure 2.2.1b): These models derived from the Kubelka-Munk theory consider the leaf as a slab of diffusing (scattering coefficient *s*) and absorbing (absorption coefficient *k*) material. The N-flux equations are a simplification of the radiative transfer theory: the solution of these equations yields simple analytical formulae for the diffuse reflectance and transmittance. A two-flux model (Allen and Richardson, 1968) and a four-flux model (Fukshansky et al., 1991; von Remisowsky et al., 1992; Richter and Fukshansky, 1996) have been successfully used in the forward mode to calculate the *s* and *k* optical parameters of plant leaves. Yamada and Fujimura (1991) later proposed a more sophisticated version in which the leaf was divided into four parallel layers: the upper cuticle, the palisade parenchyma, the spongy mesophyll, and the lower cuticle. The Kubelka-Munk theory is applied with different parameters in each layer, and solutions are coupled with suitable boundary conditions to provide the leaf reflectance and transmittance as a function of the scattering and absorption coefficients. But these authors went further, interpreting the absorption coefficient determined in the visible region in terms of chlorophyll content. By inversion, their model became a nondestructive method for the measurement of photosynthetic pigments. The leaf biochemistry has been introduced by Conel et al. (1993) who used a two-flux model to study the influence of water, protein, cellulose, lignin, and starch on leaf middle infrared reflectance. However they did not validate it. Finally, a very simple model, directly issued from the expression of the reflectance, has been used to estimate the chlorophyll content of wheat leaves (Andrieu et al., 1988).

- **Compact spherical particle models** (Figure 2.2.1c): None of these models are adapted to needle-shaped leaves due to a lack of experimental data available on such targets. Dawson et al. (1998) adapted Melamed's theory of light interaction with suspended powders (Melamed, 1963) and designed the LIBERTY model (*Leaf Incorporating Biochemistry*

Exhibiting Reflectance and Transmittance Yields) specifically to calculate the optical properties of both dried and fresh stacked conifer (particularly pine) needles. By treating the leaf as an aggregation of cells, with multiple radiation scattering between cells, output reflectance and transmittance spectra are a function of three structural parameters (cell diameter in μm, intercellular air space, leaf thickness) and the combined absorption coefficients of leaf biochemicals (chlorophyll concentration in mg m^{-2}, water content in g m^{-2}, lignin and cellulose content in g m^{-2}, and nitrogen content in g m^{-2}). To date, LIBERTY remains the only model based on this concept; however, validation studies remain sparse.

- **Radiative transfer theory** (Figure 2.2.1d): Compared with canopy level, only few models directly use the radiative transfer equation at leaf level. The poor information we have on leaf internal structure and biochemical distribution leads to strong simplifications which make such an approach less efficient as compared to more robust formulations. In Ma et al. (1990), the leaf is described as a slab of water with an irregular surface containing randomly distributed spherical particles. In LEAFMOD (*Leaf Experimental Absorptivity Feasibility MODel*), it is compared to a homogeneous mixture of biochemicals which scatter and absorb light (Ganapol et al., 1998). Each model was able to provide a faithful simulation of leaf optical properties.

- **Stochastic models** (Figure 2.2.1e): Tucker and Garatt (1977) proposed an original stochastic model where the radiation transfer is simulated by a Markov chain. A black maple leaf is partitioned into two independent tissues, a palisade parenchyma and a spongy mesophyll. Four radiation states (solar, reflected, absorbed, and transmitted) are defined, as well as the transition probabilities from one radiation state to another, between the different compartments. These probabilities are set on the basis of the optical properties of the leaf material. Starting with an initial state vector representing the incident radiation, the steady state is computed by iteratively applying the one-step transition matrix, and yields both the reflectance and transmittance. The SLOP (*Stochastic model for Leaf Optical Properties*) model (Maier et al., 1999; Maier, 2000) is an improved version of the stochastic model, which differs in that the leaf is partitioned into four different tissues.

- **Ray tracing models** (Figure 2.2.1f): Among various approaches, only ray tracing techniques can account for the complexity of internal leaf structure as it appears in a photomicrograph. They require a detailed description of individual cells and their unique arrangement inside tissues. The optical constants of leaf materials (cell walls, cytoplasm, pigments, air cavities, etc.) also have to be defined. Using the laws of reflection, refraction, and absorption, it is then possible to simulate the propagation of individual photons incident on the leaf surface. Once a sufficient number of rays have been simulated, statistically-valid estimates of the radiation transfer in a leaf may be deduced. The technique has been applied with a number of variants. The first studies were performed at the cell level (Haberlandt, 1914; Gabrys-Mizera, 1976), in particular with epidermal cells the shape of which might influence the path of the incident beams. Research efforts were also directed toward understanding the transmission path of light through entire leaves: Allen et al. (1973), and afterwards Brakke and Smith (1987) modelled an albino maple leaf by 100 circular arcs and of two media: intercellular space air and cell walls characterized by their indices of refraction. The model was used to test the specular and the diffuse nature of the reflection at the cell walls. Simulations led to an underestimation of the reflectance and an overestimation of the transmittance in the near-infrared plateau, which was demonstrated shortly afterwards by Kumar and Silva (1973) who found that the actual reflectance and transmittance could be better reproduced by

adding two more media into the model, cytoplasm and chloroplasts, thereby increasing the internal diffusion. Whatever the approach, the absorption phenomena that characterize leaf optical properties outside the near-infrared plateau has been ignored. Moreover in all these models, leaves were always described as two-dimensional objects although the three-dimensional structure of these organs is very important to their physiological function. For this reason, Govaerts et al. (1996) used a three-dimensional ray tracing model, RAYTRAN (Govaerts and Verstraete, 1998), on a virtual 3D dorsiventral leaf, to characterize the light environment, including absorption, scattering and transmission, within and between cells: Cells of variable size, cell wall thicknesses, chemistry and air spaces were modelled and implications for absorption profiles, light harvesting, and photosynthesis were successfully investigated (Ustin et al., 2001). Finally, in a completely different domain, namely image synthesis, modelling of light interaction with biological tissues such as plant leaves recently emerged with ABM (*Algorithmic BDF Model*) (Baranoski and Rokne, 1997, 1999).

Despite decades of research, much more work is required before we will accurately model leaf optical properties. Models are nevertheless essential to understand how electromagnetic radiation interacts with leaf elements, but also to directly relate observed optical properties to leaf biophysical attributes. Although several leaf models have been developed to relate leaf biochemistry and scattering parameters to leaf reflectance and transmittance signatures, only a few, detailed in the next section, are formulated to specifically include the chlorophyll fluorescence signal as shown in Table 2.2.1.

Finally, it is noticeable that PROSPECT and LIBERTY, the two most popular models to simulate the reflectance and transmittance of broad-leaves and needles respectively, do not include fluorescence, and notably PROSPECT has been validated on several datasets and is widely used in remote sensing.

a) Plate models	b) N-flux models
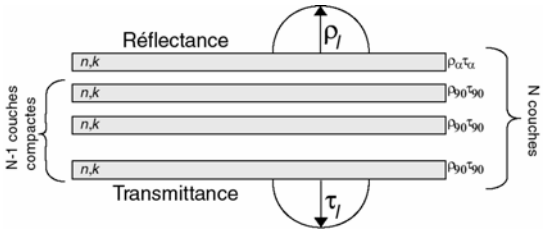	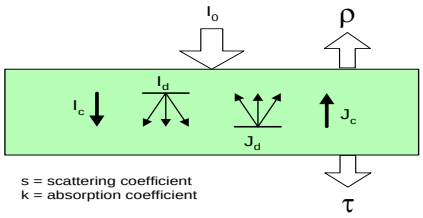
c) Compact spherical particle models	d) Radiative transfer theory
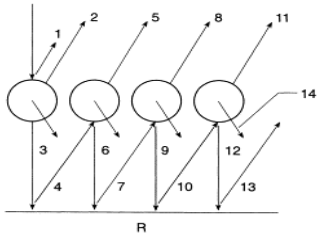	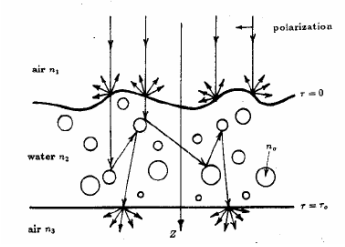
e) Stochastic models	f) Ray tracing models
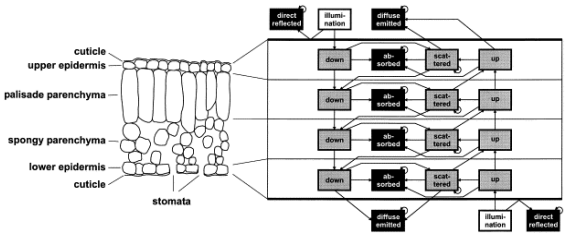	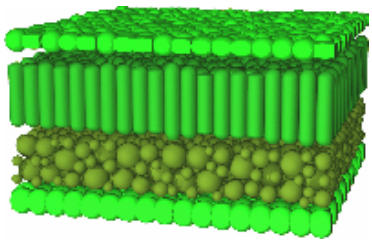

Figure 2.2.1. Different leaf optical properties models.

Table 2.2.1. Categorization of leaf optical properties models.

Type	Name	Reflectance/transmittance	Fluorescence
Beer-Lambert		Baret et al. (1988)	Ounis et al. (2001)
Plate models	PROSPECT	Allen et al. (1969), Allen et al. (1970), Jacquemoud and Baret (1990), Fourty et al. (1996), Jacquemoud et al. (1996), Baret and Fourty (1997), Jacquemoud et al. (2000)	
N-flux models	FRT	Allen and Richardson (1968), Fukshansky et al. (1991), Yamada and Fujimura (1991), von Remisowsky et al. (1992), Conel et al. (1993), Richter and Fukshansky (1996)	Fukshansky and Kazarinova (1980), Rosema et al. (1991), Zarco-Tejada et al. (2000 a&b)
Compact spherical particle models	LIBERTY	Dawson et al. (1998)	
Radiative transfer theory	LEAFMOD	Ma et al. (1990), Ganapol et al. (1998)	
Stochastic models	SLOPE	Tucker and Garatt (1977), Maier et al. (1999)	Maier (2000)
Ray tracing models	ABM, RAYTRAN	Allen et al. (1973), Brakke and Smith (1987), Kumar and Silva (1973), Govaerts et al. (1996), Baranoski and Rokne (1997, 1999), Ustin et al. (2001)	

2.2.2. Leaf fluorescence models

The possible applications of fluorescence spectroscopy in plant physiology, medical diagnostic techniques or the paper industry are numerous. However, they are limited because the measured spectrum is distorted by the absorption and scattering properties of the media. Attempts to eliminate these effects have been based on a theoretical description of light propagation in a turbid medium, producing an analytic relationship between measured and intrinsic fluorescence (Gardner et al., 1996). Different theories of light transport have been applied to fluorescence of cellular tissues.

- **Beer's law theory:** When optical properties are dominated by absorption, the Beer's law theory works well. In order to study the fluorescence of ink printed on paper, Emmel (1998, 2000), Emmel and Hersch (1998) established a mathematical formula that predicted the behaviour of a transparent medium containing fluorescent molecules (Figure 2.2.2).

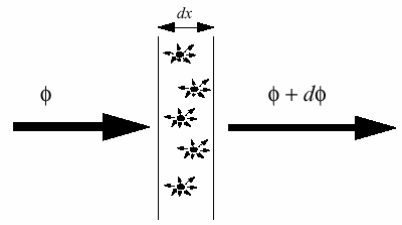

Figure 2.2.2. Absorption and emission in an infinitely thin fluorescent layer when irradiated by a diffuse light flux ϕ (after Emmel, 1998).

The intensity variation dϕ of the light emerging in the positive direction has two components: the first one is due to the light which has been absorbed, the second one is the light emitted by fluorescence,

$$\mathrm{d}\phi(\lambda,x) = -c\varepsilon(\lambda)\phi(\lambda,x)dx + \frac{1}{2}cQf(\lambda)\left[\int_{\Delta}\varepsilon(\mu)\phi(\mu,x)d\mu\right]dx \qquad [2.2.1]$$

where ε(λ) is the extinction coefficient of the fluorescent molecules, c is their concentration, Q is their quantum yield in the medium, Δ is the excitation spectrum, and f(λ) the normalized fluorescence spectrum. Richards-Kortum et al. (1989) applied a one layer model of tissue fluorescence to the human artery wall. The tissue is represented as a single layer, which is infinitely thick with respect to the penetration depth of the irradiating light. The tissue fluorescence power arriving at the detector $S(\lambda_x,\lambda_m)$, which is a function of both the excitation λ_x and emission λ_m wavelength, is written as:

$$S(\lambda_x,\lambda_m) = k\int_0^{\infty} P(\lambda_x)e^{-\mu t(\lambda x)z}\mu_a(\lambda_x)\frac{\phi(\lambda_x,\lambda_m)}{2}e^{-\mu t(\lambda m)z}dz \qquad [2.2.2]$$

where k is a proportionality factor which depends on the tissue index of refraction and the incident light, $P(\lambda_x)$ denotes the incident excitation power, $\mu_t(\lambda)$ and $\mu_a(\lambda)$ are the total attenuation and absorption coefficients of the tissue, $\phi(\lambda_x,\lambda_m)$ is the quantum yield of fluorescence, and z is the distance from the irradiated surface. Ounis et al. (2001) simulated the leaf fluorescence with such an approach.

- **Kubelka-Munk theory:** Because optical properties are often dominated both by scattering and absorption, Allen (1964) modified the Kubelka-Munk equations to include fluorescence. Radiation within the medium consists of two diffuse fluxes propagating in opposite directions. The flow of total diffuse flux across a horizontal slab of thickness dz at any wavelength λ can be written in differential form as:

$$\left.\begin{aligned}\frac{dI}{dz} &= -(k+s)I + sJ\\ -\frac{dJ}{dz} &= sI - (k+s)J\end{aligned}\right\} \Rightarrow \left\{\begin{aligned}\frac{d(I+F^+)}{dz} &= -(k+s)(I+F^+) + s(J+F^-) + \frac{1}{2}P\\ -\frac{d(J+F^-)}{dz} &= s(I+F^+) - (k+s)(J+F^-) + \frac{1}{2}P\end{aligned}\right. \qquad [2.2.3]$$

where *s* and *k* are the linear scattering and absorption coefficients for diffuse light (mm^{-1}), respectively, *I* and *J* are the upward and downward radiant fluxes at depth z, respectively, F^+ and F^- are the upward and downward fluorescence fluxes at depth z, respectively, and *P* is the fluorescence emission flux (assumed to be isotropic) at depth z. The latter assumes that all absorbed photons of *I* and *J* in the PAR region contribute to the excitation of the photosystems and is defined as an integration over the wavelength range 400-700 nm:

$$P(z) = \phi\eta\int_{400}^{700} k(I+J)d\lambda \qquad [2.2.4]$$

where ϕ is the photon fluorescence efficiency, i.e., the fraction of absorbed upward and downward flux that contributes to fluorescence excitation, and η is the fluorescence

emission spectral distribution function. Fukshansky and Kazarinova (1980), Bonham (1986), and Shakespeare and Shakespeare (2003) solved the extended Kubelka-Munk equations by successive approximations in an analytical way. Rosema et al. (1991) and later on Zarco-Tejada et al. (2000 a,b) prefered a numerical way called the "doubling method". Finally Emmel (1998, 2000), Emmel and Hersch (1998) proposed a matrix method. Of course all the methods should provide the same results.

Since plant leaves cannot be considered as homogeneous layers due to the existence of differentiated tissues (epidermis, palisade and spongy mesophylls), the matrix formulation provided by Yamada and Fujimura (1991) was used by Zarco-Tejada et al. (2000 a,b) to improve simulations. These authors assumed the leaf to be represented as a stack of three layers – top epidermal layer, compact inner layer containing the chloroplasts and cellular material, and lower epidermal layer – and calculated its apparent reflectance with the superimposed effects of fluorescence (Figure 2.2.3).

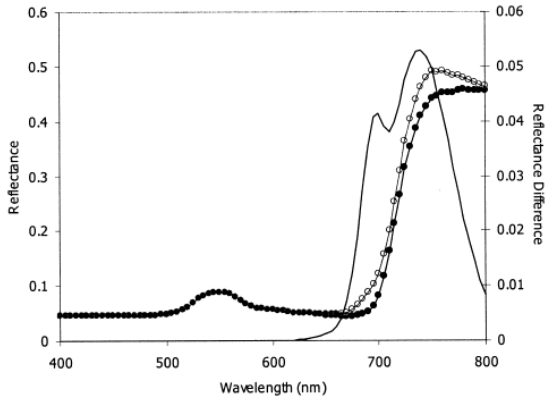

Figure 2.2.3. Leaf reflectance with fluorescence • (ϕ = 0.085, C_{ab} = 50 μg cm^{-2}, leaf thickness = 0.075 mm) and without fluorescence o simulated by the FRT (*Fluorescence-Reflectance-Transmittance*) model. The line indicates the difference between the two spectra (after Zarco-Tejada et al., 2000 a,b).

- **Stochastic theory:** Little information is available on the implementation of chlorophyll fluorescence in SLOPE (Maier, 2000). The radiative transfer has been modelled in a wavelength sequential manner, starting with the shortest one, because chlorophyll fluorescence causes an energy transfer from shorter to longer wavelengths. After the absorption in one wavelength channel has been calculated, the number of absorbed photons in each layer by each pigment are multiplied by a fluorescence quantum yield specific to this pigment. These fluorescence photons are then distributed over the longer wavelengths according to a given fluorescence spectrum. Figure 2.2.4 shows the apparent reflectance and transmittance spectra of a linden leaf.

  As can be seen, the reflectance is strongly modified in the red region, and relatively less in the red edge up to the near infrared plateau. In the red, about 50% of the radiance is due to fluorescence, which seems overestimated. The position of the red edge is shifted 3 nm to shorter wavelengths. In the near infrared plateau, fluorescence amounts only to a few percent of the signal, which agrees with experiment.

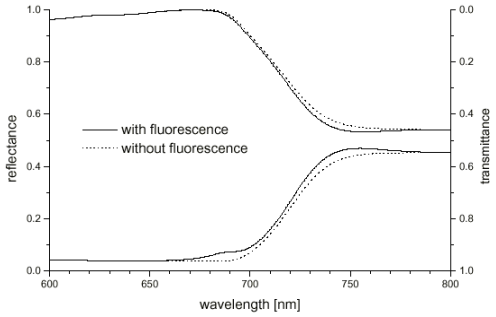

Figure 2.2.4. Reflectance and transmittance spectra of a linden leaf without fluorescence (…) and with fluorescence (—) simulated with SLOPE (after Maier et al., 1999).

- **Other theories:** Through a series of Monte Carlo simulations, Wu et al. (1993) described fluorescence in an optically thick turbid medium such as human tissue. In Welch et al. (1997), boundary conditions have been introduced to model fluorescence of multiple layer and cubic objects. An innovative rigorous analysis of tissue fluorescence based on electromagnetic theory has been proposed by Panou-Diamandi et al. (1998).

2.3. Review of canopy fluorescence models

The literature on canopy level fluorescence models is very sparse. Three canopy fluorescence models and a canopy fluorescence lifetime model will be described here.

a) Olioso model

The model of Olioso et al. (1992) assumes a Lambert-Beer law attenuation of light flux inside the canopy, and it considers only direct solar flux and the generated radiance in the view direction (a). This model also takes into account the background reflection of incident (b) and downward (c) emitted radiation. The global fluorescence signal is then the sum of three contributions:

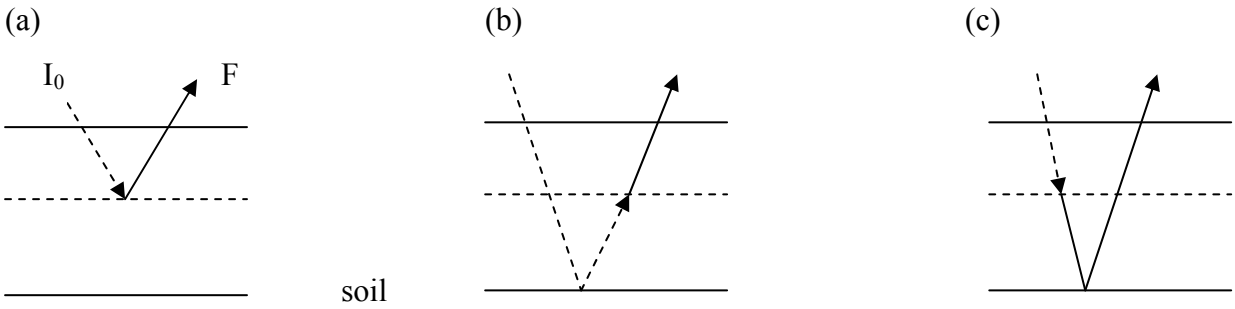

The emitted fluorescence by a layer dL at optical depth L will be:

$$\mathrm{d}F(L) = F(L)K(L)I(L)\mathrm{d}L$$

with
$F(L)$ the fluorescence efficiency
$K(L)$ the interception coefficient
$I(L)$ the incident radiation

$$I = I_0.\exp[-\int k_e(L')\mathrm{d}L']$$

k_e attenuation coefficient.

The extinction coefficients describing the attenuation of these fluxes are obtained by means of simulations with the SAIL model (Verhoef, 1984). A peculiarity is that a vertical gradient of the leaf chlorophyll content is allowed, thus accommodating the vertical leaf colour gradients often seen in canopies like wheat. The leaf chlorophyll gradient is assumed to vary exponentially, and combined with the exponential attenuation of light fluxes, this combination still allows an analytical solution to be obtained. However, a dependence of leaf fluorescence efficiency on the light level incident on leaves is not accommodated for. The fluorescence efficiency is taken to be constant at 730 nm and is described by an exponential profile at 690 nm to take into account the greater fluorescence of the leaves closer to the ground, considered to have lower chlorophyll content.

b) FLSAIL model

The FLSAIL model (Rosema et al., 1991) shares its description of canopy geometry with the one applied in SAILH (Verhoef, 1998). This model is identical to the original SAIL model, but with an extension to include the hot spot effect in the single scattering contribution. In FLSAIL all light interactions are modelled in a similar manner to SAILH, but fluorescence contributions are added. Also, a different method of solution has been chosen. Where SAILH is based on an analytical solution, in FLSAIL the doubling algorithm is used. Other properties of this model are: that the canopy layer is assumed to be homogeneous, that no dependence of leaf fluorescence on the incident light level is assumed, and that it was developed with the application to laser-induced fluorescence in mind. In FLSAIL, a simple leaf level fluorescence model is included that is based on the Kubelka-Munk equations, extended for fluorescence. This leaf level sub-model is also solved by using the doubling algorithm. The input parameters of the FLSAIL model are:

Fluorescence quantum efficiency
Relative chlorophyll concentration
Relative leaf thickness
Number of doubling steps
Leaf area index
Leaf angle distribution type
Hot spot parameter (leaf size / canopy height)
Soil reflectance (assumed spectrally flat)
Source zenith angle
Viewing zenith angle
Relative azimuth
Excitation wavelength

The reason that the doubling method is applied in FLSAIL, instead of an analytical solution like in SAIL, is that the required system of differential equations describing all radiation

interactions for both the excitation wavelength and the fluorescence wavelength is eight-dimensional and in this case an analytical solution becomes rather involved.

For an elementary canopy layer it is possible to express the reflectance, transmittance and fluorescence in terms of the optical properties of single leaves, the leaf angle distribution, and the source-object-sensor geometry. Starting from the optical properties of the elementary layer, it is possible to derive the optical properties of a stack of two elementary layers. This is called a doubling step. Repeating this process several times, it is possible to quickly compute the optical properties of a canopy layer of the desired optical thickness. For instance, for a canopy with a given LAI of L one could define an elementary layer with an LAI equal to $L/1024$, and then derive the optical properties of the thick layer in only ten doubling steps.

Advantages of the doubling method are that it is fast and numerically very stable. A disadvantage is that is can only be applied to a homogeneous medium. In case the optical properties of leaves vary throughout the layer, one has to use another method, for instance the adding method. In the adding method each elementary layer may have different optical properties. The drawback is that computation time increases considerably.

c) D.A.R.T. model

Fluorescence was also implemented into the D.A.R.T. model (Discrete Anisotropic Radiative Transfert) developed by the CESBIO (Centre d'Etude Spatiale de la BIOsphère) that simulates radiative transfer in 3-D media. In this model, the media is represented by a matrix of parallelepiped cells, which may contain different kind of elements, such as leaves, trunk, water, etc.. The elements are characterized by their architectural and optical properties. In a first step, a programme builds a realistic representation of the scene to be studied. Then, the propagation of a known incident ray is calculated using the phase function of each cell. This model was coupled with a leaf fluorescence model, which gives directional and spectral emission at given wavelength λ and direction Ω_v :

$$E_f(\lambda, \Omega_v) = \eta(\lambda)\, \alpha(\lambda)\, q\, f(\Omega_v)\, E_{fabs}(\lambda)$$

$\eta(\lambda)$: normalized spectrum of fluorescence emission without taking into account re-absorption.
$\alpha(\lambda)$: ratio of photons which are not re-absorbed by the leaf
q : fluorescence quantum yield
E_{fabs} : energy absorbed by the leaf
$f(\Omega_v)$: function of leaf angular repartition, assumed to be Lambertian.

Simulations were performed for laser-induced fluorescence. In a first stage, the DART model provides the amount of energy absorbed by each cell. Then it calculates the fluorescence emission for a given direction. The fluorescence quantum yield is assumed to be constant.

d) Canopy fluorescence lifetime model

One can also mention a canopy fluorescence lifetime model by Camenen et al. (1996). It was shown that the average lifetime is proportional to the fluorescence quantum yield under most experimental conditions. At leaf level, the principle of lifetime determination is based on the recording of the fluorescence decay during a time window of a few nanoseconds after excitation with a short light pulse. However, the recorded decay is the convolution product of the fluorescence decay with the instrumental response. A deconvolution method has then to be used to determine the fluorescence lifetime. As a laser beam directed towards a canopy will be intercepted by components situated at different levels along the laser beam, the global signal measured after a short laser pulse corresponds to the superposition of elementary signals coming from each illuminated canopy component. Thus, it was necessary to develop a specific method for retrieving fluorescence lifetime, based on the deconvolution method known for a single leaf. In a first step, the position and reflectance characteristics of each reflecting canopy element is determined from the deconvolution of the backscattered signal. In a second step, the parameters obtained are introduced into the fluorescence function to determine canopy fluorescence lifetime. This deconvolution method was validated using simulated laser shots on a 3-D canopy mockup.

2.4. Leaf-canopy fluorescence modelling approach

The modelling approach used defined the input/output variables that connect the model stages as well as the processes as follows:

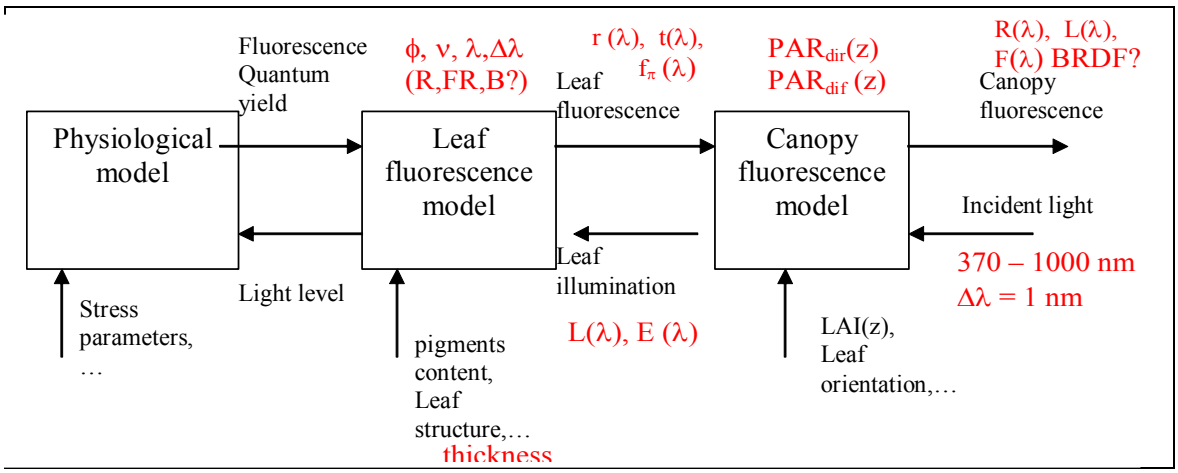

The physiological variables controlling fluorescence are defined in detail in Chapter 3. The canopy model is described in detail in Chapter 4.

2.5. Conclusions

Steady-state chlorophyll fluorescence is often a sensitive indicator of natural and stress-induced effects. One of its most powerful applications is in the early detection of physiological strain, and the capacity that affords decision-makers to initiate remedial actions before growth and productivity are constrained. Chlorophyll fluorescence analyzed from two wavebands – red and far-red – has previously been found to be responsive to changes in environmental conditions, and are a focus of passive methodologies. Two immediately available approaches to acquiring passive fluorescence data include use of a passive multidetector providing measurements at two wavelengths (687 and 760 nm), and analysis of hyperspectral signatures.

For biophysical leaf fluorescence model development, it makes sense to limit the study to one model, as time is limited. A broad-leaf model is envisaged according to existing works and to recent knowledge on chlorophyll *a* fluorescence. The latter implies it is feasible to be able to model the fluorescence quantum yield – efficiency with which the energy of a photon absorbed by this pigment is emitted as fluorescence photon – as a function of the leaf physiological state (light intensity, etc.). Since the fluorescence signal relative to incident irradiance is quite low as compared to the reflectance or transmittance, a sensitivity analysis is essential. This crucial step ensures that the response of the computational model to the input parameters is the expected one. Recent works based on statistical methods like the Design Of Experiments for Simulation (DOES) or the Extended Fourier Amplitude Sensitivity Test (EFAST) extend research further by quantifying the relative effects of each of the input parameters, as well as their interactions. Such information may be helpful in inversion, for instance, to detect non-influential parameters. A leaf optical properties model should include the same parameters used in leaf reflectance and transmittance models, and specific input parameters to simulate fluorescence.

The literature on canopy level fluorescence models is very sparse. Three canopy fluorescence models (Olioso; FLSAIL; D.A.R.T.) and a canopy fluorescence lifetime model have been described here. The requirements for a new canopy level fluorescence model should be beyond that of FLSAIL, which was only intended for modelling of laser-induced canopy fluorescence. Coupling the canopy model to an atmospheric radiative transfer model would allow representation of the incident sun- and skylight, as well as simulation of top-of-atmosphere radiance levels in addition to surface fluorescence signals.

3. DEVELOPMENT of a NEW LEAF FLUORESCENCE MODEL: *FluorMODleaf*

3.1. Description of the PROSPECT model

3.1.1. Overview

PROSPECT is based on Allen et al. (1969, 1970) representation of the leaf as one or several absorbing plates with rough surfaces giving rise to isotropic diffusion (Figure 3.1.1). The first version of the model (Jacquemoud and Baret, 1990) used three input parameters: The structure parameter N (number of compact layers specifying the average number of air/cell walls interfaces within the mesophyll), the chlorophyll a+b concentration C_{ab} (µg cm^{-2}), and the equivalent water thickness C_w (cm or g cm^{-2}).

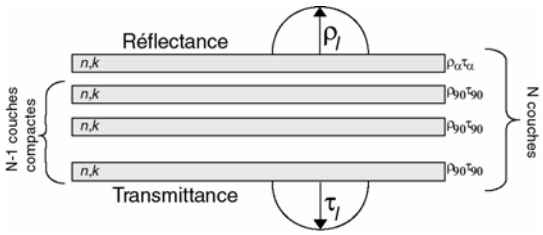

Figure 3.1.1. Schematic representation of PROSPECT.

Other biochemical constituents like cellulose and lignin (~carbon) or proteins (~nitrogen), which are potentially measurable by remote sensing thanks to the existence of specific absorption bands in the shortwave-infrared, motivated scientists to develop procedures to measure them. When trees lose their leaves, these constituents become part of the organic matter which is decomposed by soil micro-organisms. The C/N ratio is a good indicator of the rate of nitrogen mineralization, i.e., of soil respiration. The ratio is higher in Gymnosperms (which typically have thick, non-ramified, needle-shaped leaves) than Angiosperms (monocots and dicots with laminar leaves) and decomposition is slower. Since the release of carbon to the atmosphere through microbial respiration is an important component of the global carbon cycle, knowledge of C/N at different spatial scales would be particularly valuable to describe the functioning of terrestrial ecosystems.

During the summer of 1993 an experiment at the Joint Research Centre (Ispra, Italy) asembled a database, LOPEX, associating visible and infrared spectra of dry and fresh vegetation elements (leaves, conifer needles, stems, etc.) with physical measurements (thickness, water content, specific leaf area) and biochemical analyses (chlorophyll a+b, proteins, cellulose, lignin, etc.) (Hosgood et al., 1995). LOPEX was used to introduce the full leaf biochemistry into PROSPECT (Fourty et al., 1996; Jacquemoud et al., 1996; Fourty and Baret, 1998). A limit of this process arose however in the inversion of the model, when it was discovered that protein content could not be retrieved because of strong water absorption features and that cellulose and lignin could not be consistently identified and quantified. As a consequence, the model was simplified to the point that it now considers the dry matter content Cm (g cm^{-2}) as a whole instead of treating the leaf biochemical constituents individually (Baret and Fourty, 1997; Jacquemoud et al., 2000). That simplification, nevertheless, provides two interesting measures. First,C_m is equivalent to Specific Leaf Area (SLA expressed in cm^2 g^{-1}), a widely-used key variable in plant ecology because it is easily

measured and it is correlated with plant growth, light interception, gas exchange, and photosynthesis (Dijkstra, 1990; Meziane and Shipley, 1999; Shipley and Vu, 2002). For instance, after a net uptake of 1 kg of carbon, wheat (*Triticum aestivum*) will produce 20 m^2 of leaf area (allocation rate of 65%, SLA = 30 m^2 kg^{-1}) while saltbush (*Atriplex sp.*) will produce only 2 m^2 (allocation rate of 30%, SLA = 7 m^2 kg^{-1}). Second, C_m can be accurately retrieved by model inversion. In short, the four input parameters of PROSPECT today are: leaf structure parameter, the chlorophyll a+b concentration, and the equivalent water thickness, plus the dry matter content.

3.1.2. Interaction of isotropic light with a compact plant leaf: The *plate model*

The *plate model* developed by Allen et al. (1969) considers a compact plant leaf as a semi-transparent plate with plane parallel surfaces and initially assumes that the incident light is partially isotropic. That requirement is equivalent to the assumption that the surfaces are rough. Figure 3.1.2 illustrates incident light interacting with a compact plant leaf: It is partly reflected, partly transmitted and partly absorbed.

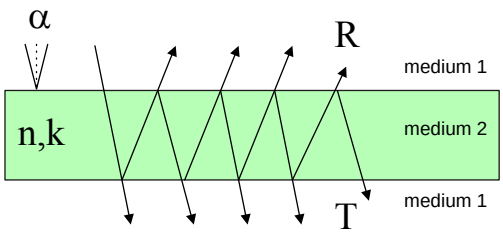

Figure 3.1.2. Multiple reflections produced by a transparent plate with rough surfaces.

The expression for the total reflectance of the plate $R_\alpha(1)$ can be derived by summing the amplitudes of successive reflections and refractions. Such derivation was first carried out by Sir George Biddell Airy in 1833 (cited by Yeh, 1988). Consider a beam incident on the plate: it is partially reflected and partially transmitted at the first interface. The transmitted part is subsequently reflected back and forth between the two interfaces as shown. We obtain:

$$\begin{aligned} R_\alpha(1) &= r_{12} + t_{12}\,\tau\, r_{21}\,\tau\, t_{21} + t_{12}\,\tau\, r_{21}\,\tau\, r_{21}\,\tau\, r_{21}\,\tau\, t_{21} + t_{12}\,\tau\, r_{21}\,\tau\, r_{21}\,\tau\, r_{21}\,\tau\, r_{21}\ldots\tau\, r_{21}\,\tau\, t_{21} + \ldots \\ &= r_{12} + t_{12}\, t_{21}\, r_{21}\,\tau^2(1 + r_{21}^2\,\tau^2 + r_{21}^4\,\tau^4 + \ldots) \\ &= r_{12} + \frac{t_{12}\, t_{21}\, r_{21}\,\tau^2}{1 - r_{21}^2\,\tau^2} \end{aligned} \qquad [3.1.1]$$

where r_{ij} and t_{ij} are the average reflectivity and transmissivity, respectively, from medium i into medium j, and τ is the fraction of light transmitted through the medium. The total transmittance of the plate $T_\alpha(1)$ is also determined by summing the components of transmissions to infinity:

$$\begin{aligned} T_\alpha(1) &= t_{12}\,\tau\, t_{21} + t_{12}\,\tau\, r_{21}\,\tau\, r_{21}\,\tau\, t_{21} + t_{12}\,\tau\, r_{21}\,\tau\, r_{21}\,\tau\, r_{21}\,\tau\, r_{21}\,\tau\, t_{21} + \ldots \\ &= t_{12}\, t_{21}\,\tau(1 + r_{21}^2\,\tau^2 + r_{21}^4\,\tau^4 + \ldots) \\ &= \frac{t_{12}\, t_{21}\,\tau}{1 - r_{21}^2\,\tau^2} \end{aligned} \qquad [3.1.2]$$

a) Transmission of light across an interface between two dielectrics

The first obstacle is the interface between air (refractive index $n_1 = 1$) and the plate (refractive index n_2). Transmissivity between media i and j will be designated t_{ij}, and the corresponding reflectivity by r_{ij}. We assume that there is no appreciable absorbance at the interface. The reflectivity is then related to the transmissivity by the simple relation $r_{ij} = 1 - t_{ij}$, and because the results for the transmissivity are somewhat simpler, we will not deal further with the reflectivity. We can identify the transmissivity for radiation whose electric vector **E** is perpendicular to the plane of incidence (plane containing the normal to the interface and the propagation vector of the incident wave) by the subscript $\perp$ and the transmissivity for radiation whose electric vector is in the plane of incidence by the subscript || (Figure 3.1.3).

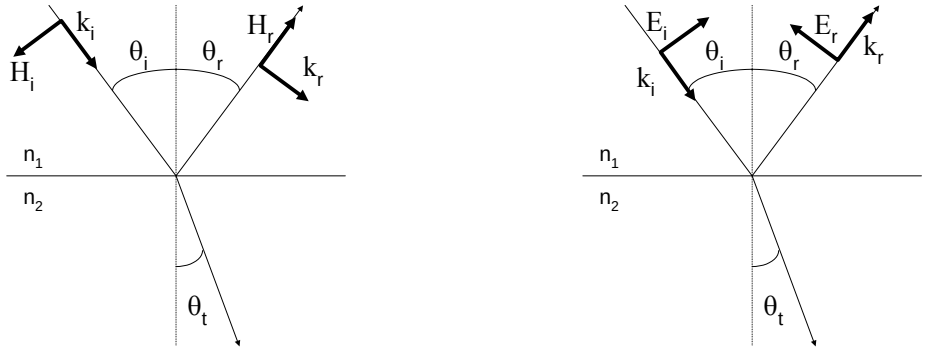

Figure 3.1.3. Reflection and refraction of a light beam a) perpendicular polarization b) parallel polarization.

When light falls at an angle θ_i on the interface, it is reflected according to the angle $\theta_r = \theta_i$ and refracted according to the angle θ_t which is related to θ_i by the Snell-Descartes law of refraction:

$$\sin\theta_i = n\sin\theta_t \qquad [3.1.3]$$

The transmission coefficients of the electric wave field from medium 1 into medium 2 across the boundary are (Schanda, 1986):

$$T_\perp(x,1,n) = \frac{2\sqrt{1-x}}{\sqrt{1-x}+\sqrt{n^2-x}} \quad \text{and} \quad T_\parallel(x,1,n) = \frac{2n^2\sqrt{1-x}}{n^2\sqrt{1-x}+\sqrt{n^2-x}} \quad \text{with} \quad x = \sin^2\theta_i \qquad [3.1.4$$

The fraction of light transmitted (transmissivity) by a non-absorbing medium is due to Fresnel who established his well-known equations in 1918:

$$t_\perp(x,1,n) = \frac{4\sqrt{1-x}\sqrt{n^2-x}}{\left(\sqrt{1-x}+\sqrt{n^2-x}\right)^2} \quad \text{and} \quad t_\parallel(x,1,n) = \frac{4n^2\sqrt{1-x}\sqrt{n^2-x}}{\left(n^2\sqrt{1-x}+\sqrt{n^2-x}\right)^2} \quad \text{with} \quad x = \sin^2\theta_i \qquad [3.1.5]$$

The average transmissivity in natural radiation is then given by:

$$t(x,1,n) = \frac{1}{2}\left(t_\perp(x,1,n) + t_\parallel(x,1,n)\right) \quad \text{with} \quad x = \sin^2\theta_i \qquad [3.1.6]$$

Of particular interest is the transmissivity for diffuse incident radiation which impinges on the phase boundary surface at all angles α between 0 and π/2, so that integration must be carried out over all these angles and the average obtained. Since the radiation flux impinging on a unit surface is proportional to the cosine of the angle of incidence, we have from the mean value theorem:

$$t_{av}(\alpha,1,n)=\frac{\int_0^{2\pi}d\varphi\int_0^{\alpha}t(x,n)\cos\theta\sin\theta\ \ d\theta}{\int_0^{2\pi}d\varphi\int_0^{\alpha}\cos\theta\sin\theta\ \ d\theta}=\frac{1}{2}\left(t_{\perp,av}(\alpha,1,n)+t_{\parallel,av}(\alpha,1,n)\right)\quad\text{with}\quad x=\sin^2\theta \qquad [3.1.7]$$

The integration leading to $t_{av}(\alpha,1,n)$ has been carried out by Judd (1942) and Stern (1964) for $\alpha=\pi/2$, and by Allen (1973) for any value of α. Figure 3.1.4 shows that the transmissivity for diffuse incidence ($\alpha=\pi/2$) is smaller than that for perpendicular incidence ($\alpha=0$). Simple formulations of $t_{av}(\alpha,1,n)$ can be provided when $\alpha=0$:

$$t_{av}(0,1,n)=t_{\perp,av}(0,1,n)=t_{\parallel,av}(0,1,n)=\frac{4n}{(n+1)^2} \qquad [3.1.8]$$

and when $\alpha=\pi/2$:

$$t_{\perp,av}(\frac{\pi}{2},1,n)=\frac{4(2n+1)}{3(n+1)^2}\quad\text{and}\quad t_{\parallel,av}(\frac{\pi}{2},1,n)=\frac{4n^3\left(n^2+2n-1\right)}{\left(n^2+1\right)^2\left(n^2-1\right)}-\frac{2n^2\left(n^2+1\right)}{\left(n^2-1\right)^2}\log n+\frac{2n^2\left(n^2-1\right)^2}{\left(n^2+1\right)^3}\log\frac{n(n+1)}{n-1} \qquad [3.1.9]$$

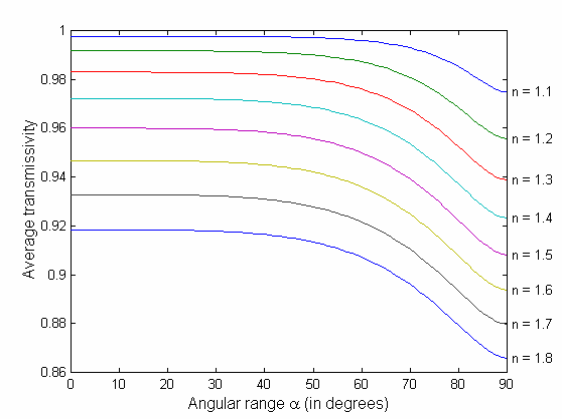

Figure 3.1.4. Average transmissivity of a plane dielectric surface for different values of the refractive index over the angular range α measured from the surface.

Finally, when the light is incident from opposite directions, i.e., from the material with the higher refractive index, Stern (1964) has shown that:

$$t_{av}(\alpha,n,1)=n^{-2}t_{av}(\alpha,1,n) \qquad [3.1.10]$$

As a consequence in [3.1.1] and [3.1.2], the reflectivities r_{ij} and transmissivities t_{ij} can be written: $r_{12}=1-t_{12}$, $r_{21}=1-t_{21}$, $t_{12}=t_{av}(\alpha,1,n)$, and $t_{21}=n^{-2}t_{av}(90,1,n)$ according to [3.1.10].

b) Transmission of light through the medium

Next, consider an energetic flux Φ (in Watts) being propagated in a semi-transparent plate with an incident angle of $\theta_i = \theta$. The medium is characterized by its absorption coefficient k (in m^{-1}) which is here assumed to be constant in the medium. This flux becomes Φ+dΦ at x+dx.

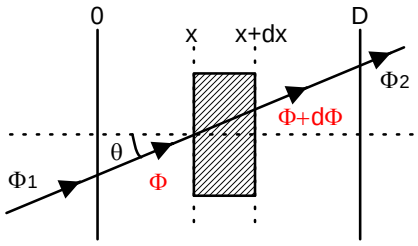

Figure 3.1.5. Transfer of radiation through a plate of thickness D.

$$d\Phi = -k\Phi dx \qquad [3.1.11]$$

Integrating [3.1.11] over the whole thickness of the layer, we have the attenuation factor of the medium (see the fundamental Beer-Lambert law):

$$\tau(\theta, D) = \frac{\Phi_2}{\Phi_1} = \exp\left(-\frac{kD}{\cos\theta}\right) \qquad [3.1.12]$$

Equation [3.1.12] can be written for any distance x:

$$\tau(\theta, x) = \exp\left(-\frac{kx}{\cos\theta}\right) \qquad [3.1.13]$$

The transmission τ for isotropic light passing through the plate is obtained by straightforward integration of [3.1.13] over the hemisphere:

$$\tau(x) = \frac{\int_0^{2\pi} d\varphi \int_0^{\pi/2} \tau(\theta, x)\cos\theta\sin\theta d\theta}{\int_0^{2\pi} d\varphi \int_0^{\pi/2} \cos\theta\sin\theta d\theta} = (1-kx)\exp(-kx) + k^2x^2\Gamma(0, kx) \qquad [3.1.14]$$

Where Γ(a,x) is the "upper" incomplete gamma function, not to be confused with the "lower" incomplete gamma function noted γ(a,x). They are given by:

$$\Gamma(a,x) = \int_x^{\infty} t^{a-1}e^{-t}dt \text{ and } \gamma(a,x) = \int_0^{x} t^{a-1}e^{-t}dt \qquad [3.1.15]$$

By definition their sum satisfies:

$$\gamma(a,x)+\Gamma(a,x)=\int_0^x t^{a-1}e^{-t}dt+\int_x^\infty t^{a-1}e^{-t}dt=\int_0^\infty t^{a-1}e^{-t}dt=\Gamma(a)$$
$$\Rightarrow \frac{\gamma(a,x)}{\Gamma(a)}+\frac{\Gamma(a,x)}{\Gamma(a)}=1\Rightarrow P(a,x)+Q(a,x)=1 \qquad [3.1.16]$$

where P(a,x) and Q(a,x) are the regularized "lower" and "upper" incomplete gamma functions. [Since the incomplete gamma function defined in Matlab is P(a,x), one has to be very careful with the definitions!] Finally, in the particular case when a = 0, Γ(a,x) is closely related to the exponential integral [which will be used in the Matlab code]:

$$\Gamma(0,x)=\int_x^\infty \frac{e^{-t}}{t}dt \qquad [3.1.17]$$

The differentiation and integration of Γ(0,x) are well known:

$$\frac{d\Gamma(0,x)}{dx}=-\frac{e^{-x}}{x} \quad \text{and} \quad \frac{d\Gamma(0,kx)}{dx}=-\frac{e^{-kx}}{x} \qquad [3.1.18]$$

$$\int\Gamma(0,x)=x\Gamma(0,x)-e^{-x} \quad \text{and} \quad \int\Gamma(0,kx)=x\Gamma(0,kx)-\frac{e^{-kx}}{k} \qquad [3.1.19]$$

Finally, the absorption coefficient k which varies as a function of the wavelength contains contributions from all of the individual leaf biochemical constituents, i.e., chlorophyll, water and dry matter:

$$k(\lambda)=\sum_{i=1}^{n}k_i(\lambda)\times C_i \qquad [3.1.20]$$

where the C_i are the concentrations of the leaf absorbers in the elementary layer and $k_i(\lambda)$ are the associated specific absorption coefficients. The latter, which are assumed to be invariable from one leaf to another, have been recently recalibrated on the basis of experimental data acquired in Angers (France) in June 2003. They are provided with a 1 nm spectral resolution.

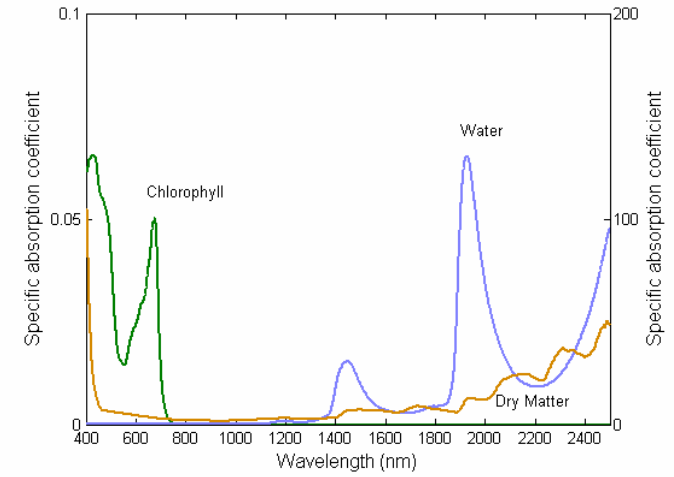

Figure 3.1.6. Specific absorption coefficients of chlorophyll a+b (left scale), water and dry matter (right scale) as used in the PROSPECT model.

3.1.3. Radiative transfer through a pile of plates: The *generalized plate model*

Plant leaves are not compact but present a wide range of anatomical structures which depend on the species (Figure 3.1.7). Variation in internal leaf structure has been a source of fascination for more than a century.

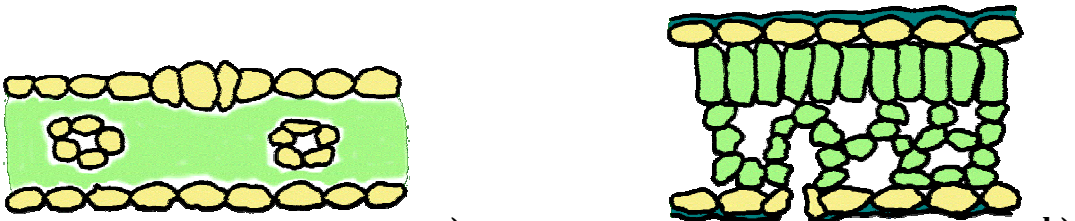

Figure 3.1.7. Schematic representation of a) Monocot and b) Dicot leaves.

As related by Allen et al. (1970), since plant leaves cannot be described as a unique compact layer, the *plate model* detailed above is not suited to simulating leaf optical properties. The *generalized plate model* which consists in stacking elementary plates has been proposed to account for the development of intercellular spaces in the leaf mesophyll. The leaf is conceptually subdivided into N homogeneous compact plates separated by N–1 air spaces (Figure 3.1.1). Such a system which has been solved for reflectance and transmittance many years ago by Stokes (1862) gave rise to an abundant literature (see for instance Gronwall, 1926; Benford, 1946; Tuckerman, 1947; Olf, 1988; Jacquemoud, 1992; Dahm and Dahm, 1999). The discrete approach can be extended to a continuous one where N need not be an integer.

a) Stokes' approach

Stokes (1862) contemplates a set of N = m + n plates and obtains the reflectance R(m+n) and the transmittance T(m+n) of this set in terms of the reflectances and transmittances of the two subsets consisting of m and n plates. The radiation flux which strikes the m plates from above is partially reflected and partially transmitted. The fraction T(m) falls on the n plates, the fraction T(m)R(n) is reflected, and the fraction T(m)T(n) transmitted. The fraction T(m)R(n) falls from beneath on the m plates, the new fraction T(m)R(n)T(m) being transmitted and the fraction T(m)R(n)R(m) reflected, etc., as indicated in Figure 3.1.8.

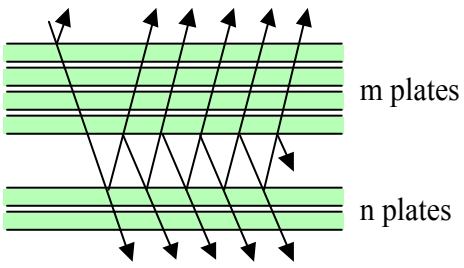

Figure 3.1.8. Pile of N = m + n plates.

By summing all the reflected and transmitted fractions, we obtain two geometrical series:

$$R(m+n) = R(m) + T(m)R(n)T(m) + T(m)R(n)R(m)R(n)T(m) + \ldots = R(m) + \frac{T(m)^2 R(n)}{1 - R(m)R(n)} \qquad [3.1.21]$$

$$T(m+n) = T(m)T(n) + T(m)R(n)R(m)T(n) + \ldots = \frac{T(m)T(n)}{1 - R(m)R(n)} \qquad [3.1.22]$$

To solve that system, Stokes first proceeded to show that the following expression is constant:

$$\frac{1 + R(m)^2 - T(m)^2}{R(m)} = \frac{1 + R(n)^2 - T(n)^2}{R(n)} = 2\cos\alpha \qquad [3.1.23]$$

For convenience, he denoted this invariant by 2 cosα and solved [3.1.23] for T^2 to obtain a simple expression for the transmittance in terms of the reflectance and, with it, to eliminate T in [3.1.22].

b) Olf's approach

For the N pile of plates, we wish to know the radiant fluxes i(ν) and j(ν), where ν is an arbitrary interlayer space number defined in Figure 3.1.9 and where i and j are the radiant fluxes per unit area of plate surface directed, respectively, downward and upward.

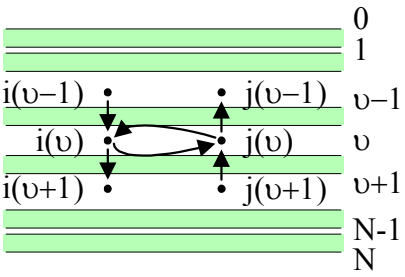

Figure 3.1.9. Pile of N plates. The plate count starts with 1 and the space count starts with 0.

We can state that:

$$\begin{cases} i(\upsilon) = T \times i(\upsilon - 1) + R \times j(\upsilon) \\ j(\upsilon) = T \times j(\upsilon + 1) + R \times i(\upsilon) \end{cases} \Leftrightarrow \begin{cases} i(\upsilon) = T \times i(\upsilon - 1) + R \times j(\upsilon) \\ j(\upsilon - 1) = T \times j(\upsilon) + R \times i(\upsilon - 1) \end{cases} \qquad [3.1.24]$$

We view these conditions as a system of two linear difference equations with constant coefficients R and T. In the particular case where N = 2, we solve [3.1.24] for ν = 1 and ν = 2:

$$\begin{cases} i(1) = T \times i(0) + R \times j(1) \\ j(0) = T \times j(1) + R \times i(0) \end{cases} \Rightarrow \begin{cases} T \times i(0) = i(1) - R \times j(1) \\ R \times i(0) - j(0) = T \times j(1) \end{cases} \Rightarrow \begin{bmatrix} i(0) \\ j(0) \end{bmatrix} = \frac{1}{T} \begin{bmatrix} 1 & -R \\ R & R^2 - T^2 \end{bmatrix} \begin{bmatrix} i(1) \\ j(1) \end{bmatrix} \qquad [3.1.25]$$

and

$$\begin{bmatrix} i(1) \\ j(1) \end{bmatrix} = \frac{1}{T}\begin{bmatrix} 1 & -R \\ R & R^2 - T^2 \end{bmatrix}\begin{bmatrix} i(2) \\ j(2) \end{bmatrix} \Rightarrow \begin{bmatrix} i(0) \\ j(0) \end{bmatrix} = \frac{1}{T^2}\begin{bmatrix} 1 & -R \\ R & R^2 - T^2 \end{bmatrix}^2\begin{bmatrix} i(2) \\ j(2) \end{bmatrix} \quad [3.1.26]$$

By setting i(0) = 1, j(0) = R_2, i(2) = T_2 and j(2) = 0 we obtain Equations [3.1.1] and [3.1.2] for homogeneous plates. Olf (1988) introduces the operation of displacement E with the fundamental property that E × i(ν) = i(ν+1) and E × j(ν) = j(ν+1), and solves Equation [3.1.26] with the theory of difference equations.

c) Jacquemoud's approach

In order to take into account the anisotropic structure of the incident beam ($\alpha = 60°$) impinging on the top of the pile, the Stokes system has been slightly modified by separating the first plate from the N–1 other ones (Figure 3.1.10a): The reflectance and the transmittance are $R_\alpha(1)$ and $T_\alpha(1)$, respectively, for the first plate and $R_{90}(N-1)$ and $T_{90}(N-1)$, respectively, for the N–1 other ones because the light flux is assumed to be isotropic inside the leaf.

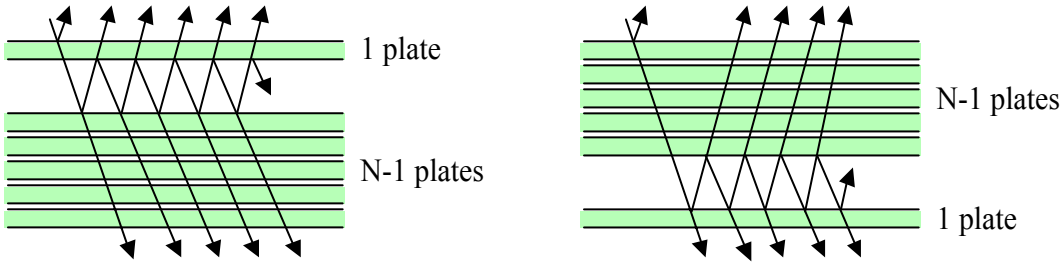

Figure 3.1.10. Pile of N plates a) 1 and N–1 b) N–1 and 1.

The reflectance (Equation [3.1.21]) and the transmittance (Equation [3.1.22]) become:

$$\begin{cases} R_\alpha(N) = R_\alpha(1) + T_\alpha(1)R_{90}(N-1)T_{90}(1) + T_\alpha(1)R_{90}(N-1)R_{90}(1)R_{90}(N-1)T_{90}(1) + \ldots \\ \qquad = R_\alpha(1) + \dfrac{T_\alpha(1)T_{90}(1)R_{90}(N-1)}{1 - R_{90}(1)R_{90}(N-1)} \\ T_\alpha(N) = T_\alpha(1)T_{90}(N-1) + T_\alpha(1)R_{90}(N-1)R_{90}(1)T_{90}(N-1) + \ldots \\ \qquad = \dfrac{T_\alpha(1)T_{90}(N-1)}{1 - R_{90}(1)R_{90}(N-1)} \end{cases} \quad [3.1.27]$$

If we now consider N–1 layers overlaying 1 layer (Figure 3.1.10b), the reflectance and the transmittance are $R_\alpha(N-1)$ and $T_\alpha(N-1)$, respectively, for the first plates and $R_{90}(1)$ and $T_{90}(1)$, respectively, for the other one.

$$\begin{cases} R_\alpha(N) = R_\alpha(N-1) + T_\alpha(N-1)R_{90}(1)T_{90}(N-1) + T_\alpha(N-1)R_{90}(1)R_{90}(N-1)R_{90}(1)T_{90}(N-1) + \ldots \\ \qquad = R_\alpha(N-1) + \dfrac{T_\alpha(N-1)T_{90}(N-1)R_{90}(1)}{1 - R_{90}(1)R_{90}(N-1)} \\ T_\alpha(N) = T_\alpha(N-1)T_{90}(1) + T_\alpha(N-1)R_{90}(1)R_{90}(N-1)T_{90}(1) + \ldots \\ \qquad = \dfrac{T_\alpha(N-1)T_{90}(1)}{1 - R_{90}(1)R_{90}(N-1)} \end{cases} \quad [3.1.28]$$

The solution of this system of recursive series has been given by Jacquemoud (1992):

$$R_\alpha(N) = \frac{R_\alpha(1)\left(ab^{N-1} - a^{-1}b^{1-N}\right) + \left(T_\alpha(1)T_{90}(1) - R_\alpha(1)R_{90}(1)\right)\left(b^{N-1} - b^{1-N}\right)}{ab^{N-1} - a^{-1}b^{1-N} - R_{90}(1)\left(b^{N-1} - b^{1-N}\right)} \quad [3.1.29]$$

$$T_\alpha(N) = \frac{T_\alpha(1)\left(a - a^{-1}\right)}{ab^{N-1} - a^{-1}b^{1-N} - R_{90}(1)\left(b^{N-1} - b^{1-N}\right)} \quad [3.1.30]$$

where $a = \frac{1 + R_{90}(1)^2 - T_{90}(1)^2 + \sqrt{\delta}}{2R_{90}(1)}$, $b = \sqrt{\frac{\beta\left(a - R_{90}(1)\right)}{a\left(\beta - R_{90}(1)\right)}}$, $\beta = \frac{1 + R_{90}(1)^2 - T_{90}(1)^2 - \sqrt{\delta}}{2R_{90}(1)}$, and

$$\delta = \sqrt{\left(R_{90}(1)^2 - T_{90}(1)^2 - 1\right)^2 - 4R_{90}(1)^2}\ .$$

3.2. Development and coding of leaf fluorescence model

We propose here an elegant and powerful way to calculate the fluorescence, first of an elementary layer, and then of a pile of N layers.

3.2.1. Fluorescence of an elementary layer

In that algebraic method, we consider fluxes as a network.

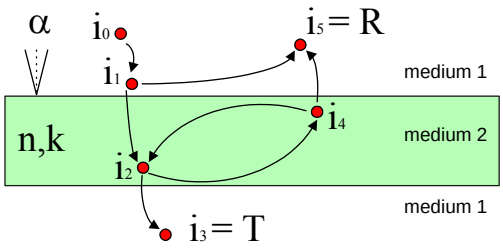

Figure 3.2.1. Flux network produced by a semi-transparent plate with rough surfaces.

The thickness of the plate D is set to unity (D = 1). We obtain a system of linear equations in i_0, i_1, i_2, i_3, i_4 and i_5 which is easily solved. The reflectance corresponds to i_5 and the transmittance to i_3:

$$\begin{cases} i_0 = 1 \\ i_1 = i_0 \\ i_2 = i_1\, t_{12,s}\, \tau_s(1) + i_4\, r_{21,s}\, \tau \\ i_3 = i_2\, t_{21,s} \\ i_4 = i_2\, r_{21,s}\, \tau_s(1) \\ i_5 = i_1\, r_{12,s} + i_4\, t_{21,s} \end{cases} \Rightarrow \begin{cases} i_5 = R = r_{12,s} + \dfrac{t_{12,s}\, t_{21,s}\, r_{21,s}\, \tau_s^2(1)}{1 - r_{21,s}^2\, \tau_s^2(1)} \\ i_3 = T = \dfrac{t_{12,s}\, t_{21,s}\, \tau_s(1)}{1 - r_{21,s}^2\, \tau_s^2(1)} \end{cases} \quad [3.2.1]$$

where $t_{ij,s}$ and $r_{ij,s}$ are the average transmissivity and reflectivity ($r_{ij,s} = 1 - t_{ij,s}$) between media i and j, respectively, and $\tau_s(1)$ is the transmission of the plate for isotropic light. The subscript

s indicates the source (excitation) wavelength. In order to calculate the fluorescence fluxes, it is necessary to know the excitation fluxes at any position within the plate. Consider an infinitesimal layer of thickness dx, parallel to the surface, at position x (Figure 3.2.2).

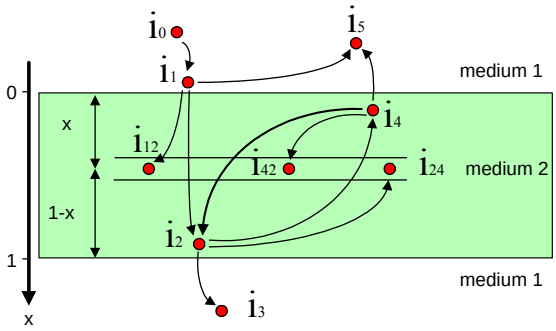

Figure 3.2.2. Flux network showing the excitation fluxes at position x.

We can set a system of linear equations similar to [3.2.1]:

$$\begin{aligned} &i_0 = 1,\ i_1 = i_0,\ i_2 = i_1\, t_{12,s}\, \tau_s(1) + i_4\, r_{21,s}\, \tau_s(1),\ i_3 = i_2\, t_{21,s},\ i_4 = i_2\, r_{21,s}\, \tau_s(1),\ i_5 = i_1\, r_{12,s} + i_4\, t_{21,s} \\ &i_{12} = i_1\, t_{12,s}\, \tau_s(x),\ i_{24} = i_2\, r_{21,s}\, \tau_s(1-x),\ i_{42} = i_4\, r_{21,s}\, \tau_s(x) \end{aligned} \qquad [3.2.2]$$

whose solution provides the same expressions for i_5 (reflectance) and i_3 (transmittance), and the following values for i_{12}, i_{24} and i_{42} at position x:

$$i_{12}(x) = t_{12,s}\, \tau_s(x) \quad \text{and} \quad i_{24}(x) = \frac{t_{12,s}\, r_{21,s}\, \tau_s(1)\, \tau_s(1-x)}{1 - r_{21,s}^2\, \tau_s^2(1)} \quad \text{and} \quad i_{42}(x) = \frac{t_{12,s}\, r_{21,s}^2\, \tau_s^2(1)\, \tau_s(x)}{1 - r_{21,s}^2\, \tau_s^2(1)} \qquad [3.2.3]$$

The total flux at position x is given by $i_{12}(x) + i_{24}(x) + i_{42}(x)$. $i_{12}(x)$ and $i_{42}(x)$ are propagating towards positive values of x, while $i_{24}(x)$ is propagating towards negative value of x. The absorbed flux in the medium between the x level and the x+dx level is calculated by considering the difference of a given flux along the direction of propagation between these two levels. Thus, we have for $i_{12}(x)$ and $i_{42}(x)$:

$$\begin{cases} i_{12}(x+dx) = i_{12}(x) - a_{12}(x)dx \\ i_{42}(x+dx) = i_{42}(x) - a_{42}(x)dx \end{cases} \qquad [3.2.4]$$

and for $i_{24}(x)$:

$$i_{24}(x+dx) = i_{24}(x) + a_{24}(x)dx \qquad [3.2.5]$$

Then, by coming back to the definition of the derivative of a function, we can link the absorbed flux with the derivative of the fluxes:

$$a(x) = \pm\frac{i(x+dx) - i(x)}{dx} = \pm di(x) \qquad [3.2.6]$$

So the amount of flux absorbed along dx is:

$$a(x)dx = \left(a_{12}(x) + a_{24}(x) + a_{42}(x)\right)dx = -\left(di_{12}(x) - di_{24}(x) + di_{42}(x)\right)dx$$
$$= -t_{12,s}\, d\tau_s(x) + \frac{t_{12,s}\, r_{21,s}\, \tau_s(1)\, d\tau_s(1-x)}{1 - r_{21,s}^2\, \tau_s^2(1)} - \frac{t_{12,s}\, r_{21,s}^2\, \tau_s^2(1)\, d\tau_s(x)}{1 - r_{21,s}^2\, \tau_s^2(1)} \qquad [3.2.7]$$

The fraction of absorbed flux by the photosynthetic pigments, namely the chlorophyll a+b in the PROSPECT model, can produce fluorescence emission. To calculate the shape and amount of emitted light which is wavelength dependent, we have to introduce a source function ϕ. The latter is a key component of the study and will be detailed later on in this chapter.

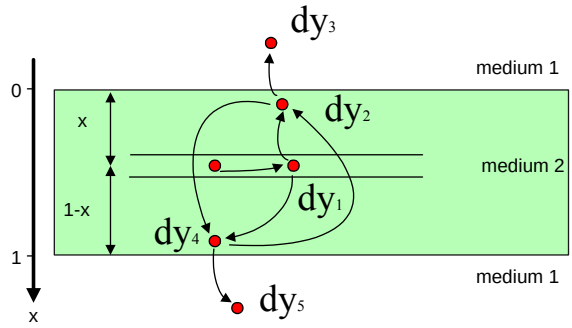

Figure 3.2.3. Flux network showing the emission flux at position x.

The network in Figure 3.2.3 corresponds to the following set of linear equations:

$$\begin{cases} dy_1(x) = a(x)\phi dx \\ dy_2(x) = \frac{1}{2} dy_1(x)\tau_m(x) + dy_4(x) r_{21,m}\tau_m(1) \\ dy_3(x) = dy_2(x) t_{21,m} \\ dy_4(x) = \frac{1}{2} dy_1(x)\tau_m(1-x) + dy_2(x) r_{21,m}\tau_m(1) \\ dy_5(x) = dy_4(x) t_{21,m} \end{cases} \qquad [3.2.8]$$

where the subscript *m* indicates the wavelength of fluorescence emission. The photons are equally distributed between the upward and downward directions in the infinitesimal layer because emission of fluorescence occurs isotropically. The system [3.2.8] can be easily solved to provide the upward dy_3 and downward dy_5 fluorescence fluxes in the infinitesimal layer dx along the leaf depth:

$$\begin{cases} dy_3(x) = -\frac{t_{12,s} t_{21,m} \phi_m}{2} \frac{\left(r_{21,m}\tau_m(1)\tau_m(1-x) + \tau_m(x)\right)\left(r_{21,s}\tau_s(1)d\tau_s(1-x) + d\tau_s(x)\right)}{\left(1 - r_{21,s}^2\tau_s^2(1)\right)\left(1 - r_{21,m}^2\tau_m^2(1)\right)} \\ dy_5(x) = -\frac{t_{12,s} t_{21,m} \phi_m}{2} \frac{\left(r_{21,m}\tau_m(1)\tau_m(x) + \tau_m(1-x)\right)\left(r_{21,s}\tau_s(1)d\tau_s(1-x) + d\tau_s(x)\right)}{\left(1 - r_{21,s}^2\tau_s^2(1)\right)\left(1 - r_{21,m}^2\tau_m^2(1)\right)} \end{cases} \qquad [3.2.9]$$

with - $t_{ij,s}$ and $t_{ij,m}$ the average transmissivities between media i and j at the excitation and emission wavelengths, respectively,
- $r_{ij,x}$ and $r_{ij,m}$ the average reflectivities between media i and j at the excitation and emission wavelengths, respectively ($r_{ij,x} = 1 - t_{ij,x}$ and $r_{ij,m} = 1 - t_{ij,m}$),

- ϕ the fluorescence source,
- $\tau_s(x)$ and $\tau_m(x)$ the transmission of the plate at position x for isotropic light at the excitation and emission wavelengths, respectively,
- and $d\tau_s(x)$ the differential of $\tau_s(x)$.

Equation [3.1.14] gives the expression of $\tau_s(x)$ and $\tau_m(x)$ as a function of x. The derivation rules of the incomplete gamma function in [3.1.18] allow the calculation of $d\tau_s(x)$ as a function of x:

$$\begin{cases} \tau_s(x) = (1-k_s x)\mathrm{e}^{-k_s x} + k_s^2 x^2 \Gamma(0, k_s x) \text{ and } d\tau_s(x) = \left(2k_s^2 x\Gamma(0,k_s x) - 2k_s e^{-k_s x}\right)dx \\ \tau_m(x) = (1-k_m x)\mathrm{e}^{-k_m x} + k_m^2 x^2 \Gamma(0, k_m x) \end{cases} \quad [3.2.10]$$

where k_s and k_m are the absorption coefficients at the excitation and emission wavelengths, respectively. Since only chlorophyll participates in the chlorophyll fluorescence process, but since the emitted light can be reabsorbed by other leaf biochemical constituents, their expressions are slightly different:

$$\begin{cases} k_s = (k_{ab} \times C_{ab})/N \\ k_m = (k_{ab} \times C_{ab} + k_w \times C_w + k_m \times C_m)/N \end{cases} \quad [3.2.11]$$

where C_{ab}, C_w and C_m are the total concentrations of chlorophyll, water and dry matter expressed in µg cm^{-2}, cm, and g cm^{-2}, k_{ab}, k_w and k_m are the corresponding specific absorption coefficients provided by the PROSPECT model (Figure 3.1.6).

The upward and downward fluorescence signals of the entire plate, $F_u(1)$ and $F_d(1)$, are then calculated by integrating dy_3 and dy_5, respectively, from x = 0 to x = 1:

$$\begin{cases} F_u(1) = \int_0^1 dy_3(x) = \int_0^1 -\phi \dfrac{t_{12,s}t_{21,m}}{2} \dfrac{\left(r_{21,m}\tau_m(1)\tau_m(1-x) + \tau_m(x)\right)\left(r_{21,s}\tau_s(1)d\tau_s(1-x) + d\tau_s(x)\right)}{\left(1-r_{21,s}^2\tau_s^2(1)\right)\left(1-r_{21,m}^2\tau_m^2(1)\right)} \\ F_d(1) = \int_0^1 dy_5(x) = \int_0^1 -\phi \dfrac{t_{12,s}t_{21,m}}{2} \dfrac{\left(r_{21,m}\tau_m(1)\tau_m(x) + \tau_m(1-x)\right)\left(r_{21,s}\tau_s(1)d\tau_s(1-x) + d\tau_s(x)\right)}{\left(1-r_{21,s}^2\tau_s^2(1)\right)\left(1-r_{21,m}^2\tau_m^2(1)\right)} \end{cases} \quad [3.2.12]$$

By rearranging [3.2.12] we obtain:

$$\begin{cases} F_u(1) = cy\left(r_{21,s}r_{21,m}\tau_s(1)\tau_m(1)\int_0^1\theta_1(x)dx + r_{21,s}\tau_s(1)\int_0^1\theta_2(x)dx + r_{21,m}\tau_m(1)\int_0^1\theta_3(x)dx + \int_0^1\theta_4(x)dx\right) \\ F_d(1) = cy\left(r_{21,s}\tau_s(1)\int_0^1\theta_1(x)dx + r_{21,s}r_{21,m}\tau_s(1)\tau_m(1)\int_0^1\theta_2(x)dx + \int_0^1\theta_3(x)dx + r_{21,m}\tau_m(1)\int_0^1\theta_4(x)dx\right) \end{cases} \quad [3.2.13]$$

With *cy* a term independent of x:

$$cy = -\phi \frac{t_{12,s}t_{21,m}}{2\left(1-r_{21,s}^2\tau_s^2(1)\right)\left(1-r_{21,m}^2\tau_m^2(1)\right)} \quad [3.2.14]$$

and $\theta_1(x)$, $\theta_2(x)$, $\theta_3(x)$, and $\theta_4(x)$ four functions of x defined by:

$$\begin{cases} \theta_1(x) = \tau_m(1-x)\, d\tau_s(1-x) \\ \theta_2(x) = \tau_m(x)\, d\tau_s(1-x) \\ \theta_3(x) = \tau_m(1-x)\, d\tau_s(x) \\ \theta_4(x) = \tau_m(x)\, d\tau_s(x) \end{cases} \qquad [3.2.15]$$

If one substitutes x for x−1 into equations [3.2.15], it can be seen that the integral from 0 to 1 of $\theta_1(x)dx$ equals the integral of $\theta_4(x)dx$, and that the integral of $\theta_2(x)dx$ equals the integral of $\theta_3(x)dx$. As a consequence, the problem is simplified.

a) Integration of $\theta_4(x)$

By combining [3.2.10] and [3.2.15] $\theta_4(x)$ can be rewritten:

$$\theta_4(x) = \tau_m(x)\, d\tau_s(x) = \left[(1-k_m x)\mathrm{e}^{-k_m x} + k_m^2 x^2 \Gamma(0, k_m x)\right] \times \left[2k_s^2 x \Gamma(0, k_s x) - 2k_s\, \mathrm{e}^{-k_s x}\right] \qquad [3.2.16]$$

The function is continuous for all x between 0 and 1, and its boundary values are:

$$\lim_{x\to 0} \theta_4(x) = -2k_s \qquad [3.2.17]$$

$$\text{and } \lim_{x\to 1} \theta_4(x) = 2\mathrm{e}^{-k_s-k_m}\, k_s \left(-1 + \mathrm{e}^{k_s}\, k_s \Gamma(0, k_s)\right)\left(1 - k_m + \mathrm{e}^{k_m}\, k_m^2 \Gamma(0, k_m)\right) \qquad [3.2.18]$$

However, we did not succeed in performing a straightforward analytical integration of [3.2.16]. Since we know that:

$$\int_0^1 \theta_4(x)\, dx = \left[\Theta_4(x)\right]_0^1 = \Theta_4(1) - \Theta_4(0) \qquad [3.2.19]$$

We tried to find the primitive $\Theta_4(x)$ of $\theta_4(x)$:

$$\Theta_4(x) = \frac{e^{-(k_s+k_m)x}}{2k_s^2 k_m^2} \begin{bmatrix} k_s k_m \left(2k_s^2 + k_s k_m (1-k_s x) + k_m^2 (k_s x + 1)(k_s x - 2)\right) \\ -e^{k_s x} k_s^4 \Gamma(0, k_s x)\left(2 + 2k_m x - k_m^2 x^2 + k_m^3 x^3\right) + e^{k_m x} k_m^4 \Gamma(0, k_m x)\left(2 + 2k_s x + k_s^2 x^2 - k_s^3 x^3\right) \\ +e^{(k_s+k_m)x} k_s^4 k_m^4 x^4 \Gamma(0, k_s x)\Gamma(0, k_m x) + 2e^{(k_s+k_m)x}\left(k_s^4 - k_m^4\right)\Gamma(0, (k_s + k_m)x) \end{bmatrix} \qquad [3.2.20]$$

When x = 1, [3.2.20] reduces to:

$$\Theta_4(1) = \frac{e^{-(k_s+k_m)}}{2k_s^2 k_m^2} \begin{bmatrix} k_s k_m \left(2k_s^2 + k_s k_m (1-k_s) + k_m^2 (k_s + 1)(k_s - 2)\right) \\ -e^{k_s} k_s^4 \Gamma(0, k_s)\left(2 + 2k_m - k_m^2 + k_m^3\right) + e^{k_m} k_m^4 \Gamma(0, k_m)\left(2 + 2k_s + k_s^2 - k_s^3\right) \\ +e^{(k_s+k_m)} k_s^4 k_m^4 \Gamma(0, k_s)\Gamma(0, k_m) + 2e^{(k_s+k_m)}\left(k_s^4 - k_m^4\right)\Gamma(0, k_s + k_m) \end{bmatrix} \qquad [3.2.21]$$

When x = 0, [3.2.20] is indeterminate. We have developed $\Theta_4(x)$ into a Taylor series about x = 0 up to order 1:

$$\Theta_4(x) = \frac{k_s k_m\left(2k_s^2 + k_s k_m - 2k_m^2\right) + 2k_s^4 \ln(k_s) - 2k_m^4 \ln(k_m) - 2\left(k_s^4 - k_m^4\right)\ln(k_s + k_m)}{2k_s^2 k_m^2} - 2k_s x + o(x)^2 \qquad [3.2.22]$$

and then:

$$\lim_{x\to 0}\Theta_4(x) = \frac{k_s k_m\left(2k_s^2 + k_s k_m - 2k_m^2\right) + 2k_s^4 \ln(k_s) - 2k_m^4 \ln(k_m) - 2\left(k_s^4 - k_m^4\right)\ln(k_s + k_m)}{2k_s^2 k_m^2} \qquad [3.2.23]$$

[3.2.19] can finally be written as follows:

$$\int_0^1 \theta_4(x)\,dx = \Theta_4(1) - \lim_{x\to 0}\Theta_4(x) \qquad [3.2.24]$$

b) Integration of $\theta_3(x)$

By combining [3.2.10] and [3.2.15], $\theta_3(x)$ can be rewritten:

$$\begin{aligned}\theta_3(x) &= \tau_m(1-x)\,d\tau_s(x) \\ &= \left[\left(1 - k_m(1-x)\right)e^{-k_m(1-x)} + k_m^2(1-x)^2\,\Gamma\left(0, k_m(1-x)\right)\right] \times \left[2k_s^2 x\Gamma(0, k_s x) - 2k_s\, e^{-k_s x}\right]\end{aligned} \qquad [3.2.25]$$

The function is continuous for all x between 0 and 1, and its boundary values are:

$$\lim_{x\to 0}\theta_3(x) = -2e^{-k_m}\,k_s\left(1 - k_m + e^{k_m}\,k_m^2\Gamma(0, k_m)\right) \qquad [3.2.26]$$

$$\text{and } \lim_{x\to 1}\theta_3(x) = 2e^{-k_s}\,k_s\left(-1 + e^{k_s}\,k_s\Gamma(0, k_s)\right) \qquad [3.2.27]$$

Once again, we did not succeed in performing a straightforward analytical integration of [3.2.25] using Mathematica, nor in finding a primitive $\Theta_3(x)$, although $\theta_3(x)$ can be numerically integrated. We tried different methods which all failed. In order to solve the problem, we have contacted mathematicians but it seems that we are confronted with an integral which does not have an "easy" analytical form, if it exists! The difficulty comes from the integral:

$$\int_0^1 x\Gamma(0, k_s x)\Gamma\left(0, k_m(1-x)\right)dx \qquad [3.2.28]$$

which contains a product of two incomplete gamma functions and cannot be calculated. The only way to surmount this problem was to integrate $\theta_3(x)$ numerically for a wide range of k_s and k_m values, in order to build a look-up table, and to compute values between ones that are tabulated using the surrounding points. Parameters k_s or k_m , which are calculated by [3.2.11], range between 0 and 10 for natural variation of leaf parameters ($N \in [1,3]$, $C_{ab} \in [0,130]$ μg cm^{-2}, $C_w \in [0.004, 0.04]$ cm, and $C_m \in [0.002, 0.0165]$ g cm^{-2}). Since the numerical integration fails for $k_s = 0$ and for $k_m = 0$, we have considered these two particular cases.

$$\lim_{k_x\to 0}\theta_3(x) = 0 \qquad [3.2.29]$$

$$\lim_{k_m \to 0} \theta_3(x) = 2e^{-k_s x} k_s \left(e^{k_s x} k_s x \Gamma(0, k_s x) - 1 \right) \qquad [3.2.30]$$

Let $I\theta_3(k_s,k_m)$ be the integral of $\theta_3(x)$ from 0 to 1 for any values of k_x and k_m. [3.2.29] implies that $I\theta_3(0,k_m) = 0$, $\forall\ k_m \neq 0$. We can integrate [3.2.30] analytically:

$$\begin{aligned} I\theta_3(k_s,0) &= \int_0^1 2e^{-k_s x} k_s \left(e^{k_s x} k_s x \Gamma(0, k_s x) - 1 \right) dx \\ &= \left[e^{-k_s x} \left(1 - k_s x + e^{k_s x} k_s^2 x^2 \Gamma(0, k_s x) \right) \right]_0^1 \\ &= e^{-k_s} \left(1 - k_s + e^{k_s} k_s^2 \Gamma(0, k_s) \right) - 1 \quad \forall k_s \neq 0 \end{aligned} \qquad [3.2.31]$$

One can see that $\lim_{k_m \to 0} I\theta_3(0,k_m) = 0$ and $\lim_{k_s \to 0} I\theta_3(k_s,0) = 0$.

Table 3.2.1. Variation domain of the function $I\theta_3(k_s,k_m)$.

$I\theta_3(k_s,k_m)$	$k_m = 0$	$k_m > 0$
$k_s = 0$	0	0
$k_s > 0$	$e^{-k_x} \left(1 - k_x + e^{k_x} k_x^2 \Gamma(0, k_x) \right) - 1$	Numerical integration

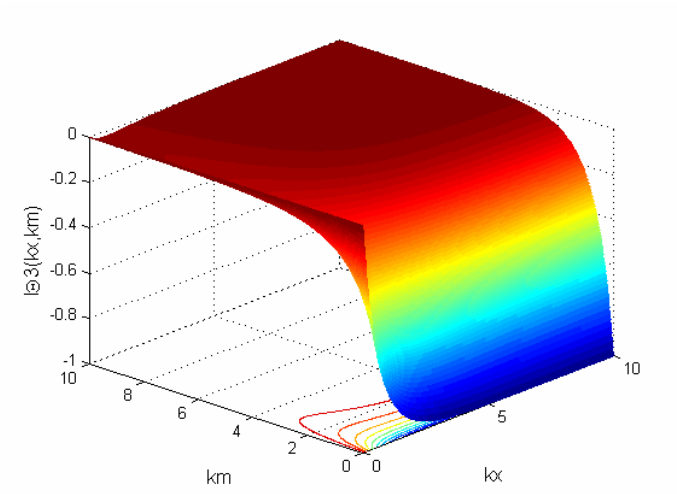

Figure 3.2.4. Surface response of $I\theta_3(k_s,k_m)$ as a function of k_s and k_m.

The two-dimensional data interpolation (look-up table) is then performed almost instantaneously for any matrices of k_x and k_m values.

3.2.2. Fluorescence of N layers

Let us consider a pile of N = m + n homogeneous plates (Figure 3.2.5) and, as seen earlier, a network of upward and downward fluxes, represented schematically by Figure 3.1.7. We obtain a system of five equations and solve it for the four unknows, i_1, i_2, j_0 and j_1.

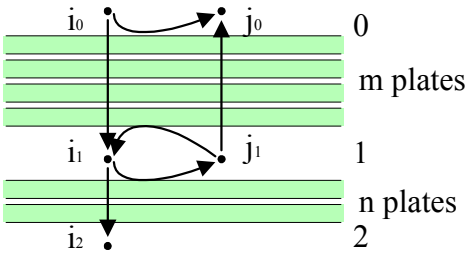

Figure 3.2.5. Pile of N = m + n plates.

$$\begin{cases} i_0 = 1 \\ i_1 = i_0\,T(m) + j_1\,R(m) \\ i_2 = i_1\,T(n) \\ j_1 = i_1\,R(n) \\ j_0 = i_0\,R(m) + j_1\,T(m) \end{cases} \Rightarrow \begin{cases} j_0 = R(m+n) = R(m) + \dfrac{T(m)^2\,R(n)}{1-R(m)R(n)} \\ i_2 = T(m+n) = \dfrac{T(m)T(n)}{1-R(m)R(n)} \\ i_1 = \dfrac{T(m)}{1-R(m)R(n)} \\ j_1 = \dfrac{T(m)R(n)}{1-R(m)R(n)} \end{cases} \qquad [3.2.32]$$

As noticed by Kortüm (1969), these equations, already derived earlier, have the same form as Equations [3.1.1] and [3.1.2] for the total reflectance and transmittance of a plane parallel plate. By setting $m = N-1$ and $n = 1$, or $m = 1$ and $n = N-1$, Equations [3.2.32] become:

$$\begin{cases} R(N) = R(N-1) + \dfrac{T(N-1)^2\,R(1)}{1-R(N-1)R(1)} = R(1) + \dfrac{T(1)^2\,R(N-1)}{1-R(N-1)R(1)} \\ T(N) = \dfrac{T(N-1)T(1)}{1-R(N-1)R(1)} \end{cases} \qquad [3.2.33]$$

In the case of an anisotropic incident beam ($\alpha = 60°$), Equations [3.2.32] become:

$$\begin{cases} i_0 = 1 \\ i_1 = i_0\,T_\alpha(m) + j_1\,R_{90}(m) \\ i_2 = i_1\,T_{90}(n) \\ j_1 = i_1\,R_{90}(n) \\ j_0 = i_0\,R_\alpha(m) + j_1\,T_{90}(m) \end{cases} \Rightarrow \begin{cases} j_0 = R_\alpha(m+n) = R_\alpha(m) + \dfrac{T_\alpha(m)T_{90}(m)R_{90}(n)}{1-R_{90}(m)R_{90}(n)} \\ i_2 = T_\alpha(m+n) = \dfrac{T_\alpha(m)T_{90}(n)}{1-R_{90}(m)R_{90}(n)} \\ i_1 = \dfrac{T_\alpha(m)}{1-R_{90}(m)R_{90}(n)} \\ j_1 = \dfrac{T_\alpha(m)R_{90}(n)}{1-R_{90}(m)R_{90}(n)} \end{cases} \qquad [3.2.34]$$

By setting $m = N-1$ and $n = 1$, we again find the results of Equations [3.1.23]. If we now add fluorescence in the system (Figure 3.2.6), one can write the flux equations for the fluorescence (those already developed in the system [3.2.32] are still valid), where $R_f(i)$ and

$T_f(i)$ are the diffuse ($\alpha = 90°$) reflectance and the transmittance of i plates at the wavelength of fluorescence emission (Equation [3.2.35]).

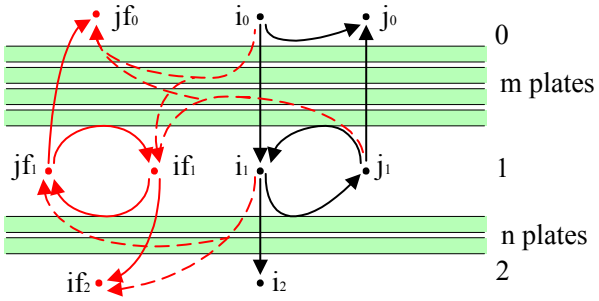

Figure 3.2.6. Fluorescence in a pile of $N = m + n$ plates.

$$\begin{cases} i_{f_1} = j_{f_1} \times R_f(m) + i_0 \times F_d(m) + j_1 \times F_u(m) \\ i_{f_2} = F_d(m+n) = i_{f_1} \times T_f(n) + i_1 \times F_d(n) \\ j_{f_0} = F_u(m+n) = j_{f_1} \times T_f(m) + j_1 \times F_d(m) + i_0 \times F_u(m) \\ j_{f_1} = i_{f_1} \times R_f(n) + i_1 \times F_u(n) \end{cases} \quad [3.2.35]$$

By solving the system of equations [3.2.35], replacing the terms i_0, i_1, j_1 by their expressions in [3.2.34], and simplifying we obtain:

$$\begin{cases} F_u(m+n) = F_u(m) + \dfrac{F_d(m)T_\alpha(m)R_{90}(n)}{1-R_{90}(m)R_{90}(n)} + \dfrac{F_d(m)T_f(m)R_f(n)}{1-R_f(m)R_f(n)} + \dfrac{T_f(m)T_\alpha(m)\left[F_u(n)+F_u(m)R_f(n)R_{90}(n)\right]}{\left[1-R_{90}(m)R_{90}(n)\right]\left[1-R_f(m)R_f(n)\right]} \\ F_d(m+n) = \dfrac{F_d(n)T_\alpha(m)}{1-R_{90}(m)R_{90}(n)} + \dfrac{F_d(m)T_f(n)}{1-R_f(m)R_f(n)} + \dfrac{T_f(n)T_\alpha(m)\left[F_u(n)R_f(m)+F_u(m)R_{90}(n)\right]}{\left[1-R_{90}(m)R_{90}(n)\right]\left[1-R_f(m)R_f(n)\right]} \end{cases} \quad [3.2.36]$$

By setting $m = N-1$ and $n = 1$, Equations [3.2.36] become:

$$\begin{cases} F_u(N) = F_u(N-1) + \dfrac{F_d(N-1)T_\alpha(N-1)R_{90}(1)}{1-R_{90}(N-1)R_{90}(1)} + \dfrac{F_d(N-1)T_f(N-1)R_f(1)}{1-R_f(N-1)R_f(1)} + \dfrac{T_f(N-1)T_\alpha(N-1)\left[F_u(1)+F_u(N-1)R_f(1)R_{90}(1)\right]}{\left[1-R_{90}(N-1)R_{90}(1)\right]\left[1-R_f(N-1)R_f(1)\right]} \\ F_d(N) = \dfrac{F_d(1)T_\alpha(N-1)}{1-R_{90}(N-1)R_{90}(1)} + \dfrac{F_d(N-1)T_f(1)}{1-R_f(N-1)R_f(1)} + \dfrac{T_f(1)T_\alpha(N-1)\left(F_u(1)R_f(N-1)+F_u(N-1)R_{90}(1)\right)}{\left[1-R_{90}(N-1)R_{90}(1)\right]\left[1-R_f(N-1)R_f(1)\right]} \end{cases} \quad [3.2.37]$$

Since the upward $F_u(1)$ and downward $F_d(1)$ fluorescence of a single layer have been calculated earlier (see Equation 3.2.12), it is possible to calculate the upward $F_u(N)$ and downward $F_d(N)$ fluorescence of 2, 3,…, N layers recursively. These values are stored in a three-dimensional matrix: the first dimension is the wavelength of excitation between, the second one the wavelength of emission, and the third one represents the five layers. The determination of the fluorescence for any real value of N amounts to "cutting a slice" in the matrix, i.e., to make a three-dimensional data interpolation (table lookup).

3.3. Spectral distribution of fluorescence emission

3.3.1 Present situation

The source function ϕ which gives rise to the fluorescence photons in Equation [3.2.8] has been generally studied at the leaf scale and related to the PSI and PSII fluorescence emission spectrum in the 680–740 nm spectral region. It is presented as the product of the quantum yield Φ (or fluorescence quantum efficiency or fluorescence yield) by the spectral distribution of fluorescence emission η(λ). Φ is the number of emitted photons divided by the number of absorbed photons in the whole photosynthetic active radiation (PAR). For a leaf, it ranges from 0% (no fluorescence) to a maximum of 10%, depending on the state of the leaf photosynthetic apparatus, but typical values are 3 to 5% (see Section 3.3.3c). η(λ) is more difficult to assess because its shape and level are difficult to measure experimentally (Durkin et al., 1994; Terjung, 1998). In SLOPE, Maier (2000) used the emission spectrum measured by Gitelson et al. (1998) for beech (*Fagus sylvatica* L.) and elm (*Ulmus minor*) leaves, in which re-absorption was assumed to be corrected. Maier recalculated the spectrum in order to have units of number of photons.

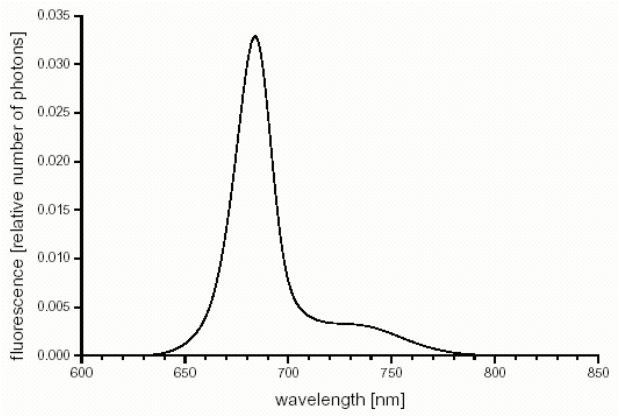

Figure 3.3.1. Chlorophyll fluorescence spectrum, taken from Gitelson et al. (1998) and recalculated to number of photons.

Zarco-Tejada et al. (2000a) used for η(λ) the function of Subhash and Mohanan (1997) who measured *in vivo* laser-induced chlorophyll fluorescence spectra on sunflower (*Helianthus annuus* L.) leaves and parameterized it mathematically as the sum of two Gaussian curves:

$$\eta(\lambda) = f_R \exp\left(\frac{-(\lambda-\lambda_L)^2}{a\Delta_L^2}\right) + \exp\left(\frac{-(\lambda-\lambda_H)^2}{a\Delta_H^2}\right) \qquad [3.3.1]$$

where f_R is the ratio of the fluorescence peak at λ_L relative to that at λ_H, Δ_L and Δ_H are the standard deviations (full-width at half maximum) of the two curves, and a is a constant set to 0.3607. The authors obtained the best results with two Gaussian curves centered on $\lambda_L \in$ [685–690 nm] and $\lambda_H \in$ [725–730 nm], with varying relative amplitudes. These peaks correspond to fluorescence maxima of the photosystems. Variations of P (see Equation [2.2.4]) for different values of photon fluorescence efficiency and a fixed fluorescence emission spectral distribution function are presented in Figure 3.3.2.

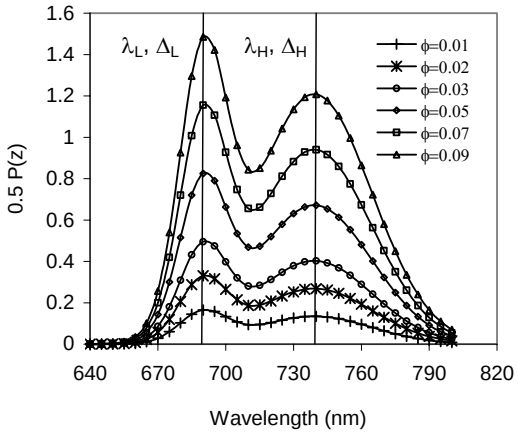

Figure 3.3.2. P(z) as a function of different values of Φ (0.01 – 0.09) for λ_L = 690 nm, λ_H = 735 nm, Δ_L = 25 nm, Δ_H = 80 nm, f_R = 1, and a = 0.3607 (after Zarco-Tejada et al., 2000a).

However, these Gaussian distributions which do not rely on a physical basis obviously do not account for re-absorption. We consequently decided to include a new source function ϕ.

3.3.2 Description of the source function

In the development of the leaf model, we solved the radiative transfer equations within the leaf considering that a fluorescence excitation was induced in each infinitesimal layer of thickness *dx*. We can reasonably liken this layer to a chloroplast or even a thylakoid which contains both photosystems I and II. To determine the excitation spectrum (Figure 3.3.3) for an emission at 760 nm, we used isolated thylakoids in solution. The quantum yield $\Phi = 4\ 10^{-5}$ obtained at the leaf level (see Section 3.4.2) for (λ_s,λ_m) = (633,758) nm was used to calibrate the intensity of the thylakoid excitation spectrum, because it is related to the lifetime of chlorophyll fluorescence which was proved to be same on isolated chloroplasts than at the leaf level (Schmuck and Moya, 1994).

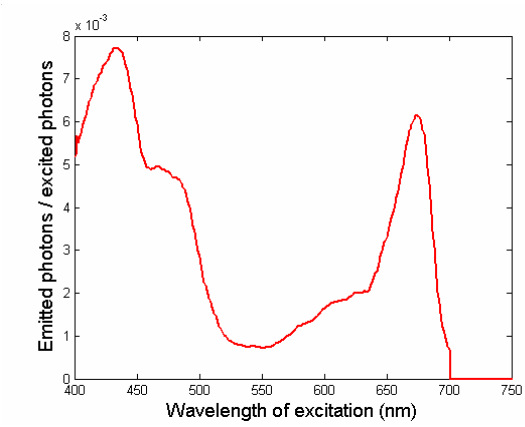

Figure 3.3.3. Thylakoid excitation spectrum EXC in number of photons measured with a Cary Eclipse fluorimeter. Emission at 760 nm.

This spectrum is normalized to 1:

$$\int_{400}^{750} EXC(\lambda) d\lambda = 1 \qquad [3.3.2]$$

The source function ϕ in Equations [3.2.9] setting the upward and downward fluorescence matrixes is now written, in W m^{-2} μm^{-1}:

$$\begin{aligned} \phi(\lambda_s, \lambda_m) &= \Phi \times \frac{k_{Cab}(\lambda_s)}{k(\lambda_s)} \times EXC(\lambda_s) \times PSIII(\lambda_m) \times \frac{E(\lambda_s)\lambda_s}{hc} \times \frac{hc}{\lambda_m} \\ &= \Phi \times \eta(\lambda_s, \lambda_m) \end{aligned} \qquad [3.3.3]$$

where the ratio k_{Cab} over k represents the fraction of light which is absorbed by chlorophyll only, Φ is the quantum yield, *EXC* is the thylakoid excitation spectrum, *PSIII* is the photosystem I+II fluorescence emission function, $E(\lambda_s)\lambda_s/hc$ is the incoming number of incident photons (expressed in photons m^{-2} s^{-1} μm^{-1} if the incoming energy E is provided in W m^{-2} μm^{-1}). The Plank constant h and the light speed in vacuum c cancel each over out. Finally, the term hc/λ_m ensures the conversion of number photons of fluorescence back into energy.

The next section surveys the literature to find PSI and PSII fluorescence emission spectra for plants at room temperature. Eventually, we will carry out laboratory experiments to measure our own spectra.

3.3.3 Photosystem I+II fluorescence emission function

The hypothesis of two light reactions (Hill and Bendall, 1960) and two pigment systems (Duysens et al., 1961) followed from Emerson's (1958) discovery of the *enhancement effect* which has been widely accepted (Govindjee and Yang, 1966).

Photosynthesis is explained with a Z scheme which accounts for the operation of the two photosystems which are linked by an electron transport chain. Both photosystems are protein complexes and contain a reaction centre with its full complements of electron transfer components, as well as an array of light harvesting (antenna) pigments (Chl a, Chl b, and carotenoids). Each reaction centre type contains its own reaction centre chlorophyll, P680 in PSII and P700 in PSI. Absorbed light is transferred from a pigment molecule to another in a non-radiative transfer process called *exciton* transfer. Finally, the exciton either arrives at the reaction centre where the chemical reactions occur, or is emitted as thermal de-excitation, or emitted as fluorescence. These three processes are in competition, which explains why photosynthesis energy conversion has to be among the fastest known chemical reactions.

At room temperature, a small fraction of the absorbed light energy is re-emitted as fluorescence. For wild type organisms, the Chl a fluorescence emission spectrum is characterized by a major peak at 683 nm (half-width of about 20 nm) attributable to PSII and a broad shoulder from 700 to 750 nm, due to both PSII and also the weak contribution of PSI (Lavorel, 1963; Wong and Govindjee, 1979). For unclear reasons, even in the F_0 state where the PSII fluorescence is minimal, there is at least a minor PSI contribution to the variable fluorescence emission of chloroplasts (Dau, 1994), *i.e.,* the PSI fluorescence seems to be

independent of the state of its reaction centre (Butler, 1978; Briantais et al., 1986). Trissl et al. (1993) gave a possible explanation since fast equilibration of excited states in PSI makes its emission spectrum independent of the excitation conditions (either direct excitation or excitation through exciton transfer from PSII to PSII or *spill-over*). So it was usually assumed that at room temperature most of this fluorescence emanates from PSII (Krause and Weis, 1991; Govindjee, 1995). Nevertheless, according to Roelofs et al. (1992), the PSI contribution is around 5% at 683 nm and around 30% at the far-red shoulder. When the PSII fluorescence is maximal (F_M), the PSI contribution is 1% at 683 nm and 6% at the far red shoulder. Pfündel (1998) found a similar result at leaf level by introducing a model to estimate the PSI contribution, estimating that at F_0 at wavelengths greater than 700 nm was about 30% and 50% in C_3 and C_4 plants, respectively. The corresponding values for the F_M fluorescence were 6% and 12%. Agati et al. (2000) studied the PSI contribution to the 735 nm fluorescence at room temperature both by time-resolved fluorescence lifetime and fluorescence yield measurements at 685 and 735 nm. They found that PSI contributed to the 735 nm fluorescence for about 40%, 10% and 35% at the minimal (F_0), maximal (F_M) and steady-state (F_s) levels, respectively. Peterson et al. (2001) obtained values between 30% and 48% at F_0 depending on the species. So even if the PSI fluorescence is small, particularly around 683 nm, it is significant and has to be taken into account.

a) Photosystem I fluorescence emission spectrum

Kok (1961) first demonstrated that the reaction centre chlorophyll of Photosystem I could be partially purified to a ratio of Chl to P700 of about 70 (in chloroplasts it is about 400) by selective extraction of light harvesting chlorophyll from chloroplasts with a critical concentration of acetone. Several attempts to purify the PSI reaction centre can also be found in the literature. Ogawa et al. (1970) applied detergent Triton X-100 to obtain a ratio of Chl to P700 of 30. Sane and Park (1970) applied the French-press treated with acetone obtaining a ratio of Chl to P700 of 16. Ikegami and Katoh (1975) used PSI particles prepared with digitonin and a diethyl ether treatment reaching a ratio of 5-9. However, it is not clear whether the reaction centre represents the PSI with respect to the fluorescence emission spectrum.

Butler and Kitajima (1975) shed light on the question proposing a theoretical basis for the existence of a specific antenna complex closely associated with PSI. Mullet et al. (1980a) added the evidence of their experiments of detergent fractionation and chloroplast developmental studies. For their functional models, Butler and Kitajima termed this component Chl a_1 and assigned the 735 nm fluorescence emission to this complex. From the structural studies of Mullet et al., the term LHC-I has been adopted, indicating the light-harvesting complex serving PSI. The LHC-I also appears in the literature as the *native* PSI complex (Haworth et al., 1983) or intact Photosystem I (Croce et al., 2000).

There is a line of research with several publications on the identification of the PSI chlorophyll proteins and the energy distribution between PSII and PSI (French, 1971; Strasser and Butler, 1977; Mullet at al., 1980a, 1980b; Haworth et al., 1983; Bassi and Simpson, 1987; Evans and Anderson, 1987; Knoetzel et al., 1992; Prakash et al., 2003). In most of the papers, the PSI fluorescence emission spectra are provided at low temperature because, as compared to room temperature, the fluorescence yield is up to 20 times higher (Mukerji and Sauer, 1993). There is also a shift in the maximum position that makes the fluorescence emission spectra at low temperature non-comparable to room temperature (Murata et al., 1966; Krause and Weiss, 1988). Very few authors show spectra at room

temperature and the latter generally only illustrate the differences between room and low temperatures, where the study is focused (Ikegami, 1976; Mukerji and Sauer, 1993; Croce et al., 1996, 2000).

Croce et al. (1996, 2000) applied the technique developed by Bassi and Simpson (1987) to obtain a ratio of Chl to P700 of 300:1, and measured the PSI fluorescence emission spectrum at several temperatures, from room temperature to 100 K. They showed that the detergent used in the extraction was clearly and markedly increasing the emission band near 680 nm, as confirmed by Mukerji and Sauer (1993). This effect was due to detergent induced coupling of the Chl a from the PSI complex, and fortunately could be eliminated.

For PSI, we chose a spectrum which shows a good correlation between the measured PSI fluorescence emission spectrum and the calculated emission spectrum applying the Stepanov equation to the absorption spectrum (Figure 3.3.4).

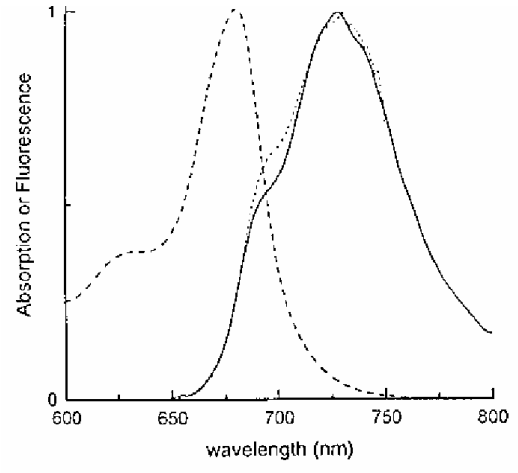

Figure 3.3.4. Comparison between calculated (dotted line) and measured (solid line) for PSI-LHCI at room temperature. Emission spectra were calculated from the measured absorption spectra (dashed line) by the Stepanov equation (after Croce et al., 1996, 2000).

b) Photosystem II fluorescence emission spectrum

In 1964, a remarkable result was reported by Boardman and Anderson (1964). They fractionated digitonin-treated spinach chloroplasts by differential centrifugation and found that the heaviest 1000 × *g* sediment with a Chl a/b ratio of 2.4 possessed PSII activity while the 50,000-144,000 × *g* fraction with a Chl a/b ratio of 6.2 possessed PSI. Ogawa et al. (1966) developed a technique to separate PSI and PSII based on the electrophoresis of chloroplasts solubilized with sodium dodecyl sulfate. Vernon et al. (1966) were the first to use detergent Triton X-100 to solubilize chloroplasts for the separation of the PSII by differential centrifugation. Later on, several authors used this technique (Anderson and Boardman, 1966; Wessels, 1966) but no fluorescence emission spectrum was available.

Yamamoto and Ke (1980) developed a technique to extract PSII by fractionation of chloroplasts with a Triton X-100 treatment, obtaining both LHC II and the reaction centre core complex. They measured the fluorescence emission spectrum at room temperature but it presented a shoulder around 720 nm due to Chl re-absorption as the content was too high.

Some years later, Dunahay et al. (1984) reviewed the most usual techniques (including a variation of the technique by Yamamoto and Ke) to fractionate the chloroplasts using detergent and salt treatments. They did not state which procedure was the best, because the different preparations showed different properties that could be advantageous in different conditions. Nevertheless, they found that the BBY technique (Berthold et al., 1981) was easier to perform and that it was more stable at room temperature. Dunahay et al. improved this technique to isolate PSII membranes with less PSI and to reduce the Triton / Chl ratio. The BBY technique is probably the most popular to extract PSII from chloroplasts. The extracted PSII (usually called BBY-grana) are considered to be in native form because both the reaction centre and the light harvesting complex (LHC-II) are present.

Van Dorsen et al. (1987) applied this technique to identify the PSII chlorophyll complexes and produced the BBY fluorescence emission spectrum at room temperature which is useful in our model (see Figure 3.3.5).

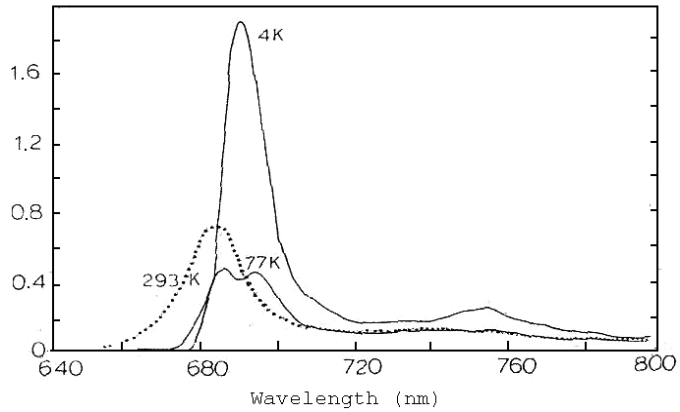

Figure 3.3.5. Emission spectra of the BBY-grana (arbitrary unit) at different temperatures.

Zucchelli et al. (1992) also used BBY-grana to identify the absorbing chlorophyll spectral species, producing another good example of fluorescence emission spectrum at room temperature. They applied a Gaussian deconvolution of the spectrum whose parameters appear in Table 3.3.1.

Table 3.3.1. Gaussian parameters for the deconvolution of the room-temperature emission spectra of spinach grana preparation (BBY-grana). FWHM stands for Full Width at Half Maximum.

Band	λ_{max} (nm)	FWHM (nm)	Area (%)
1	653.4	10.6 10.2	1.99
2	663.6	8.7 8.4	4.82
3	671.7	6.7 5.2	15.59
4	679.7	5.6 5.3	35.80
5	686.5	5.7 7.4	32.54
6	699.4	5.6 7.7	9.26

Franck et al. (2002), produced the last native PSII spectrum suitable for our model. They measured the fluorescence spectrum for several concentrations of suspensions of isolated PSII (see Figure 3.3.6). From the shape of the shoulder at far-red wavelengths it seems that the most similar spectrum to the native PSII form is the one with the minimum Chl

concentration, because it has not been re-absorbed. The three spectra that we found have very similar shape, so we are going to use the one measured by Franck et al. (2002).

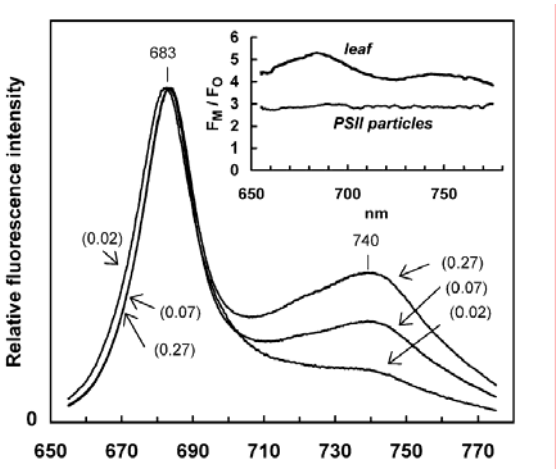

Figure 3.3.6. Room temperature fluorescence emission spectra of increasingly concentrated suspensions of isolated PSII particles (Chl concentration: 0.02, 0.07 and 0.27 mg ml^{-1}). The spectra are normalized to their maximum. Inset: comparison of the wavelength dependence of the F_M / F_0 ratio in intact leaves and in PSII particles (0.27 mg ml^{-1}).

c) PSI and PSII contribution to fluorescence

Through the introduction of the PSI and PSII fluorescence we aim at accurately describing the fluorescence emission of the infinitesimal layer *dx* in the model. This layer could be chloroplasts but for the moment it has a rather theoretical entity with a distinct emission for the two photosystems. In Figure 3.3.7 we present together and with the same scale the PSI emission spectrum of Figure 3.3.4 and the PSII emission spectrum of Figure 3.3.6 obtained with Chl content 0.02 mg ml^{-1}. The low chlorophyll content assures that red re-absorption is minimized.

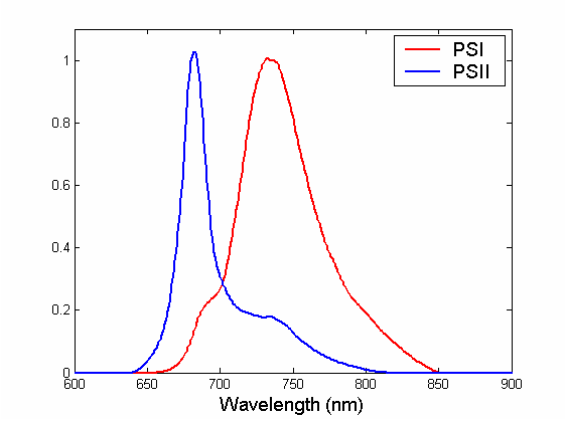

Figure 3.3.7. PSI and PSII fluorescence emission spectra used in the model

The relative contribution of PSI and PSII is a question that has to be sorted out. Franck et al. (2002) proposed a relative weight for each photosystem through the k_I and k_{II} coefficients, respectively:

$$PSIII(\lambda_m) = k_I \times PSI(\lambda_m) + k_{II} \times PSII(\lambda_m) \qquad [3.3.4]$$

They neglected the PSI variable fluorescence due to *spill-over* and found that $k_I = 1$ and $k_{II} = 5.85$, although they suggested that k_{II} could be species dependent. Another possible approach for the PSI and PSII contribution uses the stoichiometry of PSII/PSI reaction centres. The advantage would be that the plants adjust their stoichiometry as a long-term regulatory response to environmental conditions (Murakami, 1997). Taiz and Zeiger (1998) suggest that the ratio PSII/PSI is about 1.5 under many conditions, but it changes according to growth conditions. Chow et al. (1988) found that PSII/PSI increased with irradiance during growth, and values for different species were supplied. As an adaptive response to a change from low to high irradiance, the stoichiometry may increase in a few days. The PSII/PSI reaction centre ratios are close to one when plants are grown under shade or low light. They are lower than those found in sun leaves. They concluded that sun/shade acclimation or adaptation to irradiance combined two strategies: adjustments in both the PSII/PSI reaction centre ratios and the antenna size of PSII.

Nevertheless, the two photosystems do not have the same fluorescence lifetimes, and consequently the chlorophyll fluorescence quantum yield is different. The quantum yield at F_s can be deduced from lifetime measurements data (Schmuck and Moya, 1994), according to $\Phi = \tau/\tau_0$ (τ_0 is about 15-18 ns). Measured mean values at F_s are $\Phi^{PSII} = 0.5/15 = 3.3\%$ for PSII and $\Phi^{PSI} = 0.1/15 = 0.66\%$ for PSI. Therefore we will consider that the PSII is five times more efficient than the PSI by multiplying the stoichiometry values by 5. After normalization so that the integral of PSIII over the emission wavelengths is 1, Equation [3.3.4] becomes:

$$PSIII(\lambda_m) = \frac{PSI(\lambda_m) + 5 \times Sto \times PSII(\lambda_m)}{normPSIII} \qquad [3.3.5]$$

with $normPSIII = \sum_{\lambda_m} PSI(\lambda_m) + 5 \times Sto \times PSII(\lambda_m)$. Figure 3.3.8 presents combinations of the PSI and PSII isolated emission spectra shown in Figure 3.3.7. Since the spectra in Figures 3.3.4 and 3.3.6 ended at 800 nm and 775 nm, likely due to instrumental limits, we have extrapolated them to smoothly reach zero at 640 nm and at 850 nm and avoid abruptness in the emission spectrum.

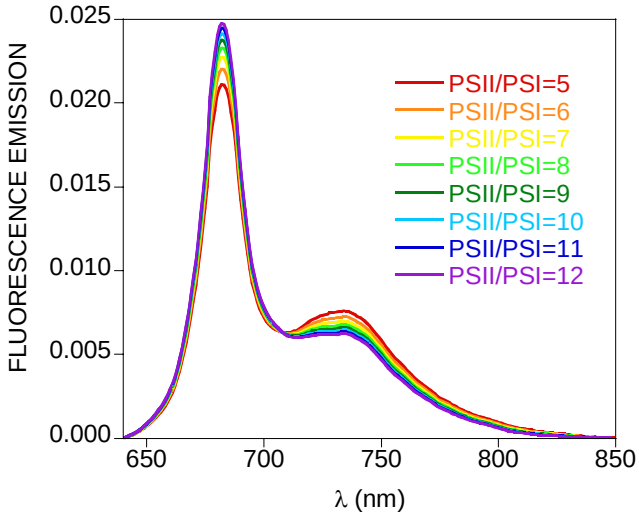

Figure 3.3.8. Elementary spectrum for several values of PSII contribution. PSI and PSII spectra were taken after Croce et al. (1996, 2000) and Franck et al. (2002), respectively.

3.4. Development of measurement protocols for laboratory and field experiments to assess leaf fluorescence model performance

We measured the fluorescence excitation and the fluorescence emission spectrum of plant leaves with a commercial fluorimeter, the Cary Eclipse (Louis, 2004). The fluorescence excitation is measured by keeping the emission wavelength constant and by varying the excitation wavelength with a monochromator and a source lamp. The fluorescence emission is measured by keeping the excitation wavelength constant and by varying the detection wavelength with another monochromator. Thus, the instrument has two monochromators, one for the excitation and one for the detection, providing measurements at 1 nm step. The sensor is a photomultiplier which measures the source before the light hits the sample and another one which measures the fluorescence signal. The Cary Eclipse has not been explicitly designed for our purpose because the spectra are not corrected for the instrument response and for the source characteristics. Furthermore, the measurements are provided in relative units while absolute units are required, so we calibrated them.

3.4.1. Correction of shape: Instrument response and calibration of the light source

a) Instrument response

We have to correct the emission spectrum because the sensitivity of the detector is spectrally dependent. Therefore we have to calibrate the shape of the measurements using a blackbody of known emission spectrum $CN(\lambda)$. We measure it with the fluorimeter $D(\lambda)$ and obtain the calibration factor as $C_s(\lambda) = CN(\lambda) / D(\lambda)$.

b) Calibration of the light source

A proper excitation spectrum is the emitted fluorescence at some wavelength when the molecules are excited for every wavelength with the same number of photons. Nevertheless, the source lamp of the fluorimeter is not flat, as seen in Figure 3.4.1, so it is necessary to correct for its shape. The latter is measured using a calibrated photodiode. The excitation spectra were calibrated by dividing them by $S(\lambda)$.

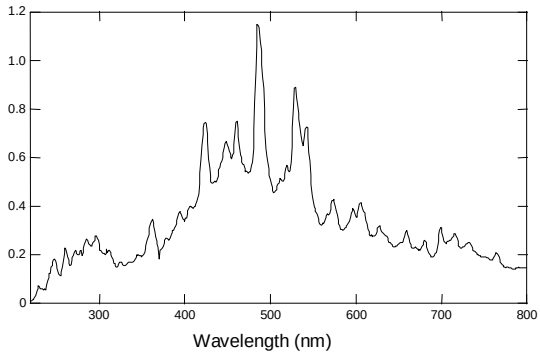

Figure 3.4.1. Emission spectrum of the xenon lamp, source of the Cary Eclipse fluorimeter.

3.4.2. Correction of intensity: Fluorescence quantum efficiency

We carried out an experiment to calibrate the excitation and emission spectra of a leaf in order to provide absolute units. These units are efficiency per nanometer. Our goal is then to

estimate the order of magnitude of the fluorescence quantum efficiency Φ_s at 760 nm, for an excitation at 632.8 nm defined as:

$$\Phi_s = \frac{\text{Number of photons emitted by fluorescence}}{\text{Number of photons absorbed}} \quad [3.4.1]$$

As it is difficult to estimate the number of photons absorbed by the leaf, we will rather measure the apparent fluorescence quantum efficiency $\Phi_{s,eff}$ which is a good approximation for Φ_s:

$$\Phi_{s,eff} = \frac{\text{Number of photons emitted by fluorescence}}{\text{Number of incident photons}} \quad [3.4.2]$$

The calibration coefficient *C* comes from the ratio:

$$C_{eff} = \frac{\Phi_{s,eff}}{I(\lambda_s, \lambda_m)} \quad [3.4.3]$$

with $I(\lambda_s,\lambda_m)$ the fluorescence corresponding to an excitation at 632.8 nm and an emission at 760 nm.

a) The reference

A wiring diagram of the experiment is shown in Figure 3.4.2. The source of excitation is a Helium-Neon laser producing 600 µmol photons m^{-2} s^{-1} at 632.8 nm. The sensor is a photodiode PIN detector PD EGG HUV 400 (ϕ = 10 mm). The non-fluorescent reference target is a block of Spectralon™ illuminated with the laser at an angle of 25°. In order to prevent the photodiode from saturating, we use a ND3 filter (Figure 3.4.3) which reduces the intensity of the beam on the detection side.

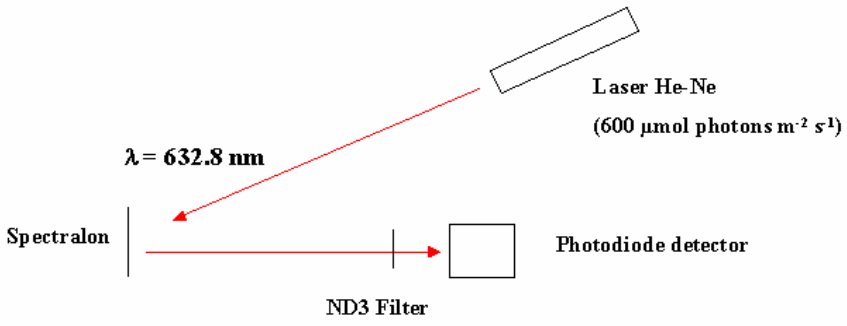

Figure 3.4.2. Spectralon reference illuminated by a laser beam. The ND3 filter prevents the detector from saturating.

Let S_1 be the signal measured by the photodiode, in Volts. One can write:

$$S_1 \times H_0 = I_L \times R_{sp} \times \Omega_{ND3}(\lambda_s) \times \xi_{il} \times \frac{N_A hc}{\lambda_s} \quad [3.4.4]$$

where H_0 is the calibration factor of the photodiode (W V^{-1}), I_L is the intensity of the laser, Ω_{ND3} is the transmittance of the filter ($\Omega_{ND3} = 0.001$), R_{sp} is the reflectance of the Spectralon (≈ 1), ξ_{il} is the area of the sample illuminated by the beam, N_A is the Avogadro number, *h* is the Planck constant, *c* is the speed of light in a vacuum, and λ_s is the wavelength of excitation. In this way, both terms of Equation [3.4.4] are expressed in Watts.

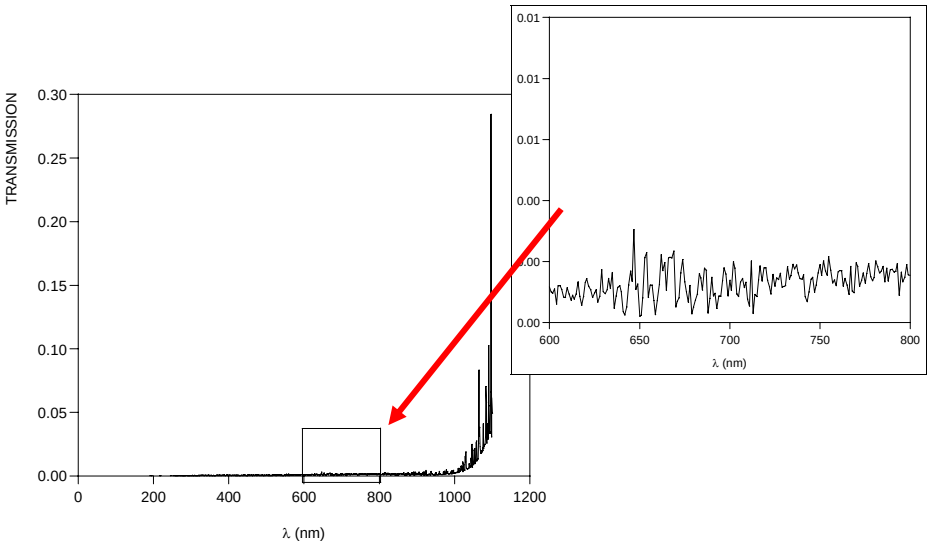

Figure 3.4.3. Transmission of the ND3 filter Ω_{ND3} measured in the laboratory (less than 0.2% in the range 600-800 nm).

b) The leaf

Figure 3.4.4 shows the configuration for the measurement of fluorescence. The leaf is put in the same geometry as the reference. We now use an interference filter 758 NB7 in order to measure the fluorescence at 758 nm.

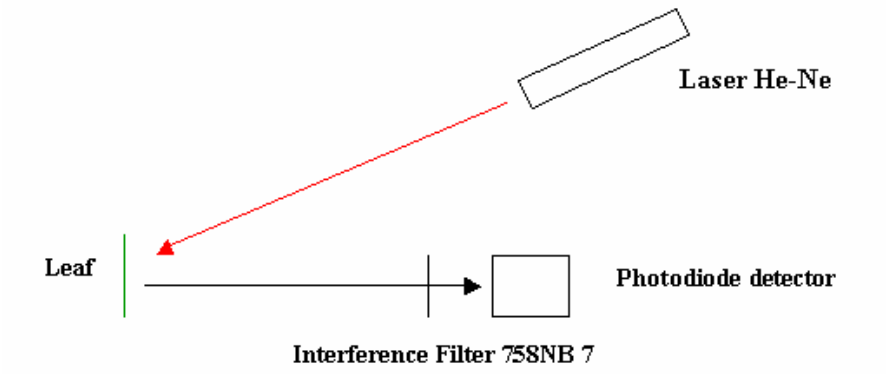

Figure 3.4.4. Leaf illuminated by a laser beam with the same geometry. The interference filter permits measurement of the fluorescence only at 758 nm.

Let S_2 be the signal measured with the photodiode. For this configuration one can write, similarly to Equation [3.4.4]:

$$S_2 \times H_0 = I_L \times R_{leaf} \times \Omega_{IF}(\lambda_s) \times \xi_{il} \times \frac{N_A hc}{\lambda_s} + I_L \times \Phi_s \times \Omega_{IF} \times \xi_{il} \times \frac{N_A hc}{\lambda_s} \qquad [3.4.5]$$

where R_{leaf} is the leaf reflectance at the geometry of the experiment and Ω_{IF} is the transmission of the interference filter (Figure 3.4.5). The signal measured with the photodiode is the sum of both the contribution from leaf reflectance and that from leaf fluorescence. The reflectance contribution is at 632.8 nm. As this wavelength is in the tail of the transmission curve, $\Omega_{IF}(\lambda_s)$ will simply be the transmission at 632.8 nm. The interference filter has a non-negligible bandpass of 7 nm around its transmission maximum located at 758 nm. The emission spectrum is a continuum, as shown in Figure 3.4.6, together with the transmission of the interference filter. This means the fluorescence measured at the detector will be not only at 760 nm but will also have the contribution at neighbouring wavelengths.

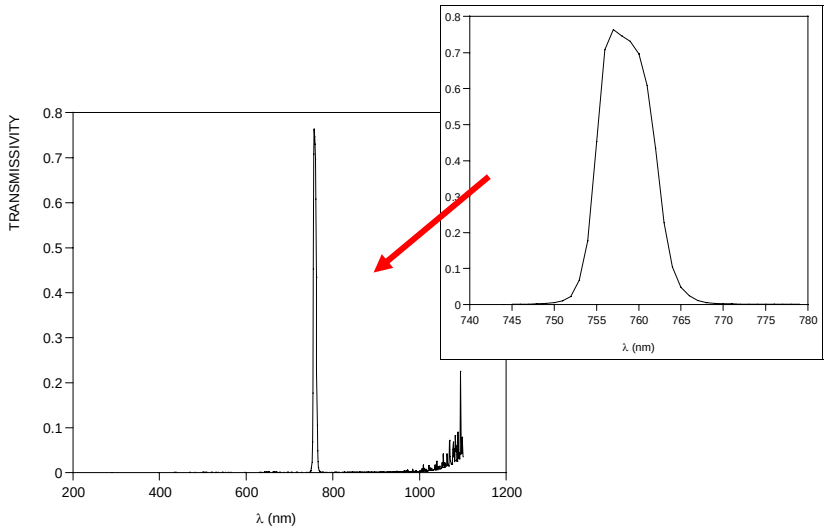

Figure 3.4.5. Transmittance Ω_{IF} of the interference filter 758 NB7 measured in the laboratory.

To correct this undesirable effect, we have to convolve the emission spectrum (number of photons of fluorescence $N_{fluo}(\lambda)$) with the transmission of the interference filter Ω_{IF}. Substituting Equation [3.4.2] in Equation [3.4.5] results in:

$$S_2 \times H_0 = I_L \times R_{leaf} \times \Omega_{IF}(\lambda_s) \times \xi_{il} \times \frac{N_A hc}{\lambda_s} + I_L \times \xi_{il} \times N_A hc \frac{1}{N_{\lambda s}} \int_{\lambda\, fluo} \frac{N_{fluo}(\lambda)}{\lambda} \Omega_{IF}(\lambda) d\lambda \qquad [3.4.6]$$

We can approximate the convolution by a simple multiplicative term of the bandpass of the filter BW_{IF}, taking the wavelength of emission $\lambda_F = 760$ nm.

$$\frac{1}{N_{\lambda s}} \int_{\lambda\, fluo} \frac{N_{fluo}(\lambda)}{\lambda} \Omega_{IF}(\lambda) d\lambda = \frac{N_{fluo}(\lambda_F)}{N_{\lambda exc}} \frac{1}{\lambda_F} BW_{IF} \qquad [3.4.7]$$

So we can write Equation [3.4.6] as follows:

$$S_2 \times H_0 = I_L \times R_{leaf} \times \xi_{il} \times \frac{N_A hc}{\lambda_{exc}} + I_L \times \xi_{il} \times \frac{N_A hc}{\lambda_F} \times \Phi_s \times BW_{IF} \qquad [3.4.8]$$

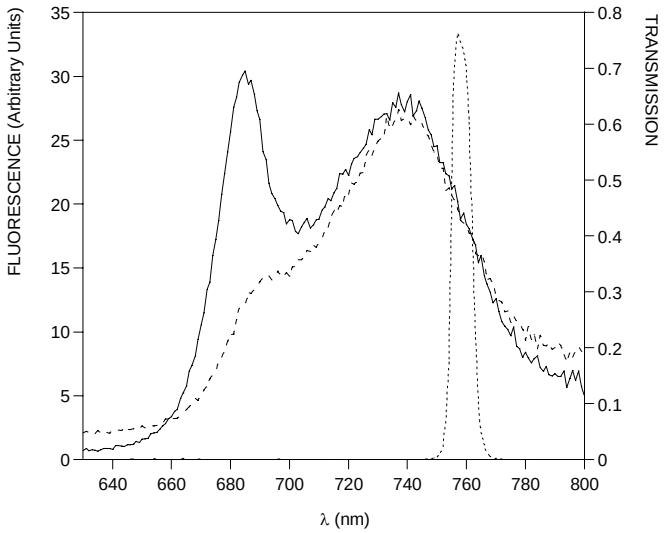

Figure 3.4.6. Fluorescence emission spectrum with excitation at 440 nm (solid line), and 535 nm (dashed line) measured for runner bean with a Cary fluorimeter. Dotted line: transmission of the interference filter.

c) Correction for artefacts

We also carried out a measurement with the Spectralon and the interference filter (S_2) and with the leaf and the ND3 filter (S_3), to correct the measurements for artefacts due to undesired signal passing through the filters. For Spectralon with the interference filter, we can write:

$$S_3 \times H_0 = I_L \times \Omega_{\mathrm{FI}}(\lambda_s) \times \xi_{il} \times \frac{N_A hc}{\lambda_s} \qquad [3.4.9]$$

On the other hand, for leaf with the ND3 filter, we can neglect the term due to fluorescence as it will be very small, and write:

$$S_4 \times H_0 = I_L \times R_{leaf} \times \Omega_{FN}(\lambda_s) \times \xi_{il} \times \frac{N_A hc}{\lambda_s} \qquad [3.4.10]$$

By solving the system of equations [3.4.4], [3.4.8], [3.4.9] and [3.4.10] we can obtain Φ_s (in nm^{-1}):

$$\Phi_S = \left(S_2 - \frac{S_3 S_4}{S_1} \right) \frac{\lambda_F}{\lambda_s} \frac{\Omega_{FN}(\lambda_s)}{BW_{FI}} \frac{1}{S_1} \qquad [3.4.11]$$

3.4.3. Results

We measured the fluorescence quantum efficiency during the summer campaign carried out in Orsay (Figure 3.4.7). We measured the leaf of a potted runner bean plant three times during ten days to check whether there was a significant variation or not. The plant was kept outdoors except for the time of this experiment. The results are shown in Table 3.4.1.

Table 3.4.1. Fluorescence quantum efficiency for three different values of Chl content measured with the SPAD sensor on the same potted plant.

Date	Chl content (μg cm^{-2})	λ_s (nm^{-1})
02/09/2003	35	3.77×10^{-5}
05/09/2003	34	4.00×10^{-5}
12/09/2003	32	3.90×10^{-5}

We can conclude that the order of magnitude of the fluorescence quantum efficiency is about 4×10^{-5} nm^{-1}. In other words, for a single wavelength of excitation, for every photon that incident to the leaf at 632.8 nm, about 4×10^{-5} photons are fluoresced at 760 nm.

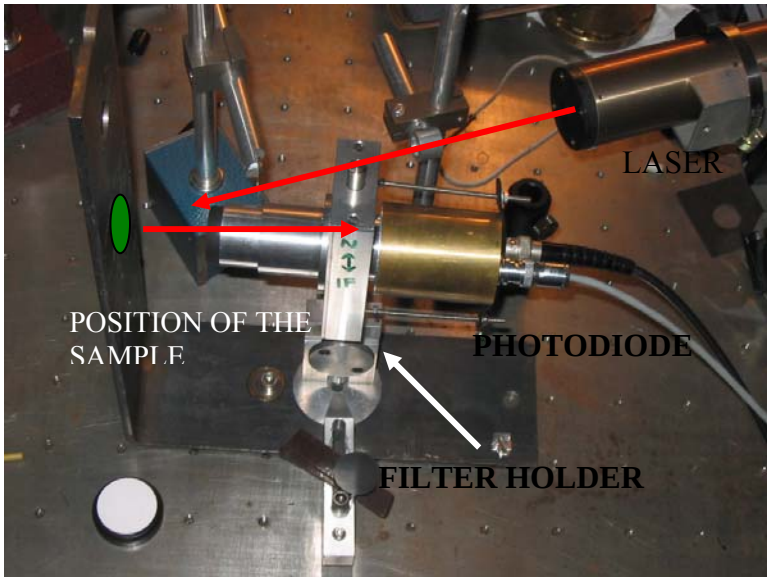

Figure 3.4.7. Photograph of the experiment showing its components.

3.5 Assessment of the leaf fluorescence model

3.5.1. Preliminary results

Let us consider a fresh-green leaf defined by its input parameters: N = 1.5, C_{ab} = 33 μg cm^{-2}, C_w = 0.025 cm, C_m = 0.01 g cm^{-2}, Φ = 0.04, species = bean, and Sto = 2.0. The elementary layer ($N = 1$) is then characterized by C_{ab}/N, C_w/N, and C_m/N. Its upward $F_u(1)$ and downward $F_d(1)$ chlorophyll fluorescence matrices have been calculated by Equations [3.2.13] for the 351 wavelengths of excitation between 400 nm and 750 nm and the 211 wavelengths of emission between 640 nm and 850 nm. The result is therefore stored in a matrix of dimension 351×211. Figure 3.5.1 compares the upward and downward fluorescence spectra of that elementary layer at the wavelength of excitation of 400 nm: Differences are noticeable in the red where re-absorption occurs. If we vary the wavelengths of excitation we obtain Figure 3.5.2.

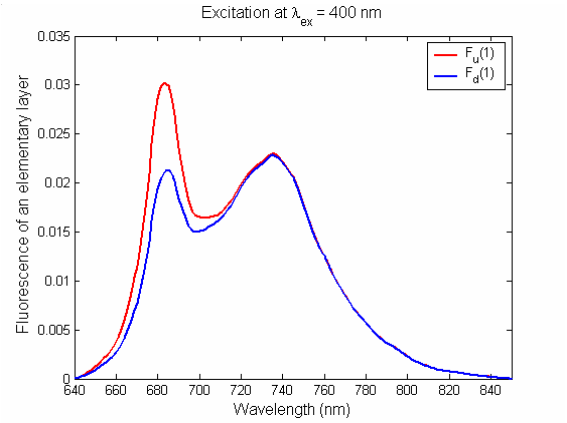

Figure 3.5.1. Modelled upward (red) and downward (blue) induced chlorophyll fluorescence of an elementary layer calculated at $\lambda_{excitation}$ = 400 nm.

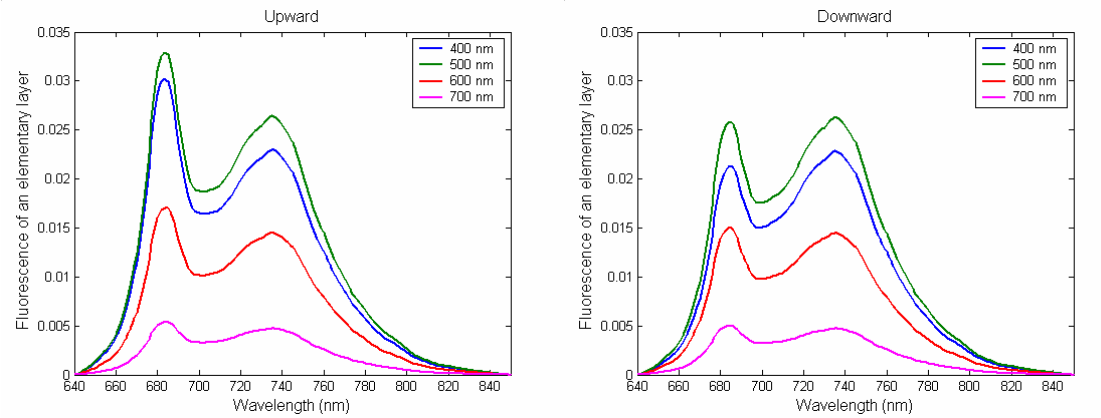

Figure 3.5.2. Modelled induced upward (left) and downward (right) chlorophyll fluorescence of an elementary layer calculated at four wavelengths of excitation.

Once the upward $F_u(1)$ and downward $F_d(1)$ fluorescence of a single layer have been calculated, Equations [3.2.37] allow us to recursively calculate the upward $F_u(N)$ and downward $F_d(N)$ fluorescence of a whole number of layers. Then, the fluorescence spectra of a real number of layers N is obtained by three-dimensional data interpolation (Figure 3.5.3).

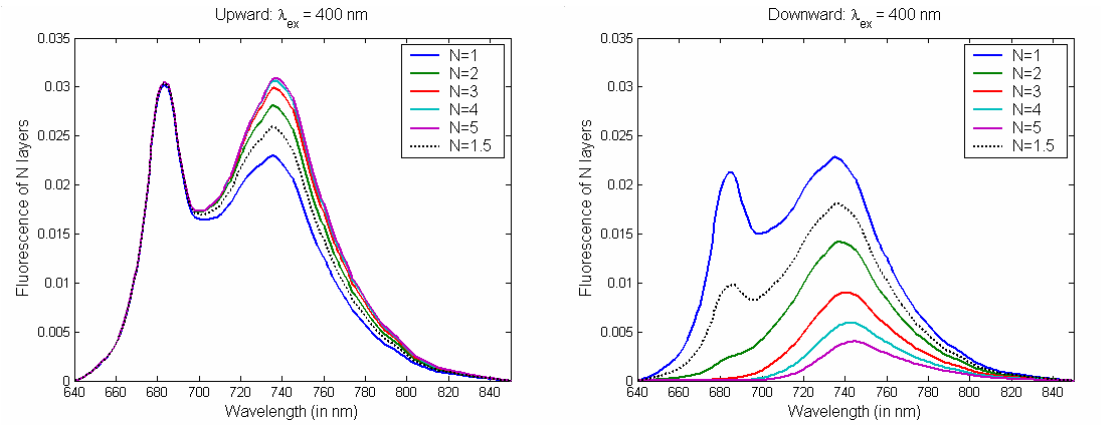

Figure 3.5.3. Modelled induced upward (left) and downward (right) chlorophyll fluorescence of N layers (N = 1,2,…,5 and N = 1.5) calculated at $\lambda_{excitation}$ = 400 nm.

3.5.2. Sensitivity analysis

A set of variables have been studied to connect the fluorescence emission to plant physiology. They were chosen because they change the fluorescence emission and because they are accessible to measurement: chlorophyll content (C_{ab}), PSI and PSII stoichiometry (Sto), fluorescence quantum efficiency (Φ), temperature (T), and light intensity or Photosynthetic Active Radiation (PAR).

a) Chlorophyll content

The main factor which drives the fluorescence emission is the Chl content. Our model is based on PROSPECT where the Chl a, Chl b and other pigments are considered as a whole. Although this might be somehow limiting, PROSPECT has shown good results modelling the reflectance and transmittance. The discrimination of the pigments in the model would require further work that has not yet been undertaken.

Figure 3.5.4 shows the variation of the fluorescence emission spectrum with Chl a+b content (C_{ab}). For the peak in the red, fluorescence increases rapidly with Chl, reaching a maximum at around 20 μg cm^{-2} and thereafter the fluorescence decreases slowly. For the peak in the near-infrared, the fluorescence increases constantly with C_{ab}. An explanation for this behaviour could be that the Chl absorption and fluorescence emission spectra overlap. This produces a re-absorption of the fluorescence reducing its intensity, which affects the peak around 683 nm much more.

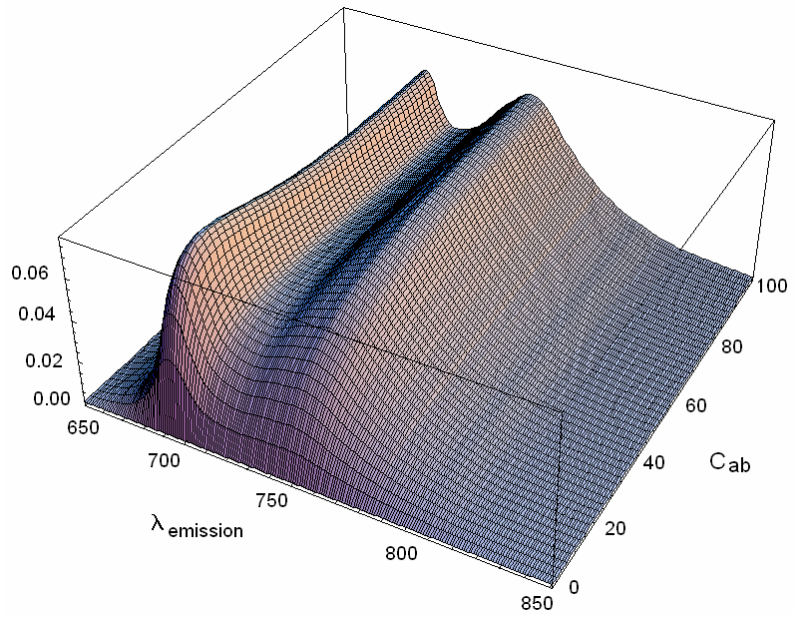

Figure 3.5.4. Variation of the upward fluorescence with C_{ab} in the range [0, 100] μg cm^{-2}. N = 1.5, C_w = 0.025 cm, C_m = 0.01 g cm^{-2}, Φ = 0.04, T = 20ºC, species = bean, and Sto = 2.0. The wavelength of excitation is λ_s = 440 nm.

b) PSI and PSII stoichiometry

The stoichiometry between the two photosystems has been introduced to account for the contribution of the photosystems to the elementary spectrum. As above-mentioned, it confers a long-term regulatory response to environmental conditions (Murakami, 1997) and its magnitude is easily measured. Figure 3.5.5 shows the variation of the upward fluorescence with the PSII:PSI stoichiometry. When the stoichiometry ratio increases, the contribution of the PSII to the elementary spectrum is greater, so the shape of the elementary spectrum changes (see Figure 3.3.8). The emission spectrum shows an increase in the peak around 683 nm, where PSII contribution is higher. There is also a decrease in the peak around 735 nm related to a weaker role of PSI.

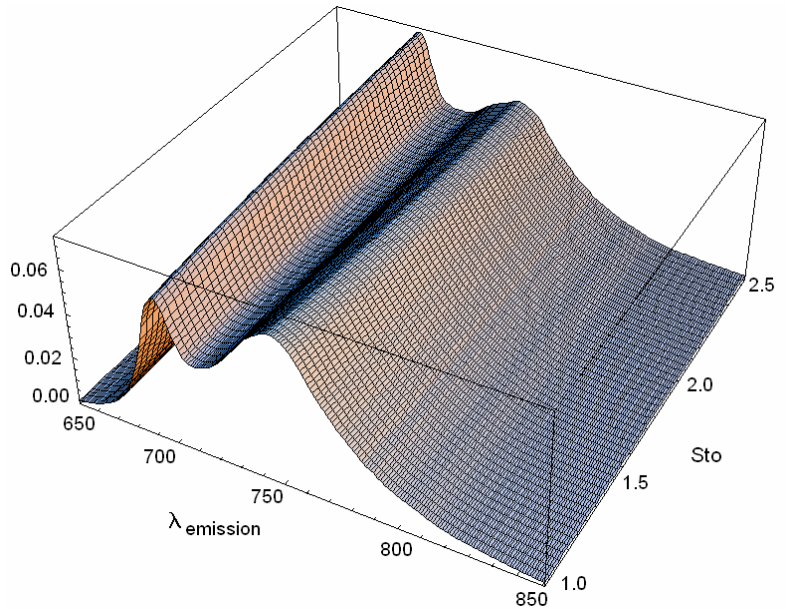

Figure 3.5.5. Variation of the upward fluorescence with PSII to PSI stoichiometry in the range [1, 2.5]. N = 1.5, C_{ab} = 33 μg cm^{-2}, C_w = 0.025 cm, C_m = 0.01 g cm^{-2}, Φ = 0.04, T = 20ºC, and species = bean. The wavelength of excitation is λ_s = 440 nm.

c) Fluorescence quantum efficiency

The quantum yield Φ (or fluorescence quantum efficiency), has been introduced previously, as it is necessary to calculate the appropriate order of magnitude of the fluorescence emission. This is an important issue because our objective is to include the fluorescence magnitude in plant canopy reflectance, not only the fluorescence shape. The quantum yield represents the ratio of emitted photons to absorbed photons. Since fluorescence lifetime is the same in isolated chloroplasts as at the leaf level, then Φ is the same at leaf and at chloroplast level (equivalent to our elementary level).

Figure 3.5.6 shows the variation of the upward fluorescence with Φ varying from 0 (no fluorescence) to 0.1 (10% of fluorescence). The fluorescence around the peak at 683 nm increases more quickly than the fluorescence around the peak at 735 nm.

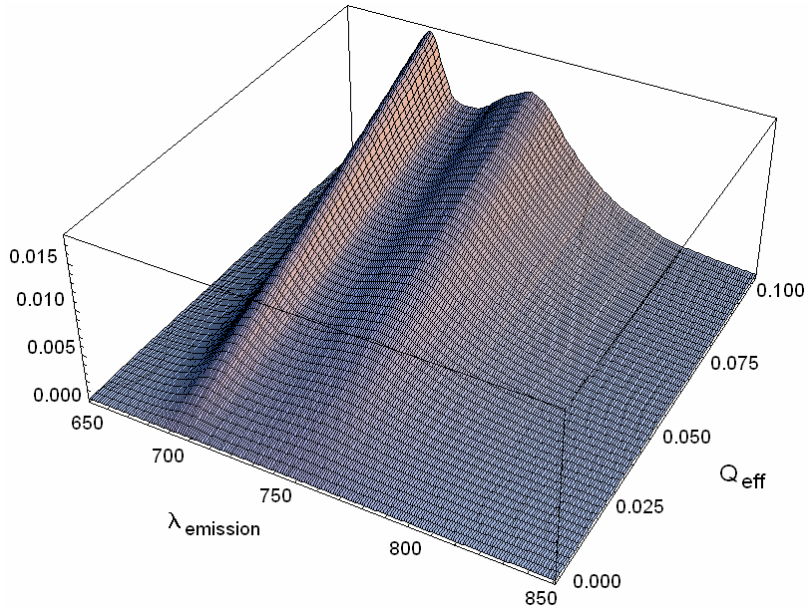

Figure 3.5.6. Variation of the upward fluorescence with Φ in the range [0, 0.01]. N = 1.5, C_{ab} = 33 µg cm^{-2}, C_w = 0.025 cm, C_m = 0.01 g cm^{-2}, T = 20ºC, species = bean, and Sto = 2.0. The wavelength of excitation is λ_s = 440 nm.

d) Temperature

Agati (1998) who studied Chl fluorescence variations for temperatures ranging from 0ºC to 25°C showed that fluorescence was increasing as leaf temperature decreased (assuming non-stress conditions). Since this trend was observed for all the investigated species, he hypothesized that it could be an intrinsic feature of higher plants. For both the 685 and 730 nm fluorescence peaks (F685 and F730, respectively), Agati found a linear relationship between the fluorescence intensity and the leaf temperature, with however a larger increase at 730 nm than at 685 nm (see Table 3.5.1). We introduced a multiplicative factor FT equal to 1 at 25 ºC and up to 3 at 0ºC.

Table 3.5.1. Linear regression for F685 and F730 versus temperature in the range [0-25] ºC. *m* is the slope and *n* the intercept (modified from Agati et al., 2000).

Plant species	$\mathbf{m_{685}}$	$\mathbf{n_{685}}$	$\mathbf{m_{730}}$	$\mathbf{n_{730}}$
Broad bean	–0.045	2.170	–0.071	2.856
Bean	–0.042	2.092	–0.054	2.404
Ficus	–0.023	1.598	–0.031	1.806
Tomato	–0.027	1.702	–0.037	1.962
Pea	–0.034	1.884	–0.046	2.196

So the multiplicative factor FT is:

$$\begin{cases} FT_{685} = m_{685} \times T(^{\circ}C) + n_{685} \\ FT_{730} = m_{730} \times T(^{\circ}C) + n_{730} \end{cases} \qquad [3.5.1]$$

where T is the temperature in degrees Celsius. Agati et al. (2000) only established the linear regression for F685 and F730. To the best of our knowledge, the temperature dependence of

the whole fluorescence emission spectrum has not been published. To overcome this problem, we will assume that the temperature dependence for the whole spectrum is linear, so for any wavelength λ (in nm) one can write the temperature dependence in the form:

$$FT_\lambda = m_\lambda \times \mathrm{T}(^{\circ}C) + n_\lambda \qquad [3.5.2]$$

with

$$\begin{aligned} m_\lambda &= m_{685} + \frac{\lambda - 685}{730 - 685}\,(m_{730} - m_{685}) \\ n_\lambda &= n_{685} + \frac{\lambda - 685}{730 - 685}\,(n_{730} - n_{685}) \end{aligned} \qquad [3.5.3]$$

An example of the dependence of fluorescence with temperature is shown in Figure 3.5.7 for broad bean leaves. The dependence with temperature is because the radiative deactivation of excited Chl, the fluorescence emission, is in competition with the photochemical reactions of photosynthesis that start a sequential electron transport among several electron-acceptor and electron-donor molecules, denoted plastoquinones. Such photochemical quenching act only on PSII since it depends on the reduction-oxidation of the first electron-acceptor molecules of PSII. Decreasing leaf temperature induces a reduction of the thylakoid membrane fluidity which inhibits the reoxidation of plastoquinones leading to an increase in the chlorophyll fluorescence yield (Havaux and Gruszecki, 1993). On the other hand, it was also correlated to a large reduction of the photochemical quenching at lower temperatures, while the non-photochemical quenching was only slightly affected by temperature in the range considered here (Bruggemann, 1992).

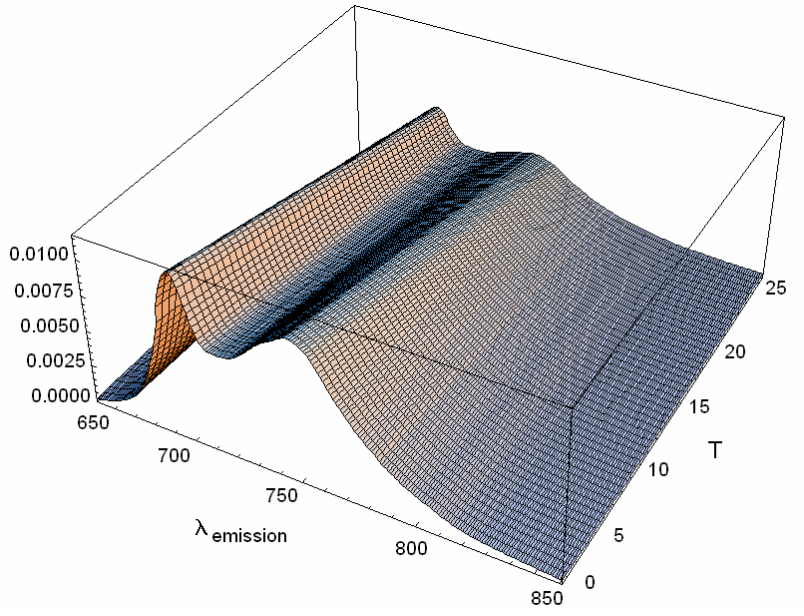

Figure 3.5.7. Variation of the upward fluorescence with temperature in the range [1, 26] ºC for broad bean species. N = 1.5, C_{ab} = 33 μg cm^{-2}, C_w = 0.025 cm, C_m = 0.01 g cm^{-2}, Φ = 0.04, species = bean, and Sto = 2.0. The wavelength of excitation is λ_s = 440 nm.

e) White light integration

We have calculated the fluorescence of the leaf for a real number N of layers by cutting a slice in the cube of dimension 351×211×5 defined by Equations [3.2.37]. 351 is the number of wavelengths of excitation between 400 nm and 750 nm (1 nm step) and 211 is the number of wavelengths of emission between 640 nm and 850 nm (1 nm step). Thus, we obtained a fluorescence matrix M_{ij} where the row number i represents the wavelength of excitation and the column number j the wavelength of emission:

$$M_{ij} = \begin{bmatrix} M_{400,640} & M_{400,641} & \cdots & M_{400,849} & M_{400,850} \\ M_{401,640} & M_{401,641} & \cdots & M_{401,849} & M_{401,850} \\ \vdots & \vdots & & \vdots & \vdots \\ M_{750,640} & M_{750,641} & \cdots & M_{750,849} & M_{750,850} \end{bmatrix} \quad [3.5.4]$$

This matrix is plotted in Figure 3.5.8.

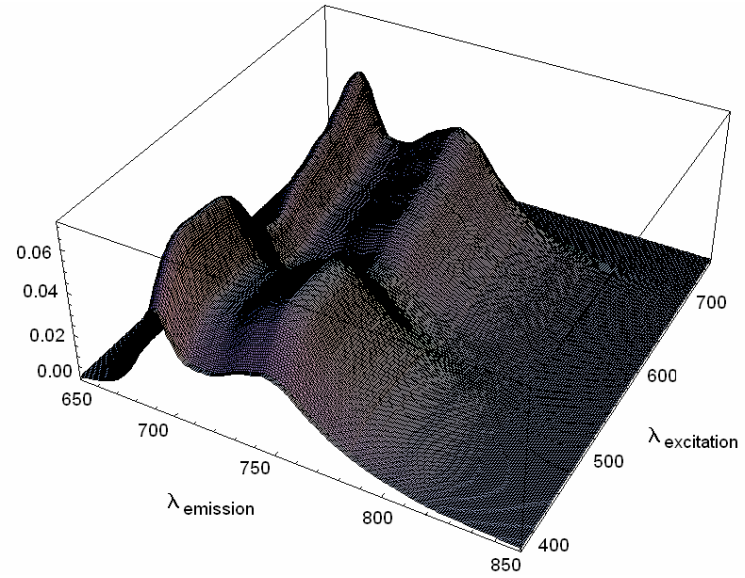

Figure 3.5.8. Fluorescence matrix. N = 1.5, C_{ab} = 33 μg cm^{-2}, C_w = 0.025 cm, C_m = 0.01 g cm^{-2}, Φ = 0.04, T = 20ºC, species = bean, and Sto = 2.0.

Let now calculate the fluorescence excited by the Sun. At each wavelength, a horizontal leaf receives the solar global irradiance noted $E(\lambda)$ and expressed in W m^{-2} μm^{-1}:

$$E(\lambda) = E_{dir}(\lambda) \times \cos\theta_s + E_{dif}(\lambda) \quad [3.5.5]$$

where $E_{dir}(\lambda)$ and $E_{dif}(\lambda)$ are the direct and diffuse irradiance, also expressed in W m^{-2} μm^{-1}, and θ_s is the Sun zenith angle. The diffuse radiation is due to Rayleigh and Mie scattering, and to multiple reflections between the ground and the atmosphere. At the ground level, these terms can be measured *in situ* with a Sun photometer or simulated using the MODTRAN 4.0 radiative transfer code, for instance (Figure 3.5.9). If the leaf inclination angle varies, which is generally the case in a plant canopy, we need to apply an irradiance model on

an inclined surface (Perez et al., 1987; Gueymard, 1987; Davies and McKay, 1989). This is accounted for by the canopy fluorescence model (see Chapter 4).

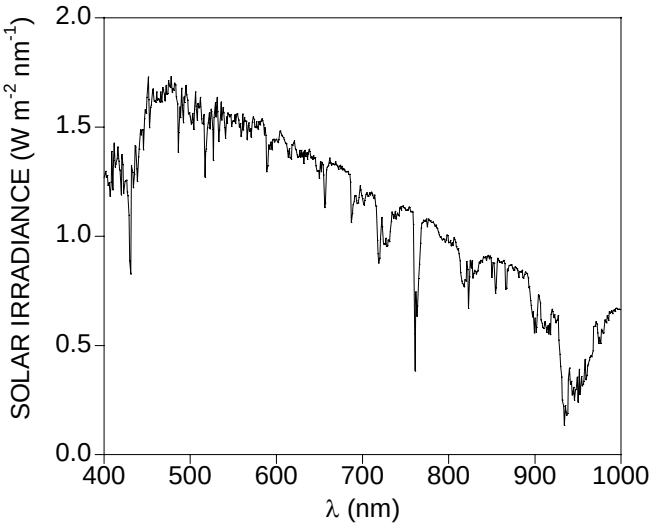

Figure 3.5.9. Solar irradiance simulated with MODTRAN 4.0 at ground level.

The white light fluorescence is obtained by integrating the fluorescence matrix over all the wavelengths of excitation, i.e. the range [400-750] nm corresponding to the photosynthetic active radiation, for each wavelength of emission. This integral is weighted by the solar global irradiance $N(\lambda)$ expressed in mol photons m^{-2} s^{-1} μm^{-1} and is normalized to the total number of incoming photons:

$$I_j = \frac{\int_{400}^{750} N(\lambda_i) M_{ij} d\lambda_i}{\int_{400}^{750} N(\lambda_i) d\lambda_i} \qquad [3.5.6]$$

The relationship between $E(\lambda)$ and $N(\lambda)$ is given by the Planck equation:

$$E(\lambda) = N(\lambda) N_a \frac{hc}{\lambda} \Leftrightarrow N(\lambda) = \frac{E(\lambda)}{N_a} \frac{\lambda}{hc} \qquad [3.5.7]$$

with h the Planck constant (6.6208×10^{-34} Js), c the speed of light in vacuum (2.99792×10^{8} ms^{-1}), N_a the Avogadro number (6.02214×10^{23} mol^{-1}), and λ the wavelength expressed in m. Thus if the latter is given in nm, it must be first converted into meter by multiplying by 10^{-9}. Figure 3.5.10 and 3.5.11a show an example of solar induced fluorescence emission spectrum. The global irradiance is the spectrum of Figure 3.5.9, simulated with MODTRAN 4.0 for a standard atmosphere and a Sun zenith angle of 23°. The reflectance and transmittance of the leaf with and without fluorescence are plotted in Figure 3.5.11b. These curves agree well with the experimental results published in the literature. The contribution of the upward and downward fluorescence to the reflectance and the transmittance, respectively, is shown in Figure 3.5.12. Kim et al. (1993) found 23% at 685 nm and 4% at 740 nm for the reflectance, although all authors do not agree with such values.

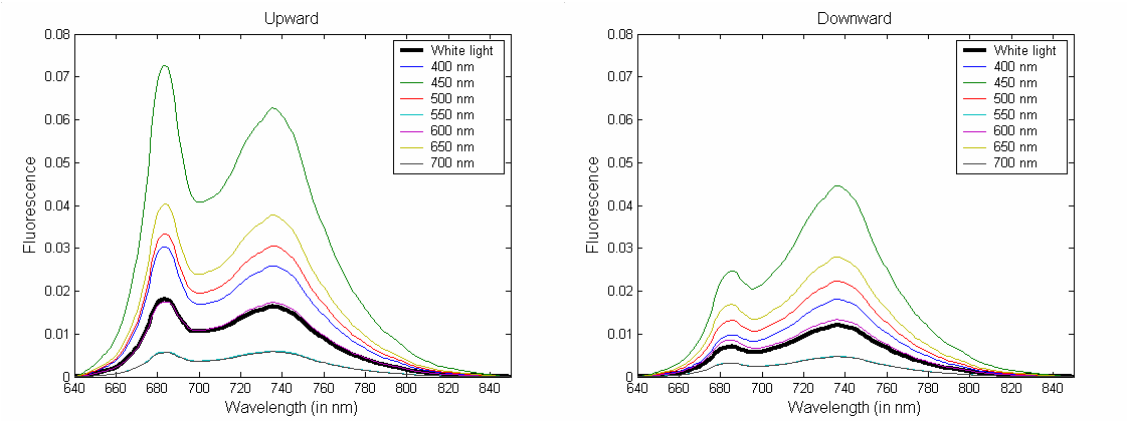

Figure 3.5.10. Example of the white light integration for the upward (left) and downward (right) fluorescence. N = 1.5, C_{ab} = 33 µg cm^{-2}, C_w = 0.025 cm, C_m = 0.01 g cm^{-2}, Φ = 0.04, T = 20ºC, species = bean, and Sto = 2.0.

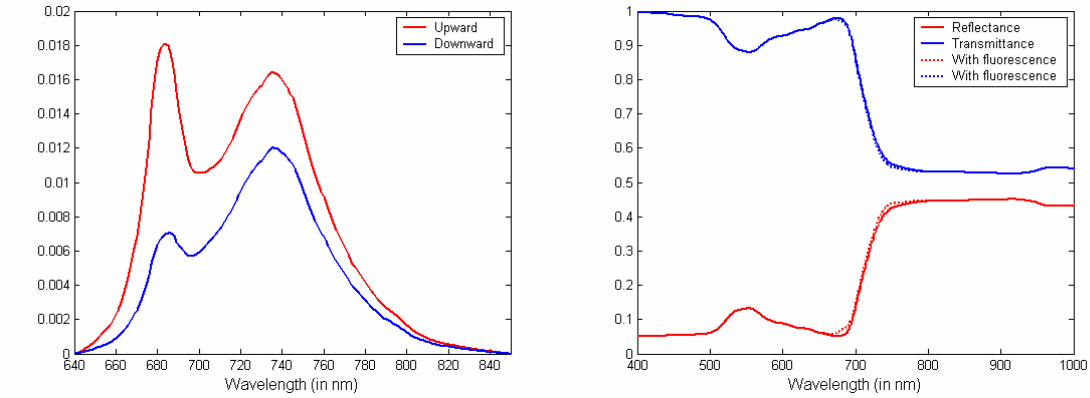

Figure 3.5.11. Upward & downward fluorescence (left) and reflectance & transmittance with and without fluorescence (right). N = 1.5, C_{ab} = 33 µg cm^{-2}, C_w = 0.025 cm, C_m = 0.01 g cm^{-2}, Φ = 0.04, T = 20ºC, species = bean, and Sto = 2.0.

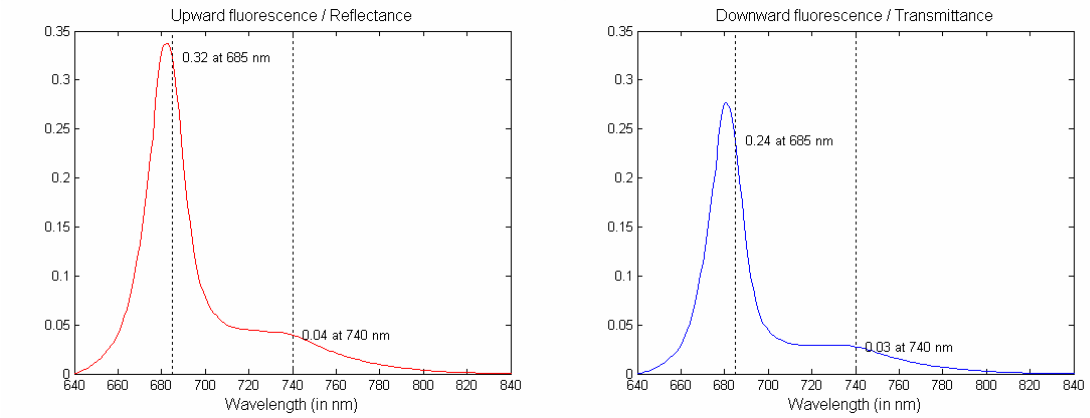

Figure 3.5.12. Contribution of the upward (left) and downward (right) fluorescence to the reflectance and the transmittance, respectively. N = 1.5, C_{ab} = 33 µg cm^{-2}, C_w = 0.025 cm, C_m = 0.01 g cm^{-2}, Φ = 0.04, T = 20ºC, species = bean, and Sto = 2.0.

f) Light intensity effects

To calculate the light intensity PAR expressed in μmol m^{-2} s^{-1} one integrates [3.5.7] on the wavelength range [400-750] nm and multiplies the result by 10^6:

$$PAR = 10^6 \times \int_{0.400}^{0.750} N(\lambda)\, d\lambda \qquad [3.5.8]$$

The PAR value for a sunny day is typically about 2100 μmol m^{-2} s^{-1}. Several authors have reported an increase of the steady state fluorescence emission with light intensity up to about 300 μmol m^{-2} s^{-1} (depending on species), followed by a slow decrease in fluorescence for higher intensities (Srivastava et al., 1995; Rosema et al., 1998; Agati, 1998; Agati et al., 2000; Flexas et al., 2000, 2002). Although the mechanisms responsible for the plant fluorescence yield are not thoroughly understood, Srivastava et al. (1995) found that the maximum level of fluorescence as a function of the light intensity was due to the increase of closed reaction centres and the concomitant increase of quenching photo-protecting mechanisms. Agati (1998) found that the slow decrease in fluorescence was due to a photo-inhibitory effect, i.e., a set of complex mechanisms aimed to protect the photosynthetic apparatus from excess light energy. This phenomenon seems to be independent of the light excitation source used. Rosema et al. (1998) parameterized the behavior of the *normalized fluorescence yield* noted $\frac{\varphi'_F}{\varphi_{F0}}$ as a function of PAR, where φ'_F is the *fluorescence yield* and φ_{F0} is the *fluorescence yield of the fully dark adapted photosystems* (reference level). In the paper of 1998, Eq-12 gives the *photosynthetic quantum yield* $\varphi'_P = \frac{\varphi'_{P0}}{1 + r_e \varphi'_{P0} PAR}$ where r_e is the electron transport resistance. Eq-18 gives the *photochemical yield* $\varphi'_{P0} = \frac{\varphi_{P0}}{1 + bPAR(1 - \varphi_{P0} - \varphi_{F0})}$ with $\varphi_{P0} = 0.82$ (*fully dark photochemical yield*) and $\varphi_{F0} = 0.01$. Eq-14 gives $\frac{\varphi'_F}{\varphi'_{F0}} = \frac{\varphi'_{FM}}{\varphi'_{F0}}\left[1 - \frac{\varphi'_{P0}}{1 + r_e \varphi'_{P0} PAR}\right] = \frac{\varphi'_{FM}}{\varphi'_{F0}}\left[1 - \varphi'_P\right]$ if one substitutes by Eq-12. The authors state that $\varphi'_{FM} = \frac{\varphi'_{F0}}{1 - \varphi'_{P0}}$. By substituting this expression in Eq-14 one obtains $\frac{\varphi'_F}{\varphi'_{F0}} = \frac{1 - \varphi'_P}{1 - \varphi'_{P0}}$. The authors state that $\frac{\varphi'_{F0}}{\varphi_{F0}} = \frac{\varphi'_{P0}}{\varphi_{P0}}$, which allows to calculate the *normalized fluorescence yield*: $\frac{\varphi'_F}{\varphi_{F0}} = \frac{\varphi'_{F0}}{\varphi_{F0}} \frac{1 - \varphi'_P}{1 - \varphi'_{P0}} = \frac{\varphi'_{P0}}{\varphi_{P0}} \frac{1 - \varphi'_P}{1 - \varphi'_{P0}}$. Then:

$$coef\_PAR = \frac{\varphi'_F}{\varphi_{F0}} = \frac{x}{0.82} \times \frac{1 - y}{1 - x} \qquad [3.5.9]$$

with $x = \varphi'_{P0} = \frac{0.82}{1 + bPAR(1 - 0.82 - 0.01)} = \frac{0.82}{1 + 0.17bPAR}$ and $y = \varphi'_P = \frac{x}{1 + r_e x PAR}$. If we set $b = 0.0035$ (variable) and $r_e = 0.005$ (variable) as recommended by Rosema et al. (1998), we obtain a curve corresponding to the upper envelope of experimental data for low light intensities (Figure 3.5.13). Due to stress or other factors, real values tend to be lower than this envelope.

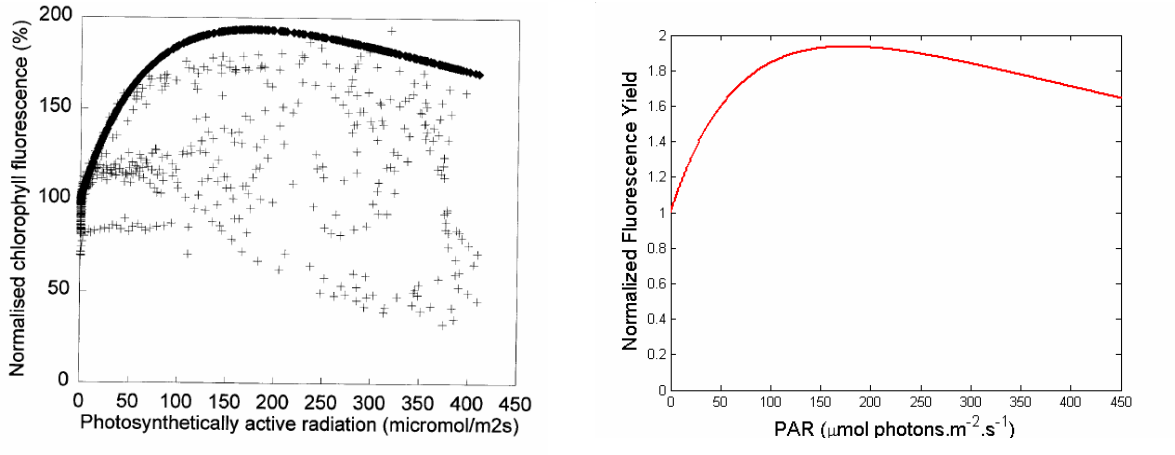

Figure 3.5.13. Scattergram of laser induced fluorescence versus PAR. Experimental measurements (on the left, after Rosema et al., 1998) and modelled function (on the right) using Equation [3.5.9].

For higher PAR values, Figure 3.5.14 shows that the *normalized fluorescence yield* can be less than 1, around 0.6 for PAR = 2100 μmol m^{-2} s^{-1}. This was actually observed and noted by Rosema et al. (1998). The dependence of fluorescence with light intensity is shown in Figure 3.5.15.

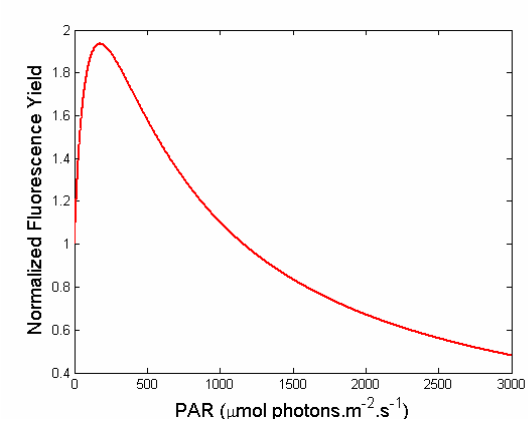

Figure 3.5.14. Normalized fluorescence yield $\frac{\varphi'_F}{\varphi_{F0}}$ calculated for a whole range of light intensities using Equation [3.5.9].

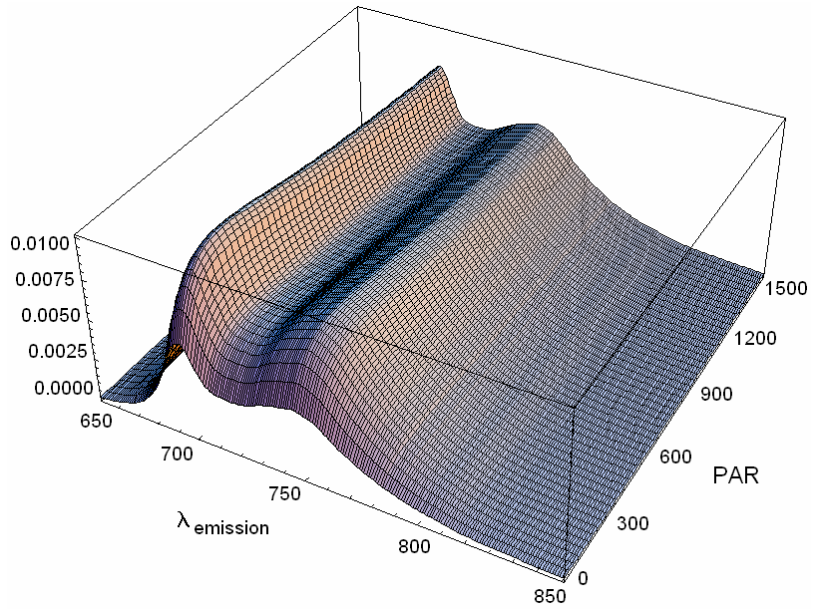

Figure 3.5.15. Variation of the upward fluorescence with PAR in the range [0, 1500] μmol m^{-2} s^{-1}, N = 1.5, C_{ab} = 33 μg cm^{-2}, C_w = 0.025 cm, C_m = 0.01 g cm^{-2}, Φ = 0.04, T = 20ºC, species = bean, and Sto = 2.0.

3.5.3. Comparison of the model outputs with measurements at leaf level

Next, we compare the measured values with the output of the model using this approach related to the stoichiometry of PSII to PSI reaction centres. The values of PSII/PSI stoichiometry are species dependent, but for high light the values are between 2.09 (*Alocasia macrorrhiza*) and 2.29 (pea, *Pisum sativum*), according to Chow et al. (1988). To evaluate the possibilities of this approach, we will consider a value of PSII/PSI stoichiometry of 2.0, which is in the range of the values suggested by Chow for plants grown in high light (outdoors, summer irradiance). This value is multiplied by 5 as above-mentioned, producing a PSII/PSI ratio of 10. The comparison of the model values and the measurements with runner beans are shown for two different Chl contents. In Figure 3.5.16 the Chl content is 17 μg cm^{-2}. The modelled values agree reasonably well with the measurements. There is a shift in the 685 peak because the elementary PSII spectrum has its maximum at 683 nm.

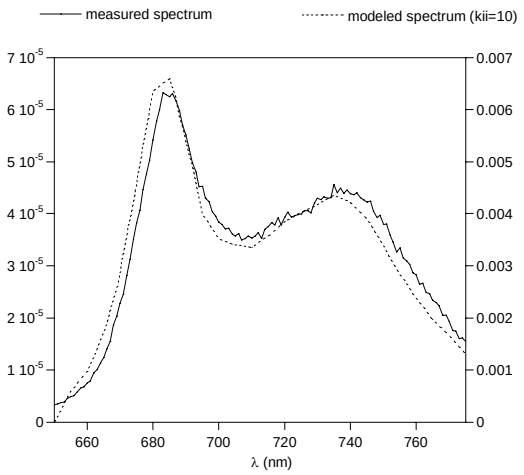

Figure 3.5.16. Fluorescence emission spectrum for a runner beam leaf with Chl content 17 μg cm^{-2} (solid line). Modelled emission spectrum using a ratio of PSII/PSI = 10 (dotted line). The excitation wavelength is 440 nm.

If we consider a leaf with a higher Chl content, it is important to note that the model reproduces the greater re-absorption of the 685 nm peak which can be seen in Figure 3.5.17 by comparing the relative heights of the two peaks.

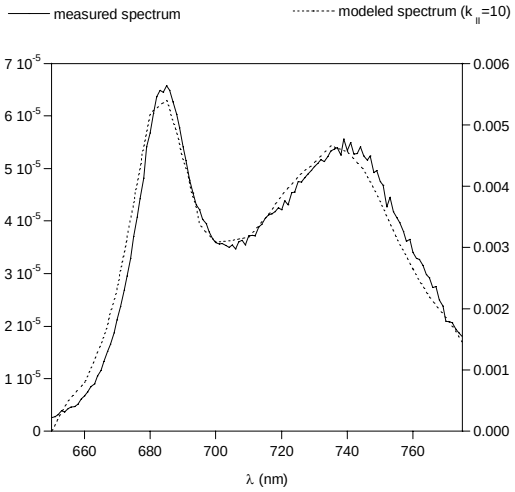

Figure 3.5.17. Fluorescence emission spectrum for a runner beam leaf with Chl content 33 μg cm^{-2} (solid line). Modelled emission spectrum using a ratio of PSII/PSI = 10 (dotted line). The excitation wavelength is 440 nm.

Although the model needs more validation work at leaf level, we can conclude that it reproduces the shape of the measured emission spectra reasonably well for different chlorophyll values.

3.6 Conclusion

Introducing chlorophyll fluorescence in PROSPECT was a challenge that we successfully took up. The equations that govern the physics of light transport (both incident and emitted) within the leaf seem to provide results consistent with experiment. The input parameters of the model are simple and most of them can be assessed experimentally. The new leaf fluorescence model is a real advance in every respect.

We improved the fluorescence emission spectrum generally used in fluorescence models through the separation of PSI and PSII contributions to the total spectrum. In this way, the fluorescence emission spectrum has a physical basis. We conducted a thorough literature review to find the elementary PSI and PSII emission spectra for plants at room temperature, and found some good examples which we used. In order to establish the relative contribution of the PSI and PSII to the total spectrum, we considered two different approaches: The first one estimates the contribution of PSI and PSII at the leaf level in a semi-empirical way. The second approach is based on the study of the PSI and PSII contributions at the elementary level using the stoichiometry of PSII to PSI reaction centres and taking into account that the PSII quantum yield is five times higher than for PSI.

We measured the fluorescence emission / excitation spectra of runner bean leaves corrected for instrument response and expressed in absolute units. For this purpose, we proceeded in two steps. First, the shape of the measured spectra was corrected. The raw emission spectra depend on the responsivity of the detector as a function of the wavelength, whereas the excitation spectra are sensitive to the light source. Once corrected for this dependence, the spectra are obtained with the right shape but in relative units. The second step was then to obtain the absolute intensity of the spectra by measuring the fluorescence quantum efficiency. This gives a conversion factor that allows expression of the spectra in absolute units of fluorescence efficiency per nm.

We applied the two procedures described as above to establish the PSII and PSI contributions and compared the model output with fluorescence measurements. They are both capable of reproducing the shape of the measured fluorescence emission spectrum for different chlorophyll contents. The advantage of the second approach is that the PSII/PSI stoichiometry is a physiological parameter related to the light conditions of the plants during growth.

However some questions remain unresolved. For instance, if we are able to predict the shape of the fluorescence emission spectrum, its magnitude still depends on a scaling factor which, to some extent, we cannot explain. We will have to find the cause of this factor and to correct it.

Other factors are known. For example, in the PROSPECT model, pigment absorption has been considered as a whole, because it was designed to simulate the reflectance and transmittance of a plant leaf. The effective absorption coefficients of the Chl actually includes Chl a, Chl b and carotenoids in the model. Unfortunately, these pigments do not absorb light equally for all wavelengths. If we consider a wavelength of excitation around 550 nm, at least 50% of the incoming light is absorbed by carotenoids and will not excite fluorescence. Nevertheless the model considers that all the pigments will excite fluorescence, leading to errors. This problem does not occur in PROSPECT because, in the calculation of the reflectance and transmittance, it does not matter which pigment is absorbing. A possible solution could be to include a

spectrum of efficiency in the energy transfer that excites chlorophyll and produces fluorescence.

In this work, contribution of second-order fluorescence to the total fluorescence flux has been neglected. Second-order fluorescence is the result of the overlap between the chlorophyll emission spectrum and chlorophyll absorption spectrum. The emission spectrum to be considered which travels in the leaf is usually dominated by the far red emission: most of the emission takes place at $\lambda > 690$ nm. *In vivo*, chlorophyll *a* which absorbs in this range is principally associated to the PSI antennae. The chlorophyll fluorescence quantum yield at F_s can be deduced from lifetime measurements data, accordingly $\Phi = \tau/\tau_0$ (τ_0 is about 15-18 ns). Measured mean values at F_s are $\Phi^{PSII} = 0.5/15 = 3.3\%$ for PS2 and $\Phi^{PSI} = 0.1/15 = 0.66\%$ for PSI. It follows that the quantum yield of second order fluorescence would be dominated by the quantum yield of PSI i.e. < 1%. In other words, by neglecting the second order fluorescence emission the error would be lower than 1%. The lifetime of second order fluorescence should be twice the lifetime of first order fluorescence. As a result a lengthening of the averaged lifetime is expected if the contribution of second order fluorescence is significant at the leaf level. It has been shown that the lifetime of chlorophyll fluorescence is the same, within the experimental error, from isolated chloroplasts as at the leaf level (Schmuck and Moya, 1994). This is in line with our assumption.

Additional efforts will be necessary to calibrate the model, i.e., to obtain the right absorption coefficients according to our approach. Subsequently, we would have to validate the model for the species of our interest, with different chlorophyll contents, temperatures, and so on. Both experiments have to be defined carefully to use the know-hows of PROSPECT calibration and validation, taking into account our approach of the fluorescence excitation and emission.

4. DEVELOPMENT of an INTEGRATED LEAF-CANOPY FLUORESCENCE MODEL: *FluorSAIL*

4.1. Development and coding of canopy fluorescence radiative transfer model

4.1.1. Introduction

Solar induced fluorescence in leaves might be used as an indicator of plant functioning and might allow the early detection of stress situations and photosynthetic deficiencies in vegetation canopies. However, the relation between fluorescence produced at the leaf level and the signal detected at the top of the canopy or even more so above the atmosphere by remote sensing techniques is very complex. Therefore models have been developed since the early nineties in order to better quantify the relation between top-of-canopy fluorescence and several factors acting upon the fluorescence from single leaves. Furthermore, these models can be used to obtain a realistic impression of the detectability of fluorescence from space.

Rosema et al. (1991) developed the model FLSAIL, which with regard to its canopy architecture was based on the SAIL (Scattering by Arbitrarily Inclined Leaves) model (Verhoef, 1984). In FLSAIL radiative transfer, including fluorescence, was modelled by means of the doubling algorithm, both at the leaf and at the canopy level. The leaf model was based on a Kubelka-Munk type formulation of radiative transfer inside the leaf. However, this model was designed with applications to laser-induced fluorescence in mind, so that a possible extension to accommodate solar-induced fluorescence, in which case high-resolution spectra of the direct and diffuse radiation inside the canopy are required, would be a non-trivial task.

In the model of Olioso et al. (1992) light extinction within the canopy is described by means of the Beer-Lambert law, which underestimates the role of scattering, especially in the near infrared. The light extinction coefficients were obtained from parallel simulations with SAIL. An exponential vertical gradient of leaf chlorophyll was assumed, and combined with the exponential light extinction this still allowed an analytical solution of the model equations.

More details on canopy fluorescence models have been given Chapter 2, Section 2.3. In neither of the above models was a dependence of leaf fluorescence on the light level considered, although it is known that the fluorescence response can depend quite substantially on the light level (Rosema et al., 1998). In this ESA-project a new canopy fluorescence model has been developed in order to include this light level dependence under natural light conditions. In this case, one has to consider that the solar flux intercepted by leaves depends strongly on their orientation with respect to the sun, and that for the diffuse upward and downward incident fluxes the spectral character of the light (the so-called light quality) changes with depth inside the canopy layer. The latter effect can be simulated very well with a numerically robust and speed-optimized recent version of the canopy reflectance model called 4SAIL, and therefore this model has been selected as a basis for the development of the model *FluorSAIL*, which simulates hyperspectral canopy fluorescence observations at both the top-of-canopy (TOC) and the top-of-atmosphere (TOA) level.

4.1.2. Design considerations

The interfaces of the *FluorSAIL* model with the outside world are determined by the spectral properties of the leaves and the soil, and by the incident radiation at the top of the canopy. For the latter, the atmospheric radiative transfer model MODTRAN4 (Berk et al., 1999) is applied. It was decided by the project team to define a spectral interval from 400 to 1000 nm, with 1 nm spectral resolution. The MODTRAN4 model is capable of providing sufficiently realistic radiance outputs, from which one can extract effective spectral parameters that describe the interaction with the earth's surface (Verhoef & Bach, 2003). The output of the leaf model *FluorMODleaf*, which becomes input to *FluorSAIL*, consists of spectra of single leaf reflectance and transmittance plus two matrices describing the fluorescence spectrum as a function of the excitation wavelength at both sides of the leaf.

Other inputs of the model are the canopy architecture, given by leaf area index (LAI), two leaf inclination distribution function (LIDF) parameters and the hot spot parameter, the angular geometry (solar zenith angle, viewing zenith angle and relative azimuth), and two parameters describing the dependence of leaf fluorescence on PAR light level.

For the latter we chose the formulation of Rosema et al. (1998), who predict the upper envelope of normalized fluorescence as a function of PAR level in $\mu\text{mol}\,\text{m}^{-2}\text{s}^{-1}$. For this, three equations are used, given by

$$\varphi'_{P0} = \frac{\varphi_{P0}}{1 + b_P\,\text{PAR}(1 - \varphi_{P0} - \varphi_{F0})}, \qquad [4.1]$$

where φ_{P0} is the fraction of the energy used for photosynthesis of the open photosystems, which is taken to be constant and equal to 0.82, and φ_{F0} is the corresponding fluorescence fraction, which is estimated at a value of 0.01.

$$\varphi'_{P} = \frac{\varphi'_{P0}}{1 + r_e\,\varphi'_{P0}\,\text{PAR}}\ , \qquad [4.2]$$

$$\text{Chl F} = \frac{\varphi'_{P0}}{\varphi_{P0}}\,\frac{1 - \varphi'_{P}}{1 - \varphi'_{P0}}, \qquad [4.3]$$

The constant b_P is called the heat dissipation constant, and r_e the electron transport resistance. These two constants must be supplied to *FluorSAIL* as inputs to introduce the light level dependence. The normalized (to the dark-adapted one) chlorophyll fluorescence is called Chl F. In Fig. 4.1.1 an example of the dependencies of Chl F and normalized photosynthesis on PAR incident light flux is shown for this model.

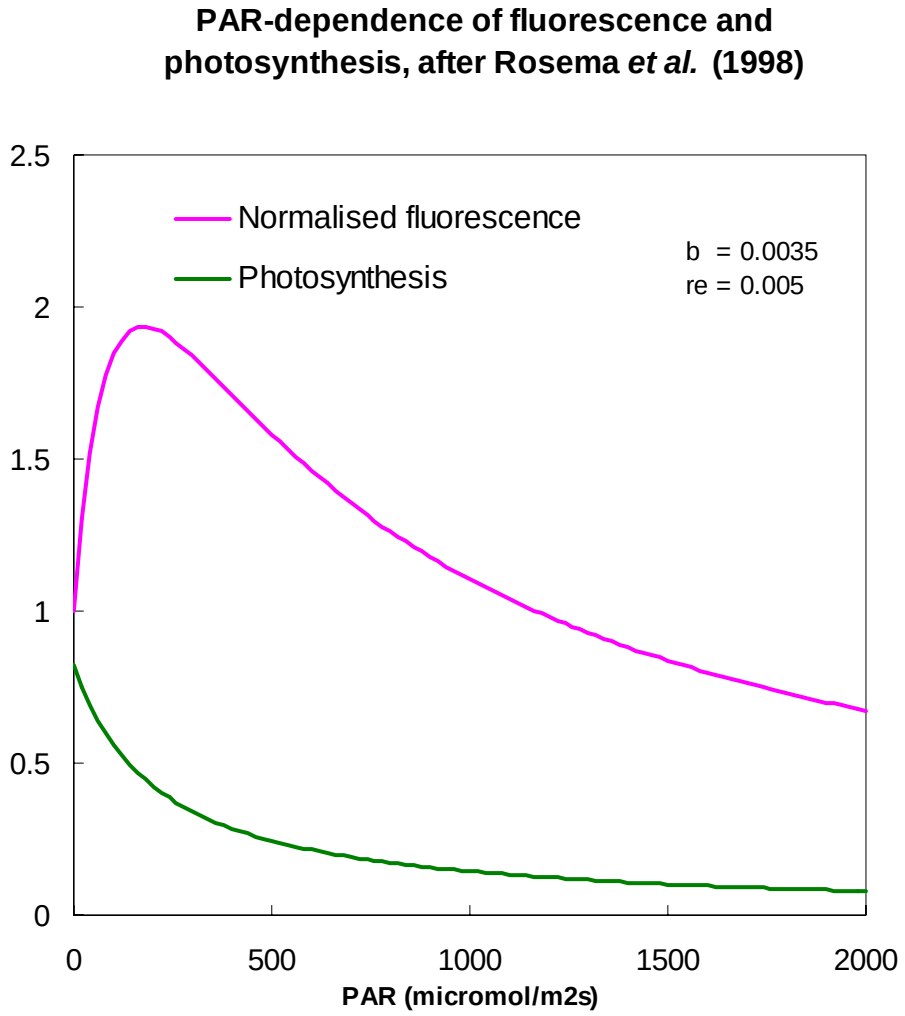

Figure 4.1.1. Dependence of normalized fluorescence and photosynthesis on PAR flux light level as modelled by Rosema et al. (1998).

In order to apply this model inside *FluorSAIL*, internal fluxes, which are usually expressed in spectral irradiance units, must be converted into photon flux densities, expressed in mols per second per unit area, and integrated over the PAR wavelength range (400 – 700 nm). For this, the following equation is applied:

$$\mathrm{PAR} = \int_{400}^{700} \frac{1000 E_\lambda}{(hc/\lambda) N_{\mathrm{Avo}}} \mathrm{d}\lambda \,, \qquad [4.4]$$

where E_λ is a radiant flux density (irradiance) in $\mathrm{mW\,m^{-2}\,nm^{-1}}$, and the wavelength λ is also expressed in nm. The product hc is Planck's constant times the speed of light $= 1.9864475 \times 10^{-16}\ \mathrm{J\,nm}$. N_{Avo} is Avogadro's number $= 6.0221367 \times 10^{23}$. Eq.[4.4] gives the PAR flux in $\mu\mathrm{mol\,m^{-2}s^{-1}}$.

In order to allow computation of all internal spectral fluxes (direct solar flux, upward and downward diffuse fluxes) in the canopy, the canopy layer is divided into 60 slabs of equal optical thickness (LAI). In each slab one can compute the spectral fluxes using the 4SAIL

radiative transfer model. This will be further discussed in the next section. Here we only note that for the direct solar incident radiation the spectral distribution and its intensity do not change inside the canopy; only the probability of sunshine changes with depth. For sunlit leaves the intercepted solar flux does strongly depend on the leaf's orientation with respect to the sun, but this effect is not position-dependent. For the diffuse fluxes both the spectral distribution and the intensity will change as a function of depth in the canopy, but the amount of diffuse flux that is intercepted by a leaf is independent of its orientation. Summarized, one can define two arrays holding the PAR incident light flux on leaves for direct solar and diffuse incident radiation, respectively.

These are given by:

$$\mathrm{PAR}_{\mathrm{sun}}(\theta_\ell,\varphi_\ell)=\int_{400}^{700}\frac{1000E_s(\lambda)\left|\cos\theta_\ell+\sin\theta_\ell\tan\theta_s\cos\varphi_\ell\right|}{(hc/\lambda)N_{\mathrm{Avo}}}\mathrm{d}\lambda \qquad [4.5]$$

$$\mathrm{PAR}_{\mathrm{dif}}(x)=\int_{400}^{700}\frac{1000[E^-(x,\lambda)+E^+(x,\lambda)]}{(hc/\lambda)N_{\mathrm{Avo}}}\mathrm{d}\lambda \qquad [4.6]$$

where $(\theta_\ell,\varphi_\ell)$ are the zenith angle and the relative azimuth angle (with respect to the sun) of the leaf's normal, θ_s is the solar zenith angle, $E_s(\lambda)$ is the direct solar spectral irradiance on a horizontal plane incident at the top of the canopy, $E^-(x,\lambda)$ and $E^+(x,\lambda)$ are the downward and upward diffuse spectral fluxes at level *x* within the canopy layer, respectively.

In *FluorSAIL* a discretized leaf angle distribution is used, consisting of frequencies at the 13 leaf inclinations of SAIL (5, 15, 25, …, 75, and 81, 83, …, 89 degrees) and a uniform leaf azimuth distribution. For the latter, the 18 discrete angles are at 5, 15, …, 175 degrees azimuth relative to the sun. Leaves that are exposed to sunlight receive an amount of incident PAR flux equal to the sum of the contributions of Eqs. [4.5] and [4.6]. Leaves in the shade receive only the latter contribution. For each level within the canopy the normalized Chl F can now be determined by applying the PAR light level dependence model of Rosema et al. for each leaf orientation and computing the weighted average according to the given leaf inclination distribution function. For leaves exposed to sunlight this gives

$$\mathrm{Chl\,F}_{\mathrm{sunlit}}(x)=\frac{\sum_{i=1}^{13}\sum_{j=1}^{18}\Phi[\mathrm{PAR}_{\mathrm{sun}}(\theta_i,\varphi_j)+\mathrm{PAR}_{\mathrm{dif}}(x)]f(\theta_i)}{18} \qquad [4.7]$$

where Φ represents the PAR light level dependence function, and $f(\theta_i)$ the leaf inclination frequency. For leaves in the shade their orientation is immaterial, so that for these one obtains simply:

$$\mathrm{Chl\,F}_{\mathrm{shade}}(x)=\Phi[\mathrm{PAR}_{\mathrm{dif}}(x)] \qquad [4.8]$$

The outputs of the model should consist of spectra of canopy reflectance, top-of-canopy radiance, and top-of-atmosphere radiance, in all cases both without fluorescence and with fluorescence included. Canopy reflectance is calculated in *FluorSAIL* by numerical

integration, in a similar manner as fluorescence. For comparison, and since this was available anyway, the canopy reflectance calculated by the model 4SAIL (which is largely based on analytical integration) is also produced as output. In addition, the direct solar and diffuse sky spectral irradiances are output. For the top-of-atmosphere radiances, two cases are considered: 1) the surroundings consist of bare soil, and 2) the surroundings are the same as the target. In these cases different top-of-atmosphere radiances result because of the atmospheric adjacency effect.

4.1.3. Computation of canopy reflectance, fluorescence and TOA radiance

The computation of canopy reflectance is based on numerical integration of the associated radiative transfer equation, here given by:

$$\frac{\mathrm{d}\,\pi L_r(0)}{L\mathrm{d}x} = w_r E_s(0) P_{so}(x) + [v_r E^-(x) + v_r' E^+(x)] P_o(x) \qquad [4.9]$$

where L is the total canopy leaf area index (LAI), and x is the relative optical height, which runs from −1 at the bottom to 0 at the canopy top. Further,

$L_r(0)$ = top-of-canopy radiance
$E_s(0)$ = direct solar irradiance on the canopy top
$E^-(x)$ = downward diffuse irradiance at level x
$E^+(x)$ = upward diffuse irradiance at level x
w_r = bi-directional scattering coefficient for sunlight
v_r = hemispherical-directional scattering coefficient for diffuse downward flux
v_r' = hemispherical-directional scattering coefficient for diffuse upward flux
$P_o(x)$ = gap viewing probability down to level x
$P_{so}(x)$ = bi-directional gap viewing probability down to level x.

The gap probabilities are derived from the SAIL direct flux extinction coefficients in the directions of the sun and the observer, which are called k and K, respectively. This gives

$$P_o(x) = \exp(KLx) \qquad [4.10]$$

$$P_{so}(x) = \exp[(K+k)Lx + \sqrt{Kk}L(1-\mathrm{e}^{\alpha x})/\alpha] \qquad [4.11]$$

where $\alpha = \frac{d_{so}}{s_\ell}\frac{2}{K+k}$ is the factor that controls the hot spot effect. The angular distance measure of the hot spot here is given by $d_{so} = \sqrt{\tan^2\theta_s + \tan^2\theta_o - 2\tan\theta_s \tan\theta_o \cos\psi}$, where θ_o and ψ are the viewing zenith angle and the relative viewing azimuth angle, respectively. The canopy hot spot size parameter s_ℓ is equal to the ratio of the correlation length of leaf projections in the horizontal plane and canopy height. The correction factor $2/(K+k)$ is applied in the more recent versions of SAIL in order to compensate the effect of shadow lengthening that occurs for inclined leaves at larger zenith angles (Bréon et al., 2002).

The scattering coefficients of the SAIL models can all be generically defined by means of the purely geometrical functions *G* and *F*. For instance, the scattering coefficients mentioned above are defined by:

$$w_r = \rho G_{so} + \tau F_{so}$$
$$v_r = \rho G_{do} + \tau F_{do}$$
$$v_r' = \tau G_{do} + \rho F_{do}$$

where ρ and τ are the single leaf reflectance and transmittance, respectively. The subscripts attached to the functions *G* and *F* indicate the flux types on incidence and exit, *s* for solar flux, *d* for diffuse upward or downward flux, and *o* for flux (radiance) in the observer's direction. In 4SAIL these functions are only computed if the geometry has changed with respect to the previous call, so that *e.g.,* hyperspectral simulations under a constant angular geometry can be carried out very efficiently.

Similar coefficients can be defined for the fluorescence contributions as well. In that case one obtains (with *f* indicating fluorescence):

$$w_f(\lambda_e,\lambda_f) = \phi_u(\lambda_e,\lambda_f)G_{so} + \phi_d(\lambda_e,\lambda_f)F_{so}$$
$$v_f(\lambda_e,\lambda_f) = \phi_u(\lambda_e,\lambda_f)G_{do} + \phi_d(\lambda_e,\lambda_f)F_{do}$$
$$v_f'(\lambda_e,\lambda_f) = \phi_d(\lambda_e,\lambda_f)G_{do} + \phi_u(\lambda_e,\lambda_f)F_{do}$$

where $\phi_u(\lambda_e,\lambda_f)$ and $\phi_d(\lambda_e,\lambda_f)$ are elements of the upward and downward fluorescence matrices of single leaves, for excitation wavelength λ_e and fluorescence wavelength λ_f. These coefficients are subsequently applied in order to accumulate the total fluorescence contribution by numerical integration (over canopy depth) of the following equation:

$$\frac{\mathrm{d}\,\pi L_f(0,\lambda_f)}{L\mathrm{d}x} = \int_{400}^{1000} \left\{ \begin{array}{l} w_f(\lambda_e,\lambda_f)E_s(0,\lambda_e)P_{so}(x)\mathrm{Chl\ F_{sun}}(x) \\ +[v_f(\lambda_e,\lambda_f)E^-(x,\lambda_e) + v_f'(\lambda_e,\lambda_f)E^+(x,\lambda_e)]P_o(x)\mathrm{Chl\ F_{shade}}(x) \end{array} \right\} \mathrm{d}\lambda_e \qquad [4.12]$$

Note that, regardless of the fluorescence wavelength, spectral integration is carried out over the full spectrum of excitation wavelengths. This is done in order not to exclude beforehand the possibility of "anti-Stokes" fluorescence (in which case $\lambda_f < \lambda_e$).

From Eqs.[4.9] and [4.12] it becomes clear that in order to be able to carry out the required integrations, one has to know all three flux types at each wavelength, and the diffuse fluxes also at all 60 depth levels. In order to determine these fluxes, first the atmospheric parameters from MODTRAN4 are combined with the hemispherical canopy reflectances computed by means of 4SAIL in order to establish the direct solar and diffuse sky irradiances at the canopy top. This gives:

$$E_{\mathrm{sun}} = \tau_{ss}^a E_s^o \cos\theta_s \qquad [4.13]$$

$$E_{\text{sky}} = \frac{\tau_{sd}^{a} + \tau_{ss}^{a} r_{sd} \rho_{dd}^{a}}{1 - r_{dd} \rho_{dd}^{a}} E_{s}^{o} \cos\theta_{s} \qquad [4.14]$$

where

E_{s}^{o} = extraterrestrial spectral solar irradiance
E_{sun} = top-of-canopy spectral solar irradiance
E_{sky} = top-of-canopy spectral sky irradiance
τ_{ss}^{a} = direct transmittance of the atmosphere for sunlight
τ_{sd}^{a} = diffuse transmittance of the atmosphere for sunlight
ρ_{dd}^{a} = spherical albedo of the atmosphere
r_{sd} = hemispherical canopy reflectance for direct solar incident flux
r_{dd} = hemispherical canopy reflectance for diffuse incident flux

Eq. [4.14] suggests that the sky irradiance is partly a function of the target reflectance. This is true under the assumption that the surroundings of the target pixel consist of the same material. If this is known to be not the case, then the hemispherical surface reflectance factors should be replaced by those of the surroundings. The extraterrestrial solar irradiance and the three effective atmospheric parameters (with superscript *a*) are obtained from three MODTRAN4 runs (for surface albedos of 0, 0.5 and 1, respectively) as explained in Verhoef & Bach (2003).

The next step is computing the internal diffuse fluxes inside the canopy layer. This is accomplished by making use of several auxiliary output quantities provided by the 4SAIL model. In the terminology of this model the diffuse fluxes are expressed by:

$$E^{-}(x) = [T_1(x) + r_{\infty} T_2(x)]/(1 - r_{\infty}^{2})$$
$$E^{+}(x) = [r_{\infty} T_1(x) + T_2(x)]/(1 - r_{\infty}^{2})$$

where r_{∞} is the bi-hemispherical canopy reflectance for infinite optical thickness, and the functions $T_1(x)$ and $T_2(x)$ are linearly transformed fluxes given by:

$$T_1(x) = \delta_1 \, \mathrm{e}^{mLx} + (s' + r_{\infty} s) J_1(x) E_s(0)$$
$$T_2(x) = \delta_2 \, \mathrm{e}^{-mL(1+x)} + (r_{\infty} s' + s) J_2(x) E_s(0)$$

Here s and s' are the SAIL (back- and forward) scattering coefficients for sunlight, $E_s(0)$ is the top-of-canopy direct solar flux, *m* is the positive eigenvalue of the diffuse flux system of differential equations, $J_1(x)$ and $J_2(x)$ are special combinations of exponential functions that are numerically safe by pro-active interception of singularities, and δ_1 and δ_2 are constants that are determined by the boundary conditions, given by the diffuse fluxes at the top and the bottom of the canopy.

Once the radiance at the top of the canopy is known, the top-of-atmosphere (TOA) radiance can also be estimated. This is particularly useful for signal analysis studies to evaluate a spaceborne fluorescence mission. For this, one needs three more atmospheric parameters,

which can also be extracted from the output of the three MODTRAN4 runs. Then the TOA radiance is obtained from

$$\pi L_o^{\mathrm{TOA}} = \rho_{so}^a E_s^o \cos\theta_s + \tau_{do}^a E_{\mathrm{upw}} + \tau_{oo}^a \pi L_o^{\mathrm{TOC}} \qquad [4.15]$$

where

E_{upw} = upwelling diffuse flux from target and surroundings at TOC level
L_o^{TOC} = top-of-canopy radiance
τ_{oo}^a = direct atmospheric transmittance in the observer's direction
τ_{do}^a = diffuse transmittance of the atmosphere in the observer's direction
ρ_{so}^a = bi-directional reflectance of the atmosphere

The upwelling diffuse flux E_{upw} is responsible for the atmospheric adjacency effect, and in the program *FluorSAIL* it is computed for surroundings of bare soil, and for the case of an extensive target, so that the surroundings can be considered the same as the target. It is given by:

$$E_{\mathrm{upw}} = \frac{r_{sd} E_{\mathrm{sun}} + r_{dd} E_{\mathrm{sky}}}{E_{\mathrm{sun}} + E_{\mathrm{sky}}} \qquad [4.16]$$

As *FluorSAIL* assumes a Lambertian soil reflectance, in the case of bare soil surroundings both above hemispherical reflectances are taken equal to the soil's reflectance factor. For the case of the extensive target they are taken from the associate reflectance factors computed by 4SAIL, so fluorescence from the surroundings is not taken into account here.

4.2. Simulations for specific scenarios on the model

First some results from MODTRAN4 simulations are illustrated in Fig. 4.2.1. Here the solar and sky spectral irradiances are shown at 1 nm resolution for a solar zenith angle (sza) of 30 degrees and 23 km visibility. All relevant MODTRAN4 input data for this simulation are summarized in Table 4.2.1. Figures 4.2.2 and 4.2.3 show internal radiation profiles for a canopy with an LAI of 4 as computed by means of the model 4SAIL. The fluxes are shown at the top and the bottom of the canopy, and at three intermediate levels. From Fig. 4.2.3 it becomes clear that the direct solar flux changes only in magnitude, not in spectral shape. Fig. 4.2.4 shows the profiles for the diffuse downward flux inside the canopy. This clearly demonstrates that the diffuse flux changes not only in magnitude, but also in spectral shape. Due to the selective absorption of radiation by the leaf canopy the spectral signature changes gradually from the blue sky top-of-canopy irradiance spectrum into a typical green vegetation signature. Especially the blue radiation is quickly absorbed, so that in the deeper layers it contributes less to fluorescence.

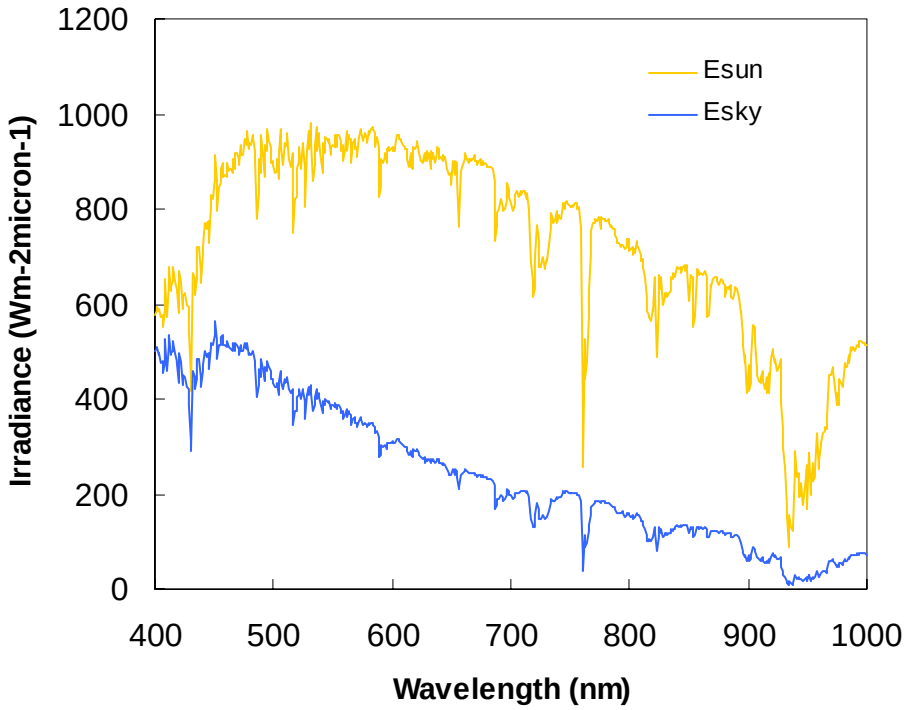

Figure 4.2.1. Direct solar and diffuse sky irradiance spectra at 1 nm resolution derived from MODTRAN4 for solar zenith angle of 30 deg and 23 km visibility.

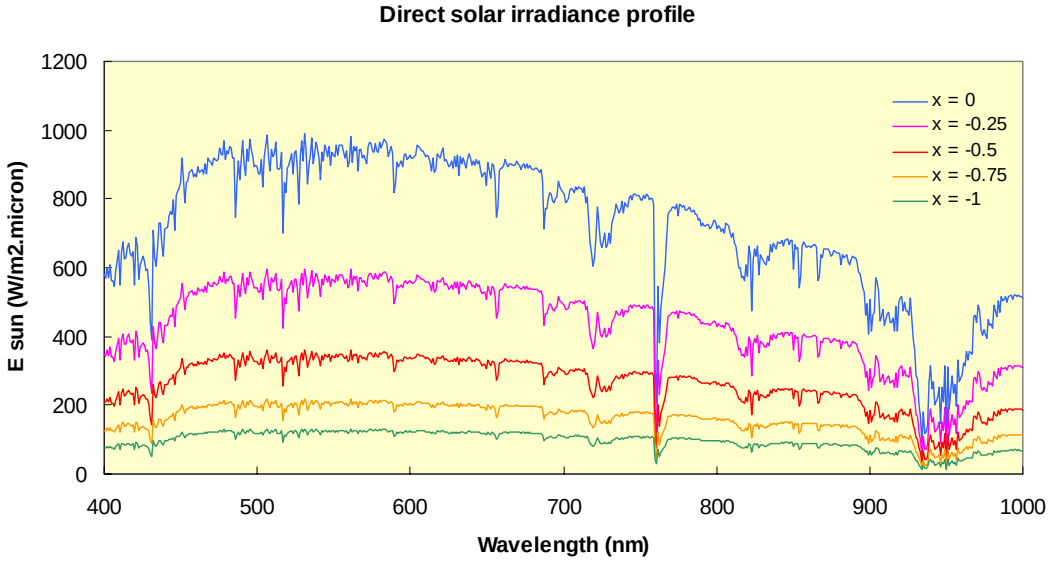

Figure 4.2.2. Internal vertical profile of direct solar irradiance spectrum in a vegetation canopy.

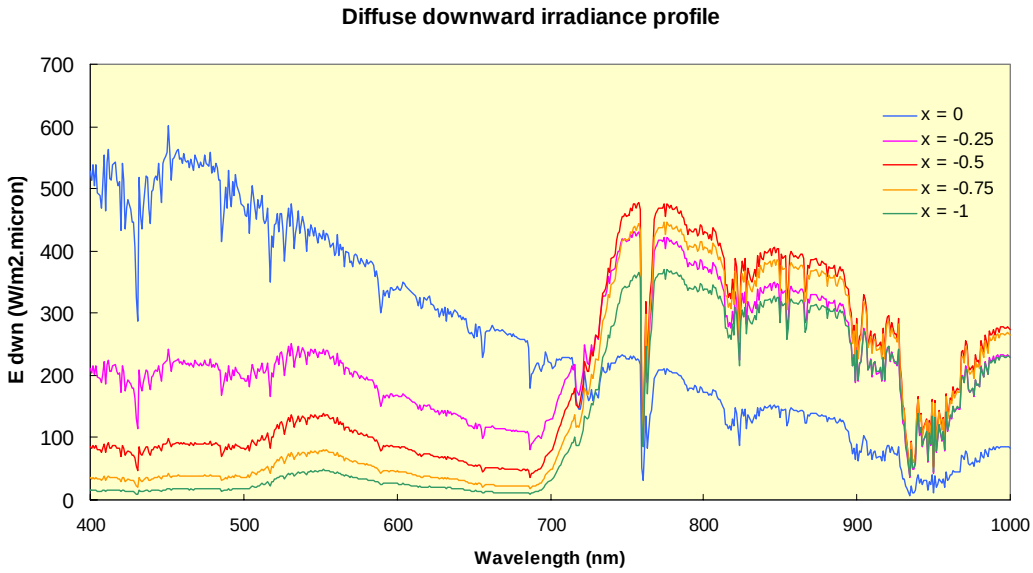

Figure 4.2.3. Internal vertical profile of downward diffuse irradiance spectrum in a vegetation canopy as computed according to the 4SAIL model.

Table 4.2.1. Input parameters and options for MODTRAN4.

Parameter	**Value**
Atmospheric profile	Mid-latitude summer
Use DISORT	Yes
Azimuth dependence	Yes
Number of streams	4
CO2 mixing ratio	365 ppm
Aerosol extinction model	Rural
Stratospheric aerosol	Background profile and extinction
Visibility	23 km
Sensor altitude	674 km
Target altitude	0 km
Aerosol phase functions	Internal Mie-generated
Day of year	162
Spectral range	400 – 1000 nm
Interval	1 nm
FWHM	1 nm
Slit function	Gaussian

Figures 4.2.4 to 4.2.6 show the computed bi-directional canopy reflectance factor (BRF) and the fluorescence contribution for the same solar zenith angle and visibility and for a nadir viewing angle. The modelled BRF is similar to the reflectance that would be measured in the field, i.e., by using an ideal white Lambertian reference panel. The leaf model input data are given in Table 4.2.2 and the canopy model input data (including PAR-dependence parameters) in Table 4.2.3. In Fig. 4.2.4 the contribution of fluorescence is best visible in the chlorophyll absorption band at 670 nm and in the atmospheric oxygen absorption band at 760 nm. A closer look in Fig. 4.2.5 shows that in the red part of the spectrum fluorescence induces an apparent shift of the chlorophyll absorption maximum from 675 to 665 nm, and an increased signal at 680 nm of about 0.5% reflectance, which relative with respect to the pure reflectance means an increase of nearly 25%. Fig. 4.2.6 shows that in the region from 750 to

770 nm similar apparent increases are found, but in the oxygen absorption band at 761 nm the increase is approximately doubled to about a 1% reflectance increase, causing a significant peak in the apparent reflectance at this wavelength.

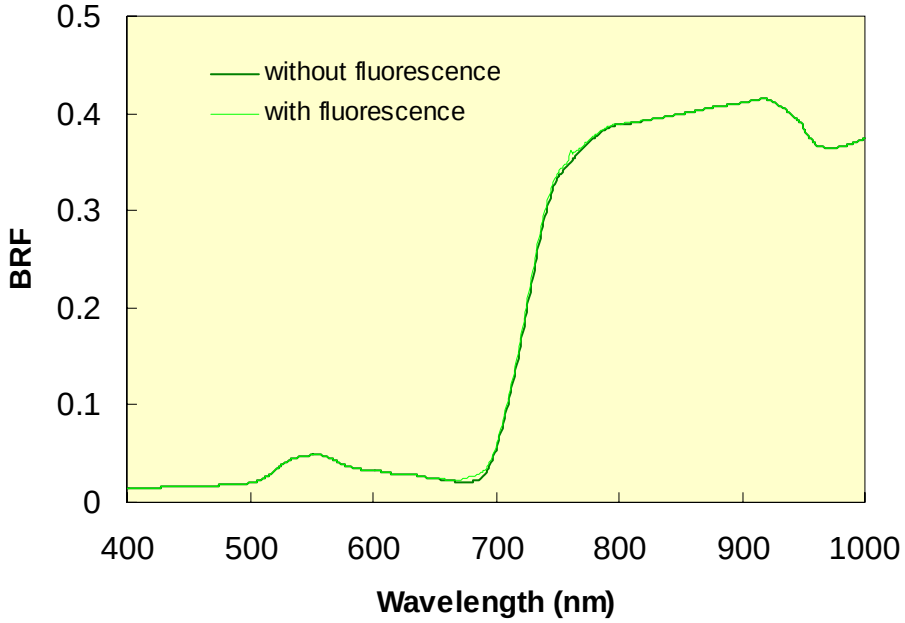

Figure 4.2.4. Spectrum of the canopy bi-directional reflectance factor (BRF) with and without fluorescence.

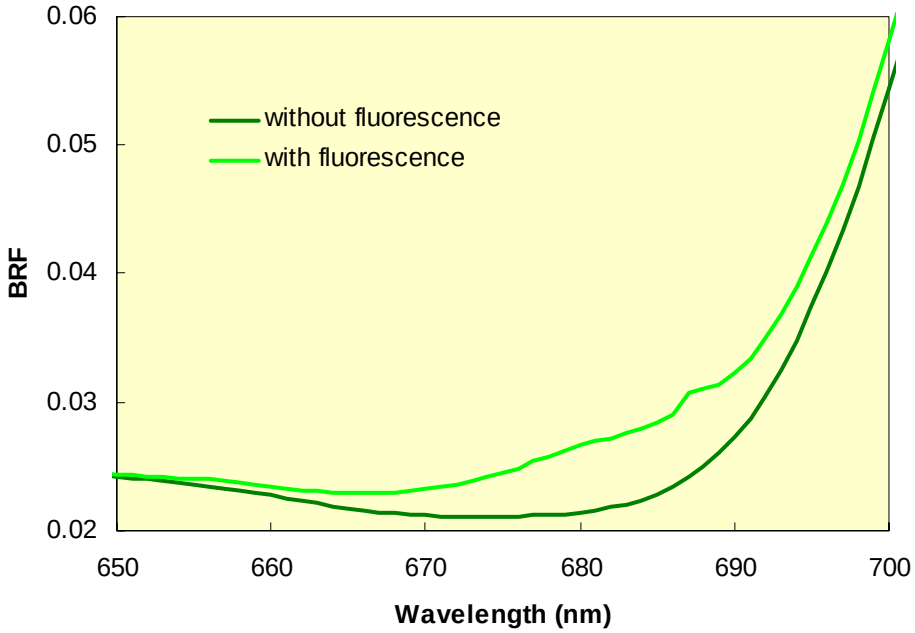

Figure 4.2.5. Same as Fig. 4.2.4, but for detail close to the red edge.

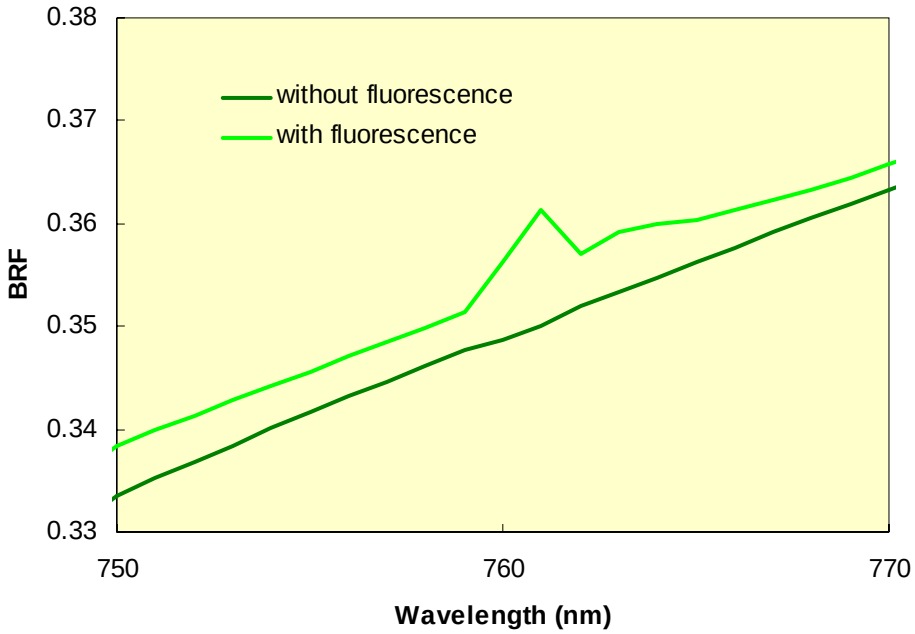

Figure 4.2.6. Same as Fig. 4.2.4, but for detail in the oxygen absorption band.

Table 4.2.2. Input parameters for the leaf fluorescence model.

Parameter	**Value**
Internal structure parameter *N*	1.5
Chlorophyll ab	50
Leaf water	0.025
Dry matter	0.01
Fluorescence efficiency factor	0.04
Temperature	20 C
Species	2 (bean)
Stoichiometry PSII / PSI	2.0 (high light)

Table 4.2.3. Input parameters for *FluorSAIL* canopy model (including PAR-dependence constants).

Parameter	**Value**
LAI	4
LIDF	spherical (a = –0.35, b = –0.15)
Hot spot size parameter	0.1
bP (heat dissipation constant)	0.0035
re (electron transport resistance)	0.005

How the radiance spectrum that would be measured on the ground is influenced by fluorescence is shown in Figures 4.2.7 (overall spectrum) and 4.2.8 (detail from 640 to 700 nm). Especially from Fig. 4.2.8 it becomes obvious that, according to the present leaf model and the assumed fluorescence quantum efficiency, in the so-called Hα Fraunhofer line at 656 nm the fluorescence signal is still quite modest, about 0.15 $\mathrm{mWm^{-2}nm^{-1}sr^{-1}}$. However, at 685 nm (Fraunhofer line Fe I) a radiance increase of nearly 2 $\mathrm{mWm^{-2}nm^{-1}sr^{-1}}$ due to fluorescence is possible for a quantum efficiency of 0.04.

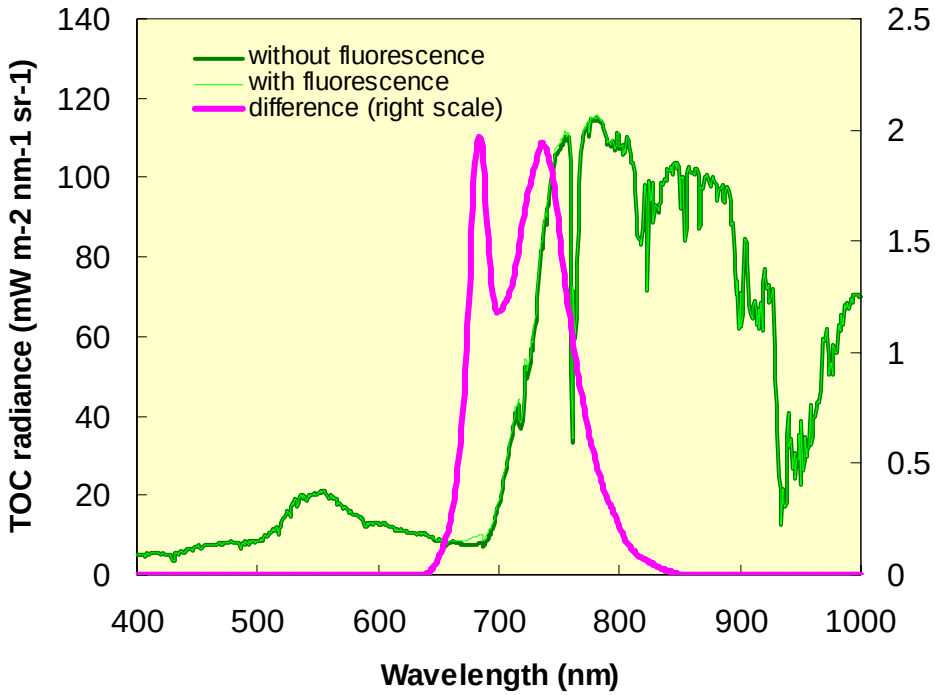

Figure 4.2.7. Top-of-canopy radiance spectra with and without fluorescence.

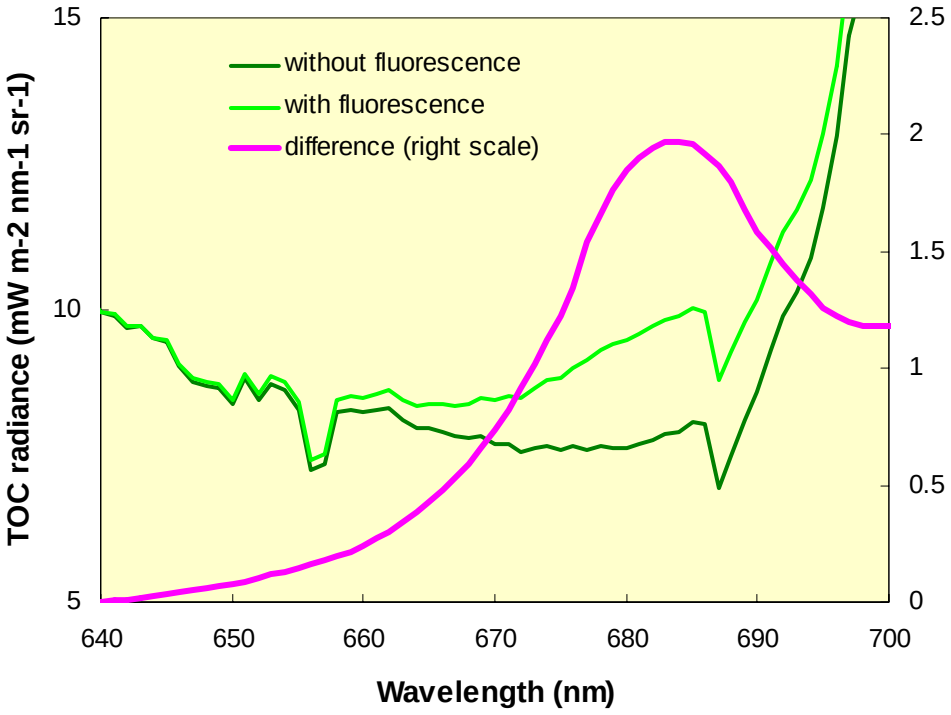

Figure 4.2.8. Same as Fig. 4.2.7, but for detail close to the red edge.

On the ground the fluorescence spectrum is relatively smooth due to the integration over the excitation wavelengths. However, spectral smoothness is partly lost again for observations from space, as illustrated in Figures 4.2.9 and 4.2.10, which show the top-of-atmosphere radiances under otherwise the same conditions as in Figures 4.2.7 and 4.2.8. The fluorescence radiance signals for TOC and TOA observations are compared in Fig. 4.2.11. From this it can be concluded that maximum TOA fluorescence is found at wavelengths of about 683 nm and 740 nm and in both cases the contribution to the total radiance is about 1.5 $\mathrm{mWm^{-2}nm^{-1}sr^{-1}}$.

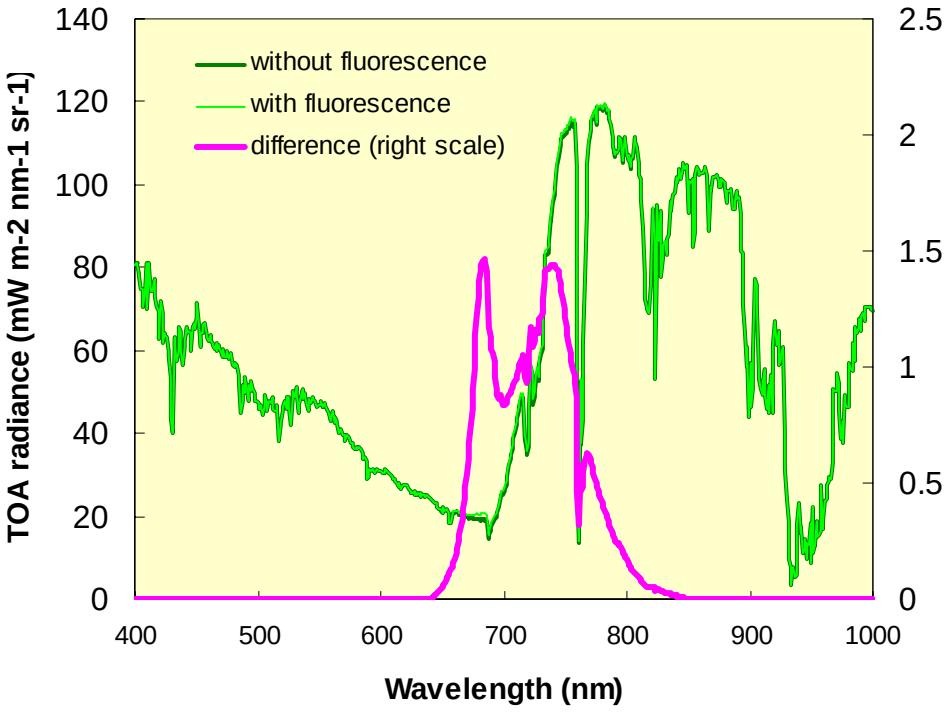

Figure 4.2.9. Top-of-atmosphere radiance spectra with and without fluorescence, nadir viewing.

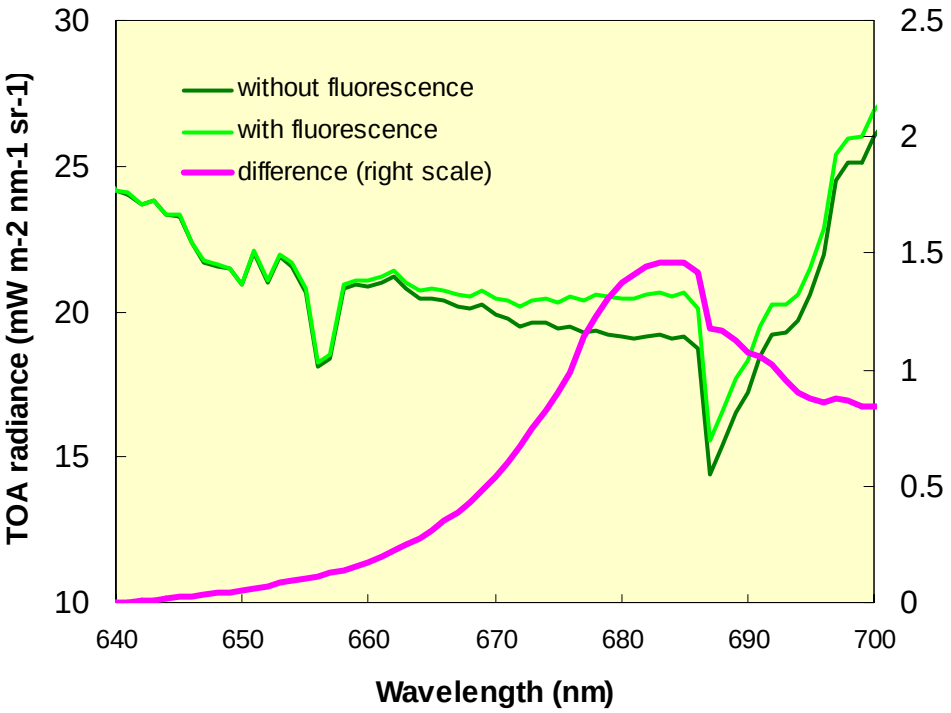

Figure 4.2.10. Same as Fig. 4.2.9, but for detail close to the red edge.

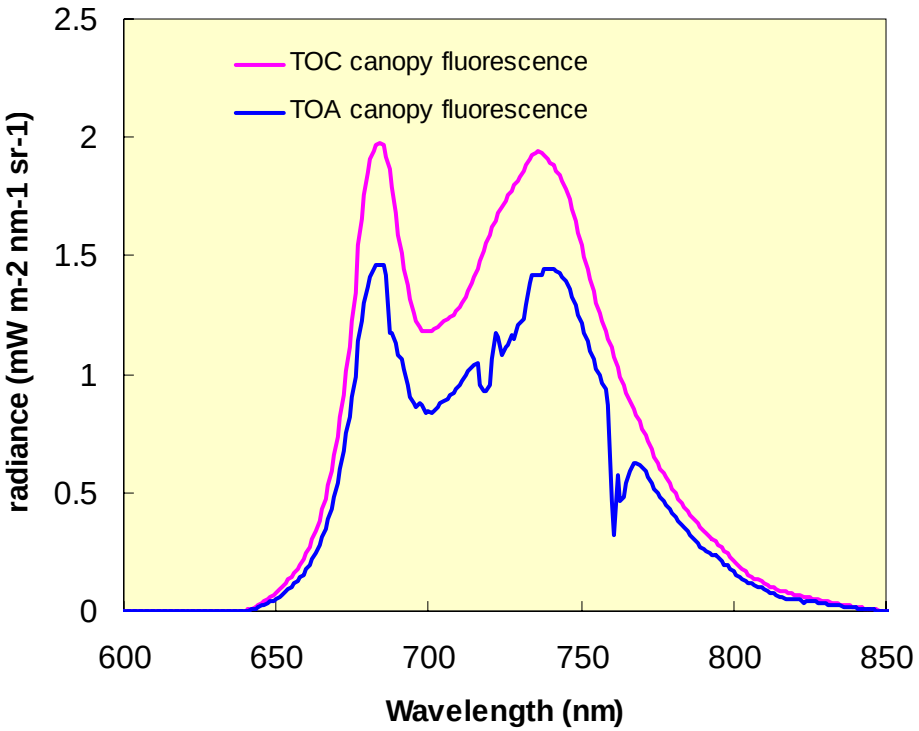

Figure 4.2.11. Comparison TOC and TOA fluorescent radiance spectra.

Finally the simulation results for fluorescence detection in the oxygen atmospheric absorption band at 761 nm are discussed in some more detail. Figures 4.2.12 and 4.2.13 show simulated measurements of the directional reflectance factor on the ground under 45 degrees viewing zenith angle, but for two different relative azimuth directions. Fig. 4.2.12 is for zero relative azimuth (this is with the sun at the back of the observer) and Fig. 4.2.13 for a relative azimuth of 180 degrees (this is with the sun opposite of the viewing direction). In Fig. 4.2.12 the fluorescence peak is somewhat more pronounced and the reflectance levels are higher than in Fig. 4.2.6, which was for nadir viewing, but otherwise the behaviour is similar. However, in Fig. 4.2.13 one can observe a dip in the pure reflectance curve at 761 nm, which is filled up by fluorescence, but effectively the fluorescence peak is nearly neutralized and therefore it becomes practically unobservable. By this it is demonstrated that sharp atmospheric absorption bands not only increase the relative contribution of fluorescence in the measured surface reflectance, but also induce fluctuations in the pure reflectance spectrum (without fluorescence) which, depending on the particular angular geometry, are able to neutralize the effects of fluorescence.

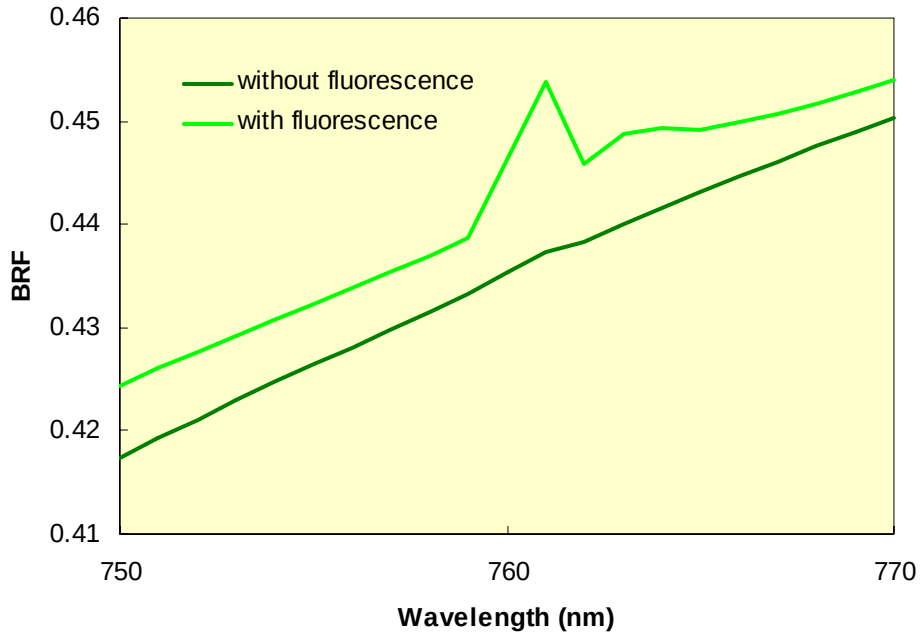

Figure 4.2.12. Detail BRF in the oxygen band for vza = 45 deg and raa = 0 deg (backscattering side in the principal plane).

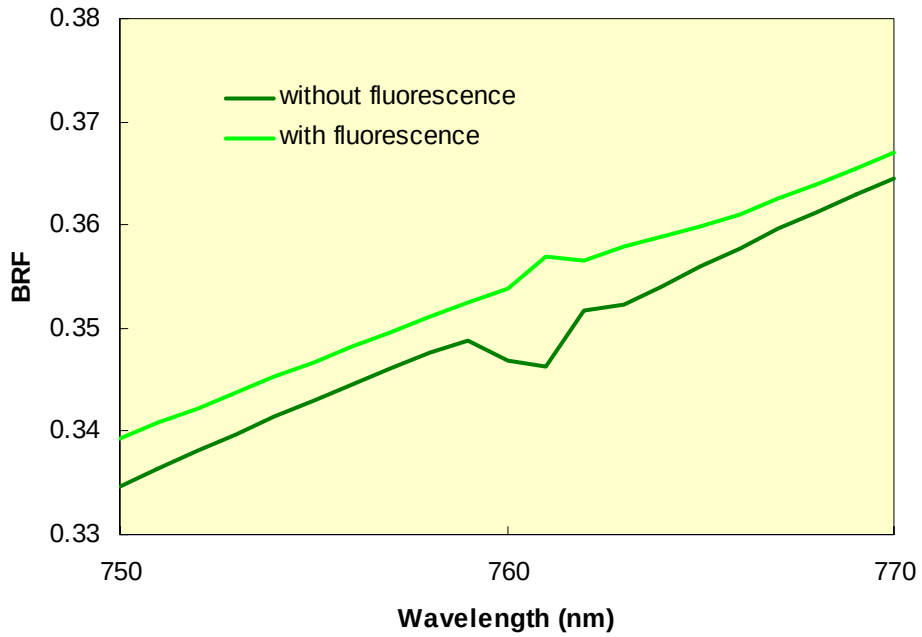

Figure 4.2.13. Detail BRF in the oxygen band for vza = 45 deg and raa = 180 deg (forward scattering side in the principal plane).

One might wonder why atmospheric absorption bands would be able to cause fluctuations in the measured bi-directional reflectance factor (BRF) on the ground, since such a measurement is relative and (ideally) simultaneous to the one of a reference panel. After all, for object and reference panel the incident flux is reduced by the same amount. However, it has been found from the MODTRAN4 results that even the fraction incident sky radiation shows fluctuations related to atmospheric absorption. This is illustrated in Fig. 4.2.14. Below

550 nm the fraction sky irradiance is a smooth function of wavelength, but especially from 680 nm onwards absorption bands show up clearly in the spectrum. One of the strongest dips occurs in the oxygen band at 761 nm. At this wavelength the fraction sky irradiance shows an abrupt decrease, and since the measured BRF is a weighted average of the BRFs for direct solar flux and diffuse incident flux, the weight of the direct solar component suddenly increases here. Depending on the difference between both reflectance components, either an increase or a decrease of the measured BRF will be found. In Fig. 4.2.15 both reflectance components are shown as a function of the viewing zenith angle in the principal plane as computed with 4SAIL, and for otherwise similar object properties. Especially on the right side of the principal plane (vza positive) diffuse incident flux is reflected more strongly than direct solar flux, which means that if the proportion of diffuse incident flux suddenly drops, also the weighted sum will suddenly drop, and this is exactly what is observed in Fig. 4.2.13. However, at the canopy hot spot (vza = –30 deg in Fig. 4.2.15) the reflectance for sunlight is much higher than the one for diffuse incident flux, so here the magnitude of the effect will be much stronger and also in the opposite direction. Here a relatively high positive peak at the absorption wavelength can be expected, which however should mainly be attributed to BRDF effects, in addition to fluorescence.

The phenomenon of atmospheric absorption bands showing up in the fraction sky irradiance is most likely to be dependent on the solar zenith angle. For relatively small solar zenith angles such as in the case illustrated above (sza = 30 degrees) direct sunrays travel through the atmosphere along a shorter path than the average scattered flux would, so this explains why direct sunrays are absorbed less. For large solar zenith angles (greater than 60 degrees) probably the opposite behaviour would be found.

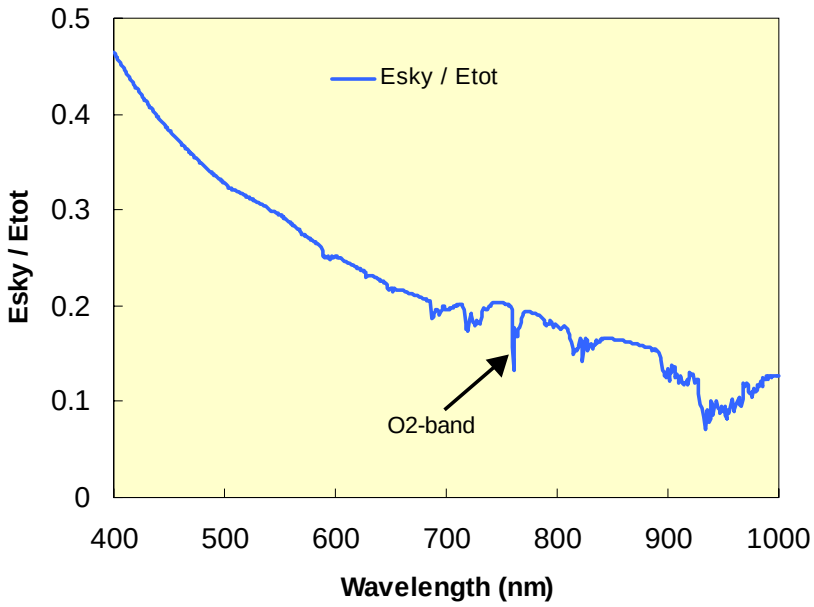

Figure 4.2.14. Spectrum of the fraction diffuse incident radiation. Note that atmospheric absorption bands still cause fluctuations in this fraction.

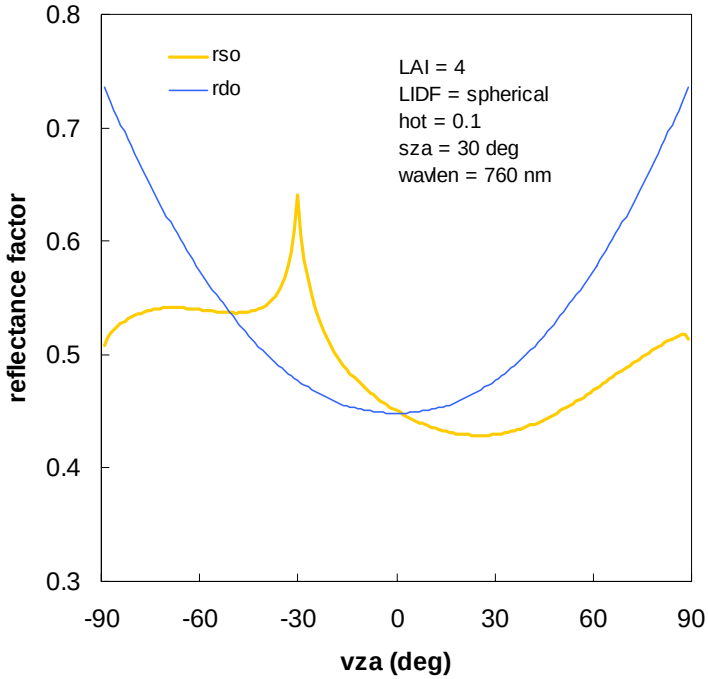

Figure 4.2.15. Directional reflectance factors for direct solar flux (rso) and diffuse incident flux (rdo) in the principal plane for sza = 30 degrees and a similar canopy object as computed with 4SAIL model.

4.3. Conclusion

It can be concluded that the new canopy fluorescence model allows the investigation of quite subtle interactions between atmospheric absorption on one hand and the directional fluorescence and BRDF effects on the other. This is necessary for a correct interpretation of *in-situ* measurements and airborne or spaceborne hyperspectral radiance data obtained under passive illumination conditions.

5. GRAPHIC USER INTERFACE for the SPECTRAL SIMULATION of LEAF and CANOPY CHLOROPHYLL FLUORESCENCE: *FluorMODgui* V3.0

5.1 Introduction

The *FluorMODgui* V3.0 Graphic User Interface (GUI) presented here provides a seamless link between inputs and outputs required for running both *FluorMODleaf* and *FluorSAIL* models, facilitating consistent user interaction and enabling the setup of multiple runs to simulate diurnal effects under different viewing geometries. This chapter provides a description of the graphic interface that will be used as a tool for leaf and canopy model validation through the use of existing and future field datasets in the context of this ESA project and the interested scientific community. This interface developed under the FluorMOD project can facilitate the testing of various remote sensing detection scenarios for future airborne and spaceborne fluorescence missions.

5.2. Graphic user interface for the linked leaf-canopy fluorescence model

The FluorMOD Graphic User Interface (*FluorMODgui* V3.0) is developed in Visual Studio .net framework with Visual Basic code (Microsoft, Redmond, WA, USA) compiled into an executable file to run under Microsoft Windows XP operating system. A general view of the GUI can be seen in Figure 5.2.1, showing four main parts: i) *Menu Area* for full control of the interface; ii) *Irradiance File and PAR Dependence* input area; iii) *Leaf Model Area* for inputs and graphic outputs to run the *FluorMODleaf* model; and iv) *Canopy Model Area* for inputs and graphic outputs to run the *FluorSAIL* model.

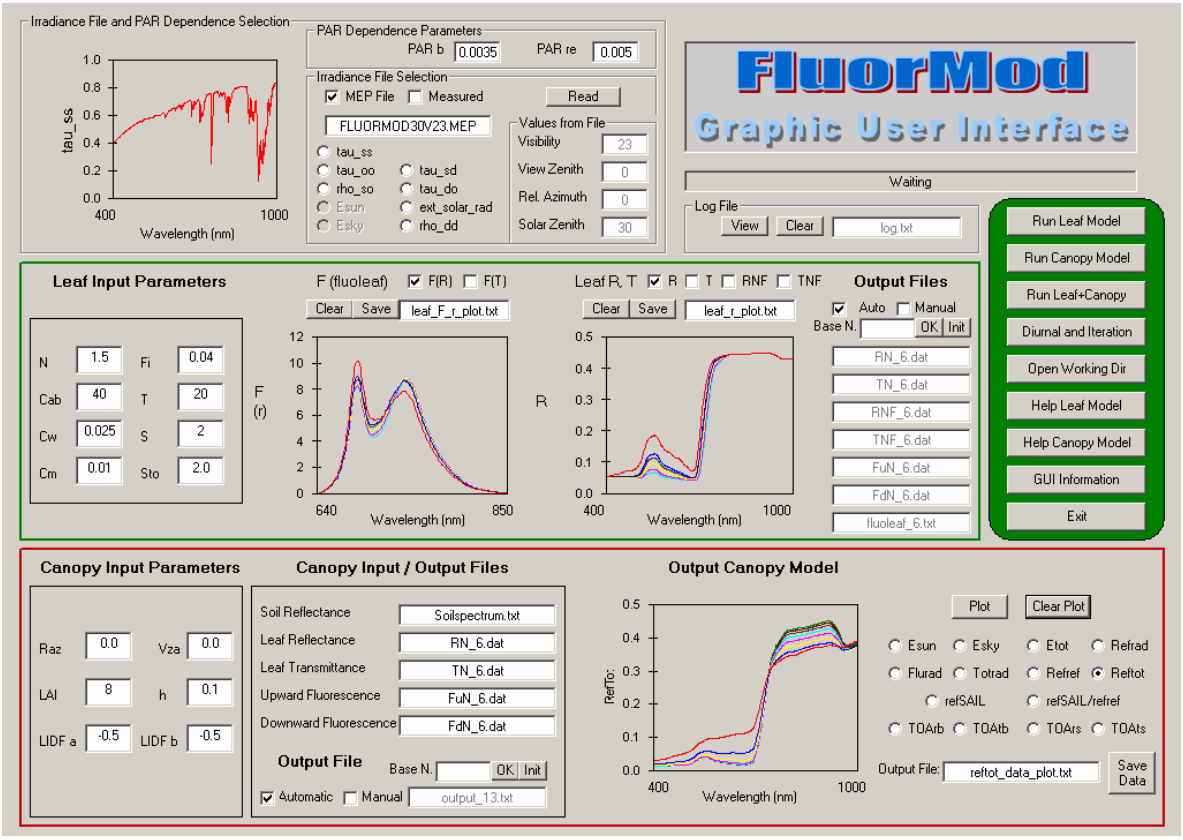

Figure 5.2.1. General view of the FluorMOD Graphic User Interface.

The *Menu Area* for full control of the interface enables the running of the leaf model or canopy model independently, or both linked together in a single run. In addition, both leaf and canopy models can be executed through a *Diurnal and Iteration Tool* to simulate the diurnal effects of a changing viewing geometry, atmospheric characteristics, and typical leaf temperature variations along the course of a day. The *Multiple Iteration Execution* option enables the execution of the models iterating a selected leaf or canopy variable as in batch processes. Other options in the *Menu Area* are tools for the user such as opening the working directory where all input and output files are stored, providing help buttons for the leaf and canopy models and GUI interface.

The *Irradiance File and PAR Dependence* input area is comprised of two subsections, one for the PAR dependence parameters, and another for the *Irradiance File Selection* with a text window for the name of the input irradiance file, with plotting capabilities. This *Irradiance File and PAR Dependence* input area is common for both the leaf and the canopy-level models.

Other main areas of the Graphic User Interface are i) the *Leaf Model Area* and ii) the *Canopy Model Area,* designed to enable the specification of leaf and canopy inputs and generation of graphic outputs with plotting capabilities. These two areas of the interface along with the *Irradiance File and PAR Dependence* input area will be described in detail in the following sections.

The *FluorMODgui* provides a convenient link between the leaf and canopy models, with proper input/output file naming and data structure. Some of the capabilities incorporated enable: error handling on file opening; an automatic and manual output naming system; a base-name input window for a flexible file naming system; help files provided in text form for both the leaf and canopy models; a direct link with the working directory to access input and output files; a *status screen* showing when the leaf or canopy model is running, disabling execution buttons in such case; graphs with plot capability for multiple series, to enable visualizations of comparisons and trends; data from plots with multiple series can be saved in a single text file for easy comparison between different model runs; a log file viewing button enables loading a text file where all inputs used for running the leaf and canopy model are stored; finally, a pop-up window with contact information for the leaf, canopy model and GUI authors is available.

5.2.1. Atmospheric and illumination inputs

The *Irradiance File and PAR Dependence* input area (Figure 5.2.2) is comprised of two subsections, one for the PAR dependence parameters, and another for the *Irradiance File Selection*. The *Irradiance File Selection Area* enables a selection of the irradiance file that will be used in the simulations. If the *MEP File* option is selected, a MEP file format from MODTRAN-4 will be used as input for the simulations, enabling the graphic view of the input file data. The beginning of each MEP file is a copy of the associated so-called ".tp5" file used as input for MODTRAN-4, containing among others the values for visibility, and solar zenith, view zenith and relative azimuth angle. The MEP file contains effective optical parameters in the 400-1000 nm spectral range such as the direct transmittance in sun direction (tau_ss), direct transmittance in view direction (tau_oo), diffuse transmittance for sunlight (tau_sd), diffuse transmittance in view direction (tau_do), atmospheric path reflectance (rho_so),

spherical albedo (rho_dd), and the extraterrestrial radiance of a white horizontal plane (ext_solar_rad) in $mW \cdot cm^{-2} \cdot \mu m^{-1} sr^{-1}$.

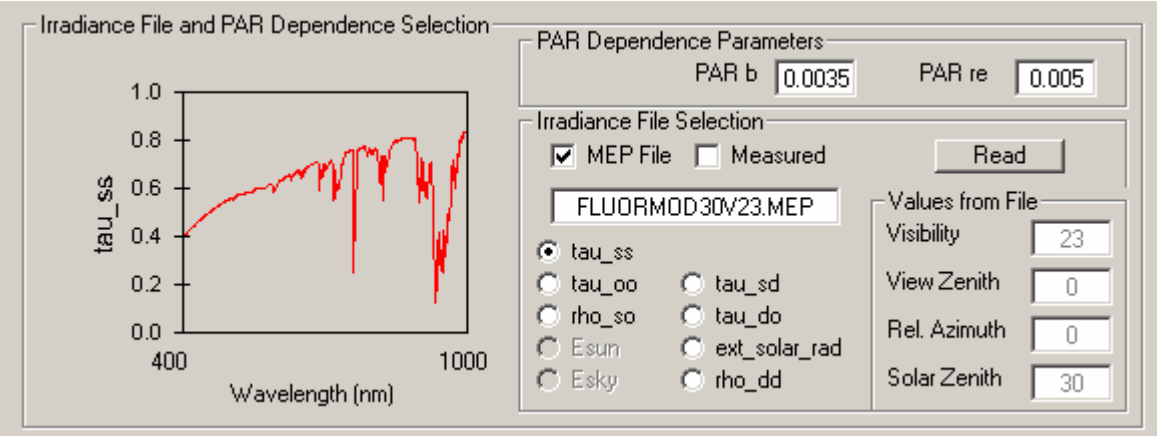

Figure 5.2.2. View of the Atmospheric File input area of the FluorMOD Graphic User Interface.

If the *Measured* option is selected, simulations will be conducted with collimated (direct solar) irradiance (Esun) and diffuse (sky) irradiance (Esky) measured by the user in $W \cdot m^{-2} \cdot \mu m^{-1}$. The description of the input parameters for the atmospheric and illumination conditions for *FluorMODleaf* and *FluorSAIL* models can be seen in Table 5.2.1. Plotting capabilities enable visualization of the MODTRAN-simulated MEP file or the measured illumination file used as input for simulations. In addition, the file header from the MEP or measured irradiance files is read to show the visibility, view zenith, relative azimuth, and solar zenith angles for which the MODTRAN simulated file was produced or the user irradiance file was measured.

The *PAR Dependence* input area allows specification of the electron transport resistance (PAR_{re}) and heat dissipation constant (PAR_b), which relates the *Photosynthetic Active Radiation* (PAR) with the rate constant for dissipation and the lowest value of this constant for dissipation. The combination of PAR_{re} and PAR_b parameters is used to relate PAR and fluorescence (Rosema et al., 1998). The PAR_{re} and PAR_b parameters are used in *FluorMODleaf* model to simulate leaf reflectance and transmittance with added fluorescence effects, and in *FluorSAIL* to generate canopy reflectance with the fluorescence addition.

Table 5.2.1. Input parameters for the atmospheric and illumination conditions for *FluorMODleaf* and *FluorSAIL* models.

Parameter	Description	Range	Units
MEP File from MODTRAN	*Atm. Simulation with MODTRAN*		
tau_ss	Direct transmittance in sun direction	-	-
tau_oo	Direct transmittance in view direction	-	-
tau_sd	Diffuse transmittance for sunlight	-	-
tau_do	Diffuse transmittance in view direction	-	-
rho_so	Atmospheric path reflectance	-	-
rho_dd	Spherical albedo	-	-
ext_solar_rad	Extraterrestrial radiance of a white Lambertian horizontal panel	-	$mW \cdot cm^{-2} \cdot \mu m^{-1} sr^{-1}$
Measured Irradiance File	*Irradiance measurements made*		
Esun	Direct solar irradiance at the surface	-	$W \cdot m^{-2} \cdot \mu m^{-1}$
Esky	Diffuse sky irradiance at the surface	-	$W \cdot m^{-2} \cdot \mu m^{-1}$
PAR Dependence	*PAR dependence parameters*		
PAR_{re}	Electron transport resistance	0-1	-
PAR_b	Heat dissipation constant	0-1	-

5.2.2. The *FluorMODleaf* leaf model interface

The *FluorMODleaf* Leaf Model Interface area (Figure 5.2.3) is comprised of: i) a *Leaf Input Parameters* area; ii) two graphic outputs with multiple series capability; and iii) a set of text windows where the output files produced by *FluorMODleaf* are shown.

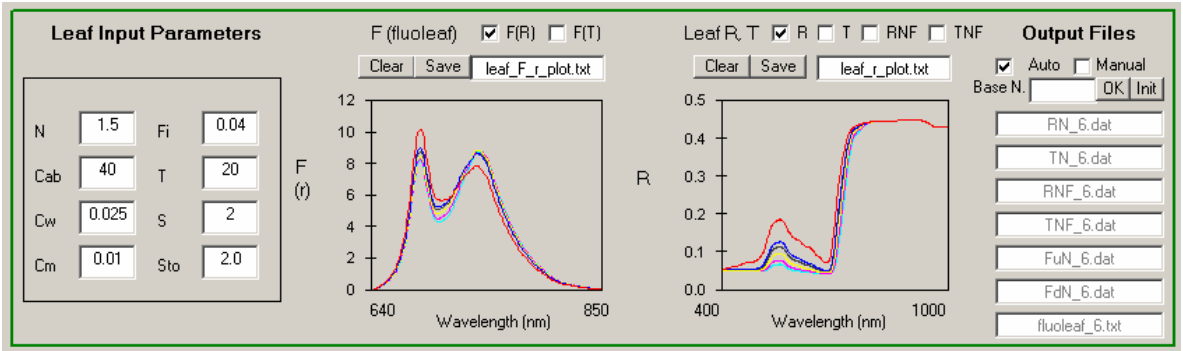

Figure 5.2.3. View of the Leaf Model area of the FluorMOD Graphic User Interface.

The *Leaf Input Parameters* area requires a total of 8 inputs, such as the number of layers in PROSPECT (N); chlorophyll a+b content in $\mu g/cm^2$ (C_{ab}); water equivalent thickness in cm (C_w); dry matter content in µg (C_m); fluorescence quantum efficiency (Fi), from 0 (no fluorescence) to 0.1 (10% fluorescence); leaf temperature in degrees Celsius (T); species temperature dependence (S) (after Agati, 1998), with 1=broad bean; 2=bean; 3=ficus; 4=tomato; and 5=pea; and stoichiometry of PSII to PSI reaction centres (Sto), which depends

on species and light conditions during plant growth, with values for high light around 2 and low light around 1. The inputs for *FluorMODleaf* fluorescence model are shown in Table 5.2.2, including the ranges and units for each parameter considered acceptable according to the model formulation.

Table 5.2.2. Input parameters for *FluorMODleaf* fluorescence model.

Parameter	**Description**	**Range**	**Units**
N	Internal structure parameter	1-3	-
C_{ab}	Chlorophyll a+b	5-100	$\mu g/cm^2$
C_w	Leaf water content	0-0.05	cm
C_m	Dry matter content	0.002-0.02	μg
F_i	Fluorescence quantum efficiency	0-0.1	-
T	Temperature	5-25	ºC
S	Species Temperature Dependence	1: broad bean; 2: bean; 3: ficus; 4: tomato; 5: pea	-
Sto	Stoichiometry of PSII to PSI	high light: Sto ~ 2; low light: Sto ~ 1.1	-

The outputs generated after execution of the *FluorMODleaf* fluorescence model are a set of 7 text files containing the leaf reflectance and transmittance without fluorescence (RN and TN), the leaf reflectance and transmittance with fluorescence (RNF and TNF) using the PAR parameters to produce the fluorescence emission at the leaf level (fluoleaf), and two matrices (FuN and FdN), containing the upward and downward fluorescence matrices corresponding to excitation wavelengths in the 400-750 nm range and fluorescence emission in the 640-850 nm range. Outputs RN, TN, RNF and TNF are generated for the 400-1000 nm range at 1 nm resolution, and fluoleaf fluorescence emission in the 640-850 nm range at 1 nm resolution. The outputs of the *FluorMODleaf* fluorescence model are shown in Table 5.2.3, indicating the spectral ranges and resolution. The output spectral files with the fluorescence emission at the leaf level (fluoleaf) and the reflectance and transmittance with and without the fluorescence emission (RN, TN, RNF and TNF) can be plotted in the leaf model area of the GUI, enabling the displaying of multiple series for comparison purposes. An automatic or manual-naming scheme for the leaf files generated can be selected using a specific base name for each simulation experiment. The graphs with multiple series plotted can be saved in a text file containing the same series displayed on the plot. This capability avoids the need to load every single output from a set of simulations for a given parameter. Outputs from *FluorMODleaf* model required as inputs for the *FluorSAIL* canopy model are automatically updated in the input windows of the *FluorSAIL* interface area described in the next section.

Table 5.2.3. Outputs from *FluorMODleaf* fluorescence model.

File	Description	Range
RN.dat	Leaf Reflectance without Fluorescence	400-1000 nm at 1 nm resolution
TN.dat	Leaf Transmittance without Fluorescence	400-1000 nm at 1 nm resolution
RNF.dat	Leaf Reflectance with Fluorescence	400-1000 nm at 1 nm resolution
TNF.dat	Leaf Transmittance with Fluorescence	400-1000 nm at 1 nm resolution
FuN.dat	Upward Fluorescence matrix	Excitation wavelengths in the 400-750 nm range; fluorescence emission in the 640-850 nm range
FdN.dat	Downward Fluorescence matrix	Excitation wavelengths in the 400-750 nm range; fluorescence emission in the 640-850 nm range
fluoleaf.txt	Solar induced fluorescence	640-850 nm at 1 nm resolution

5.2.3. The *FluorSAIL* canopy model interface

The *FluorSAIL* Canopy Model Interface (Figure 5.2.4) is divided into three different areas with: i) the input area for the canopy parameters; ii) the area for selection of the input spectral files required to run *FluorSAIL*, as well as the name for the output file generated after execution; and iii) a plotting area where the generated output file with different spectral variables can be graphed.

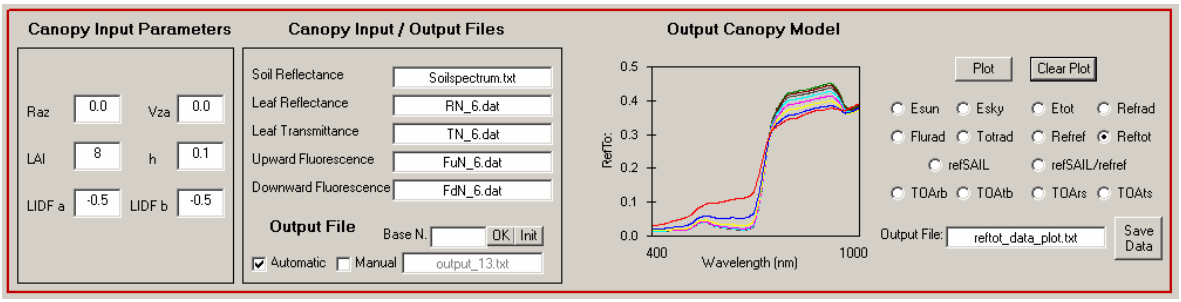

Figure 5.2.4. View of the Canopy Model area of the FluorMOD Graphic User Interface.

The input area for the canopy parameters requires the input for the viewing zenith angle in degrees (Vza), relative azimuth angle in degrees (Raz), the canopy leaf area index (LAI), the hot spot parameter (h), and the leaf inclination distribution function (LIDF) parameters, LIDF*a* and LIDF*b*.

The input spectral files required to run *FluorSAIL* are the soil spectrum file, and the four output files from the *FluorMODleaf* model which are inputs for the canopy model, such as the leaf reflectance without fluorescence (RN), leaf transmittance without fluorescence (TN), and the upward (FuN) and downward (FdN) fluorescence matrices. An output file name containing the simulation results is automatically created, using either the automatic naming system or that manually supplied by the user. Table 5.2.4 shows the input parameters and spectral files required to run the *FluorSAIL* canopy model, describing the parameters and ranges.

Table 5.2.4. Input parameters/files for *FluorSAIL* canopy model.
* abs ($LIDF_a$)+abs($LIDF_b$) < 1 (Verhoef, 1998)

Parameter/File	Description	Range	Units
Raz	Relative Azimuth Angle	0-180	Deg
Vza	Viewing Zenith Angle	0-85	Deg
LAI	Leaf Area Index	0-8	-
h	Hot Spot Size Parameter	0.01-1	-
$LIDF_a$; $LIDF_b$	Leaf Inclination Distribution Function*	spherical (a = –0.35, b = –0.15) planophile (a = 1, b = 0) erectophile (a = –1, b = 0) plagiophile (a = 0, b = –1) extremophile (a = 0, b = 1) uniform (a = 0, b = 0)	
soilspectrum.txt	spectral soil reflectance file	400-1000 nm at 10 nm resol.	-
RN.dat	Leaf Reflectance without Fluorescence in the 400-1000 nm range	400-1000 nm at 1 nm resol.	-
TN.dat	Leaf Transmittance without Fluorescence in the 400-1000 nm range	400-1000 nm at 1 nm resol.	-
FuN.dat	Upward Fluorescence matrix with excitation and fluorescence emission	Excitation wavelengths in the 400-750 nm range and fluorescence emission in the 640-850 nm range	-
FdN.dat	Downward Fluorescence matrix with excitation and fluorescence emission	Excitation wavelengths in the 400-750 nm range and fluorescence emission in the 640-850 nm range	-

The output simulation file after *FluorSAIL* execution contains the solar irradiance in $Wm^{-2}\mu m^{-1}$ (Esun); sky irradiance in $Wm^{-2}\mu m^{-1}$ (Esky); total irradiance in $Wm^{-2}\mu m^{-1}$ (Etot); reference (= without fluorescence) radiance in $Wm^{-2}\mu m^{-1}sr^{-1}$ (refrad); fluorescence radiance in $Wm^{-2}\mu m^{-1}sr^{-1}$ (flurad); total radiance in $Wm^{-2}\mu m^{-1}sr^{-1}$ (totrad); reference reflectance factor (refref); total reflectance factor (including fluorescence) (reftot); reference reflectance factor according to SAIL model (Verhoef, 1984) (refSAIL); ratio SAIL /*FluorSAIL* for reference reflectance factor (ref SAIL /refref); reference top-of-atmosphere radiance for bare soil surroundings in $Wm^{-2}\mu m^{-1}sr^{-1}$ (TOAref_bare); total top-of-atmosphere radiance for bare soil surroundings in $Wm^{-2}\mu m^{-1}sr^{-1}$ (TOAtot_bare); reference top-of-atmosphere radiance for surroundings same as target in $Wm^{-2}\mu m^{-1}sr^{-1}$ (TOAref_same); and total top-of-atmosphere radiance for surroundings same as target in $Wm^{-2}\mu^{-1}sr^{-1}$ (TOAtot_same) (Table 5.2.5).

The plotting area where the generated output file can be graphed enables visualization of any of the 14 spectral parameters generated by *FluorSAIL* execution. Plotting capabilities permit multiple overlays of several model runs into the same canopy output chart. The data from a single or multiple run for any selected output variable can be saved into a text file that can easily be loaded into spreadsheet software for further data analysis. The output canopy simulation chart plot can be cleared at any time to start a new series of runs, also clearing the output text file created with the simulation results.

Table 5.2.5. Description of the output file from *FluorSAIL* canopy model.
*All spectral ranges in 400-1000 nm

Parameter	Description	Units
Esun	Solar irradiance on the ground	$W \cdot m^{-2} \cdot \mu m^{-1}$
Esky	Sky irradiance on the ground	$W \cdot m^{-2} \cdot \mu m^{-1}$
refrad	Reference radiance (without fluorescence) on ground level	$W \cdot m^{-2} \cdot \mu m^{-1} \cdot sr^{-1}$
flurad	Fluorescence radiance on ground level	$W \cdot m^{-2} \cdot \mu m^{-1} \cdot sr^{-1}$
totrad	Total radiance on ground level	$W \cdot m^{-2} \cdot \mu m^{-1} \cdot sr^{-1}$
refref	Reference reflectance on the ground (without fluorescence)	-
reftot	Total reflectance factor on the ground (with fluorescence)	-
refSAIL	Reflectance factor computed analytically with 4SAIL model	-
refSAIL/refref	Ratio included for validation of numerical procedures	-
TOAref bare	TOA reference radiance for bare soil surroundings	$W \cdot m^{-2} \cdot \mu m^{-1} \cdot sr^{-1}$
TOAtot bare	TOA total radiance for bare soil surroundings	$W \cdot m^{-2} \cdot \mu m^{-1} \cdot sr^{-1}$
TOAref same	TOA reference radiance for surroundings same as target	$W \cdot m^{-2} \cdot \mu m^{-1} \cdot sr^{-1}$
TOAtot same	TOA total radiance for surroundings same as target	$W \cdot m^{-2} \cdot \mu m^{-1} \cdot sr^{-1}$

5.3. Diurnal simulation and multiple iteration tool

Two objectives adopted by the FluorMOD science team for validating functionality with the *FluorMODgui* were: i) to facilitate diurnal simulation of effects on canopy reflectance; and ii) to accommodate the execution of multiple runs for selected input variables at specified steps. These two objectives are facilitated by the *Diurnal Simulation and Multiple Iteration Tool* built as a pop-up window that the user can execute from the main menu (Figure 5.3.1). The inputs that the user can modify in the diurnal setup are i) the illumination file, either as a MEP file or a measured irradiance file; ii) the leaf-level model variable temperature (T); and iii) canopy-level variables such as relative azimuth (Raz) and view zenith angles (Vza). Any of these input variables can be set to a fixed value, or ramped up or down as function of a simulated or real diurnal variation measured by the user in the laboratory or in the field.

The *Multiple Iteration Tool* enables the selection of a leaf or canopy variable and set the start, end, and step increment for a multiple simulation. The multiple run and diurnal execution can be started by first clearing the output plot, or by overlaying new output simulation data to the plot. The multiple simulation tool provides the user with information regarding the number of runs to complete as a function of the start, end, and step increments for the given variable, showing the runs left to complete the series of simulations during execution time. The execution process for both the diurnal and multiple iteration can be cancelled at any time by the user.

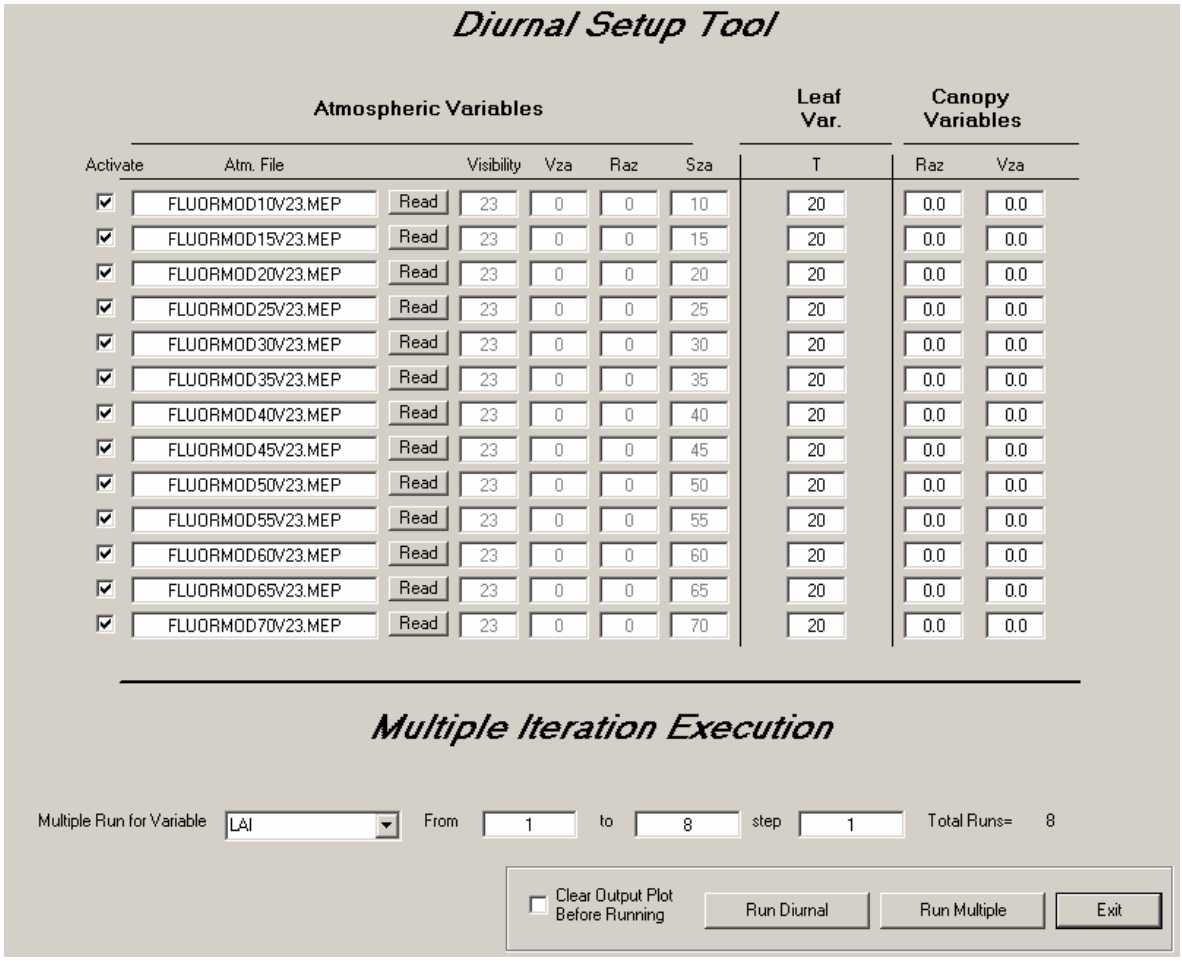

Figure 5.3.1. View of the Diurnal Setup and Multiple Iteration Execution Tools of *FluorMODgui*.

5.4. Simulation results with *FluorMODgui*

The linked *FluorMODleaf* and *FluorSAIL* models through the *FluorMODgui* interface can now be used to simulate the spectral effects of the chlorophyll fluorescence at the leaf and canopy levels. The interface is provided to the user with a set of pre-calculated MODTRAN effective parameter files at 1 nm resolution for solar zenith angles ranging from 10 to 70 degrees and 23 km visibility. The input parameters used to generate the set of MEP files from MODTRAN-4 are shown in Table 5.4.1.

To demonstrate the capabilities of the *FluorMODgui* model, a set of sample simulations were conducted for a range of input parameters. The simulation of upward and downward fluorescence emission spectra at the leaf level as a function of the chlorophyll concentration and quantum fluorescence efficiency are shown in Figure 5.4.1. As expected, the spectral distribution of chlorophyll fluorescence shows that upward emission is greater than downward emission for both levels of chlorophyll concentrations (Figure 5.4.1 a,c for upward; Figure 5.4.1 b,d for downward emission). With increasing chlorophyll concentration from 30 to 80 $\mu g/cm^2$, upward flux decreases slightly for the emission peak maximum centered at 685 nm (that mainly corresponds to PSII), with a slight increase of the peak maximum centered at 740 nm (that mainly corresponds to PSI) (Figure 5.4.1 a,c). On the other hand, the downward flux is highly affected by chlorophyll concentration levels due to

re-absorption effects, generating a substantial decrease in fluorescence emission at 685 nm in the downward flux when chlorophyll fluorescence is high (Figure 5.4.1 b,d).

Table 5.4.1. Input parameters used to generate the MEP files from MODTRAN-4 provided with the interface.

Parameter	**Value**
Atmospheric profile	Mid-latitude summer
Use DISORT	Yes
Azimuth dependence	Yes
Number of streams	4
CO_2 mixing ratio	365 ppm
Aerosol extinction model	Rural
Stratospheric aerosol	Background profile and extinction
Visibility	23 km
Sensor altitude	674 km
Target altitude	0 km
Aerosol phase functions	Internal Mie-generated
Day of year	162
Spectral range	400 – 1000 nm
Interval	1 nm
FWHM	1 nm
Slit function	Gaussian

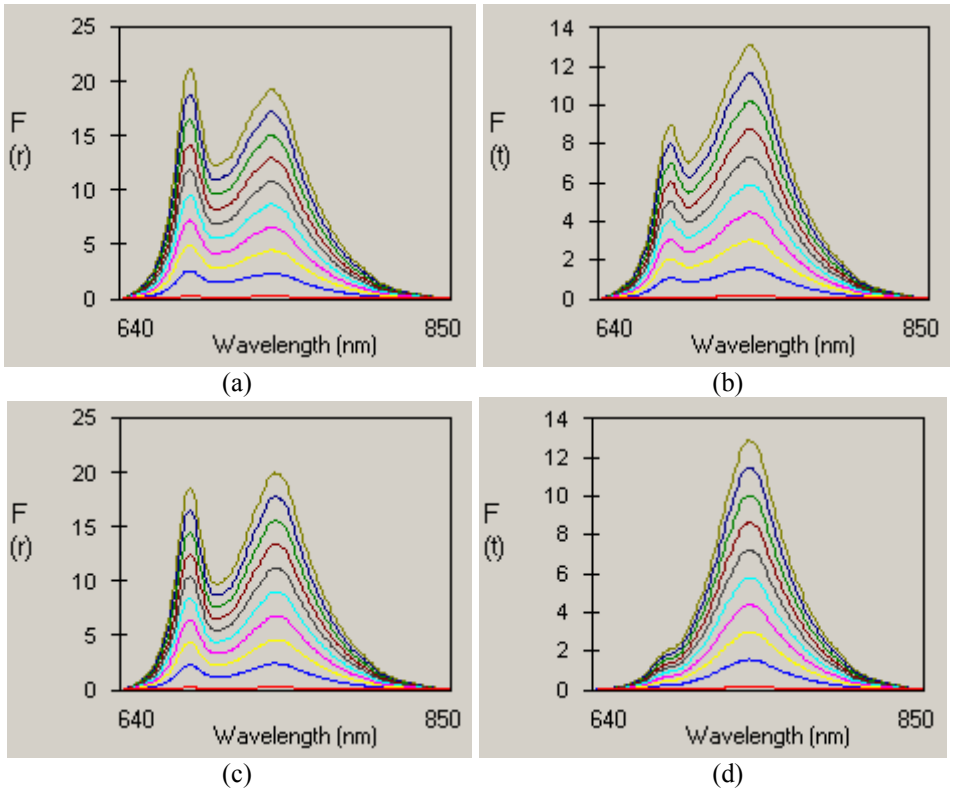

Figure 5.4.1. Chlorophyll fluorescence emission spectra simulated with *FluorMODgui* in upward (a, c) and downward (b, d) direction for C_{ab}=30 µg/cm^2 (a, b) and C_{ab}=80 µg/cm^2 (c, d) for a range of fluorescence quantum efficiencies (Fi=0.001 to 0.1). Other input parameters used for the simulation were N=1.5, Cw=0.025, Cm=0.01, T=20, S=2, Sto=2.0, PARb=0.0035, and PARre=0.005.

The simulated upward and downward spectral fluorescence emission can then be used to generate the leaf reflectance and transmittance with and without the fluorescence effects. Figure 5.4.2 shows the leaf reflectance (Figure 5.4.2a,c) and transmittance (Figure 5.4.2b,d) without (Fi=0) and with (Fi=0.1) fluorescence simulation for low chlorophyll concentration of 30 μg/cm^2 (Figure 5.4.2a,b) and high concentration of 80 μg/cm^2 (Figure 5.4.2c,d). The fluorescence spectra superimposed on top of the reflectance and transmittance can be observed along the red edge spectral region, and more specifically over the chlorophyll absorption maximum at 685 nm and on the reflectance shoulder at 740 nm.

The outputs generated from the *FluorMODleaf* model simulating the spectral fluorescence signature and leaf reflectance and transmittance are then used as input for the *FluorSAIL* canopy model. This linked scheme simulates the radiance, reflectance and other parameters at the canopy level with and without the fluorescence effects for a range of inputs (Figure 5.4.3). The effects of chlorophyll concentration for C_{ab} ranging from 30 to 80 μg/cm^2 (Figure 5.4.3a) and leaf area index ranging from 1 to 7 (Figure 5.4.3b) can be observed for a fixed set of other leaf and canopy parameters, enabling the quantification of such other parameters on the retrieval of fluorescence signature from canopy reflectance. As an example of such fluorescence effects, canopy reflectance spectra were simulated with *FluorMODgui* for C_{ab}=30 μg/cm^2 (Figure 5.4.4a,c,e) and C_{ab}=80 μg/cm^2 (Figure 5.4.4b, d, f) showing the canopy reflectance with and without fluorescence addition. An emission peak at 761 nm can be observed in the apparent reflectance spectra due to the fluorescence *in-filling* effects at the oxygen band (Moya et al., 2004, Zarco-Tejada et al., 2005) (Figure 5.4.4 e,f), where for this simulation the input parameters used were: Fi=0.1, T=5, N=1.5, Cw=0.025, Cm=0.01, S=2, Sto=2.0, PARb=0.0035, PARre=0.005, LAI=4, Raz and Vza=0, h=0.1, and LIDFa=LIDFb=-0.5.

An example of the diurnal simulation using the *Diurnal Simulation Tool* can be seen in Figure 5.4.5 for a number of spectral parameters obtained. The diurnal simulation was setup for a solar zenith angle ranging from 10º to 70º, showing the simulation for solar irradiance (Figure 5.4.5a); sky irradiance (Figure 5.4.5b); total irradiance (Figure 5.4.5c); radiance without fluorescence (Figure 5.4.5d); fluorescence radiance (Figure 5.4.5e); total radiance (Figure 5.4.5f); reference reflectance (Figure 5.4.5g); and total reflectance including fluorescence (Figure 5.4.5h). Changes observed on the fluorescence emission simulated for a diurnal setting indicate that viewing angle effects should be seriously considered when retrieving the fluorescence signature from canopy reflectance under natural light conditions due to the effects caused by the sun angles for a fixed fluorescence quantum efficiency value (Figure 5.4.5e).

This simulation tool with linked leaf and canopy models therefore enables the quantification of the fluorescence effects at the canopy level as a function of leaf, canopy and viewing and atmospheric/illumination inputs. Further developments of the leaf and canopy models after future validations for calibration purposes will probably modify the absolute emission levels and other effects of the fluorescence spectra at both leaf and canopy models. Furthermore, currently the model is designed to simulate fluorescence effects for non-stress conditions.

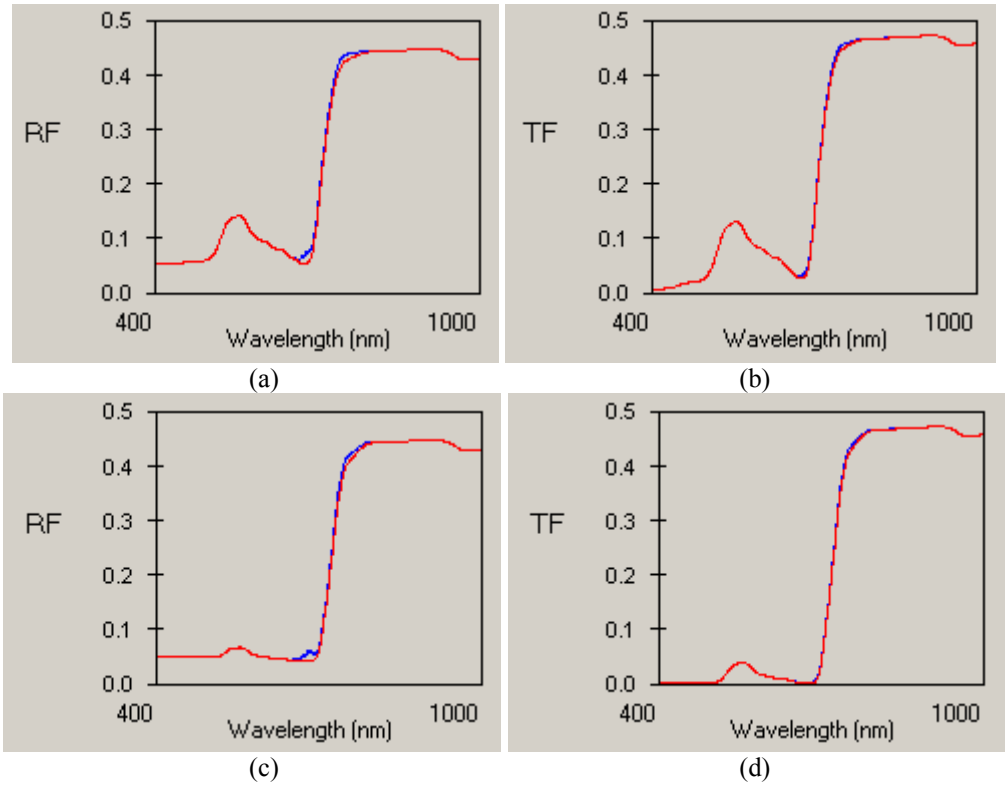

Figure 5.4.2. FluorMODgui model simulation of leaf reflectance (a, c) and transmittance (b, d) for C_{ab}=30 µg/cm^2 (a, b) and C_{ab}=80 µg/cm^2 (c, d) with and without the chlorophyll fluorescence effects.

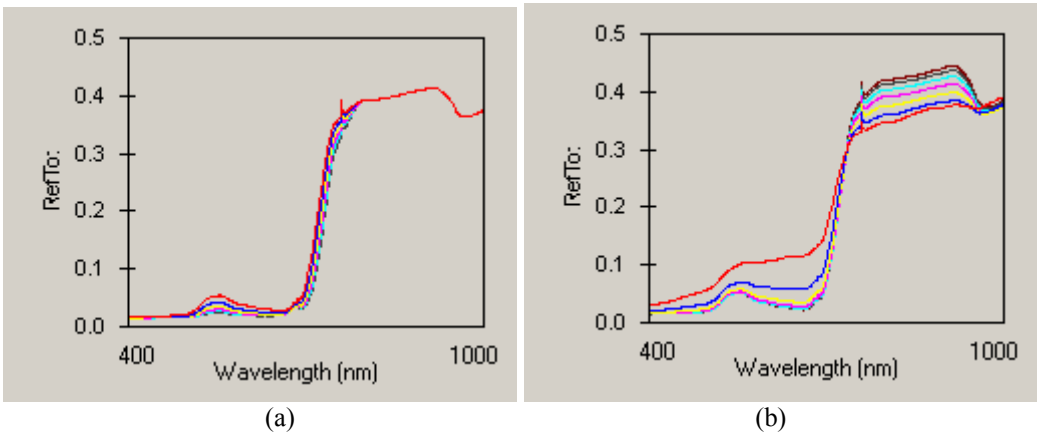

Figure 5.4.3. Canopy reflectance simulation with *FluorMODgui* for a range of C_{ab}=30 to 80 µg/cm^2 (a) and LAI=1 to 7 (b). Other input variables were Fi=0.1, T=5, N=1.5, Cw=0.025, Cm=0.01, S=2, Sto=2.0, PARb=0.0035, and PARre=0.005.

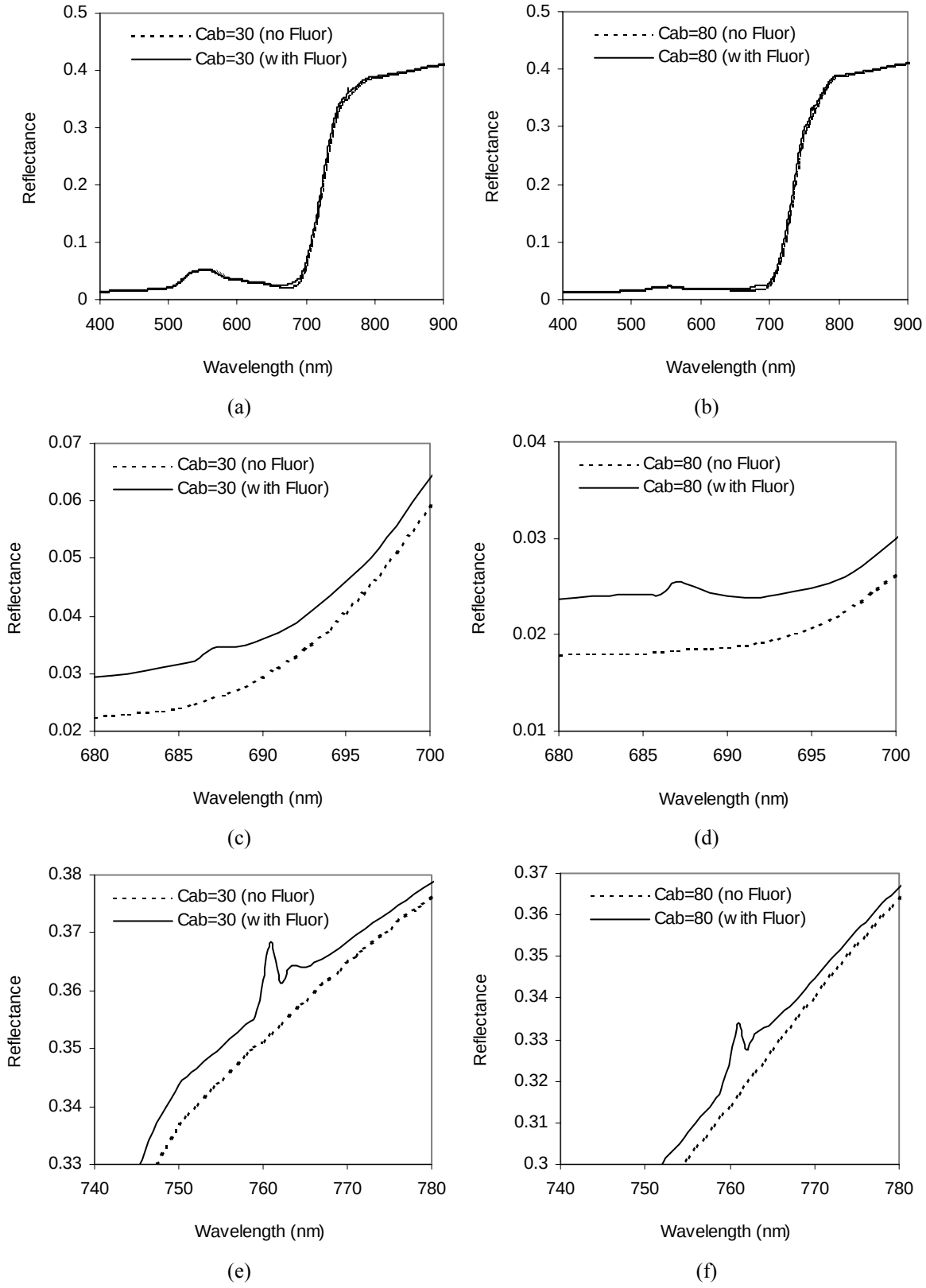

Figure 5.4.4. Simulation of canopy reflectance for C_{ab}=30 μg/cm^2 (a, c, e) and C_{ab}=80 μg/cm^2 (b, d, f) with (solid line) and without the effects of chlorophyll fluorescence (dotted line). Other input variables were Fi=0.04, T=5, N=1.5, Cw=0.025, Cm=0.01, S=2, Sto=2.0, PARb=0.0035, PARre=0.005, LAI=4, Raz and Vza=0, h=0.1, and LIDFa=LIDFb=-0.5.

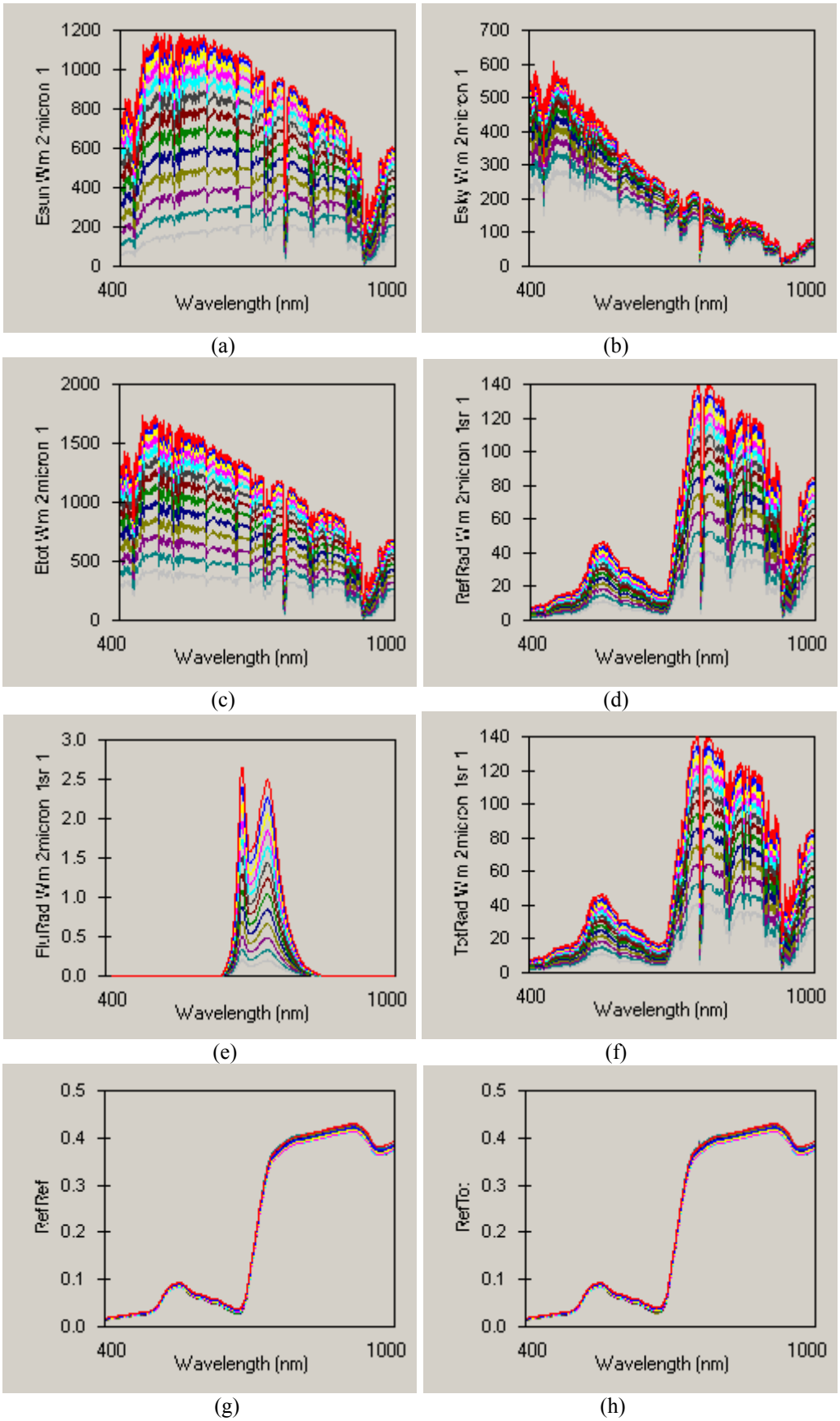

Figure 5.4.5. Diurnal simulation with *FluorMODgui* for a solar zenith angle ranging from 10º to 70º obtaining solar irradiance (a); sky irradiance (b); total irradiance (c); radiance without fluorescence (d); fluorescence radiance (e); total radiance (f); reference reflectance (g); and total reflectance including fluorescence (h).

5.5. Conclusions

The *FluorMODgui* V3.0 Graphic User Interface enables the simulation of leaf and canopy reflectance with the effects of chlorophyll fluorescence, running the leaf and canopy models *FluorMODleaf* and *FluorSAIL* independently and through a coupling scheme. The interface is designed to provide a link between the leaf and canopy models, with four main parts: a *Menu Area* for full control of the interface, an *Irradiance File and PAR Dependence* input area for controlling the light conditions and dependence, a *Leaf Model Area* for inputs and graphic outputs to run the *FluorMODleaf* model, and a *Canopy Model Area* for inputs and graphic outputs to run the *FluorSAIL* model.

The *Leaf Input Parameters* required to run *FluorMODleaf* are the number of layers, chlorophyll a+b, water equivalent thickness, dry matter content, fluorescence quantum efficiency, leaf temperature, species temperature dependence, and stoichiometry of PSII to PSI reaction centres. Outputs generated from *FluorMODleaf* fluorescence model are the leaf reflectance and transmittance without fluorescence, the leaf reflectance and transmittance with fluorescence, the fluorescence emission at the leaf level, and two matrices containing the upward and downward fluorescence.

The outputs from *FluorMODleaf* provide inputs for *FluorSAIL* along with the viewing zenith and relative azimuth angles, the canopy leaf area index, the hot spot parameter, the leaf inclination distribution function parameters, and a soil spectrum file. Outputs from *FluorSAIL* contain the solar irradiance, sky irradiance, total irradiance, radiance without fluorescence, fluorescence radiance, total radiance, reference reflectance, total reflectance, reflectance as in SAIL, the ratio SAIL/*FluorSAIL*, and reference and total top-of-atmosphere radiances.

The Graphic User Interface facilitates multiple runs with varying leaf and canopy variables, generating the model results in plots and enabling the output data to be saved in text files for further analysis. A *Diurnal and Multiple Iteration Tool* is presented which facilitates the user's simulation of the diurnal effects of fluorescence as function of variables that typically change in a diurnal setting. A set of pre-calculated atmospheric files to simulate the typical range of atmospheric conditions for different sun viewing angles and a standard 23 km visibility atmosphere is made available with the graphic user interface. Other simulated atmospheric conditions can be calculated with MODTRAN-4 and used as user-defined input for *FluorMODgui*.

It is expected that the *FluorMODgui* interface will be used as a tool for leaf and canopy model validation through existing and future field datasets under the frame of this ESA project and by the interested scientific community. Ongoing research will improve *FluorMODleaf*, *FluorSAIL* and *FluorMODgui* graphic interface with current validation efforts being conducted. The up-to-date models, graphic interface version, and documentation can be obtained by interested collaborators from a dedicated web page at **http://www.ias.csic.es/fluormod**

6. VALIDATION of the LEAF-CANOPY FLUORESCENCE MODEL

Chlorophyll Fluorescence Detection with a High-Spectral Resolution Spectrometer through *in-filling* of the O_2-A band as a function of Water Stress in Olive Trees

Validation efforts for the FluorMOD project require the acquisition of canopy-level spectral radiance and reflectance under different viewing geometries, stress levels, and species. This chapter summarizes initial validation results obtained for the project.

6.1. Introduction

In this study, the main objective was to determine if water stress levels caused by different irrigation treatments in olive tree crops would affect the crown-level natural fluorescence emitted, assessing the potential for its detection through the fluorescence *in-filling* effects in the O_2-A band at 760 nm.

6.2. Field data collection

Reflectance measurements were collected from the top of the olive tree crowns using a 0.065 nm FWHM Ocean Optics HR2000 fibre-optics spectrometer installed on a pole with a head where a cosine (downwelling irradiance) and a bare fibre (upwelling radiance) were attached. The experimental design consisted of a study area of olive trees where 3 irrigation treatments were applied, with 35 m^3 water/week (control treatment R), 3.6 m^3/week (stress treatment S1), and an intermediate treatment (S2) (Figure 6.2.1). Temperature from the crowns was collected continuously using Apogee IRTS-P (Apogee, UT, USA) thermal sensors. Conductance, photosynthesis, water potential, and chlorophyll fluorescence were measured diurnally and weekly over the summer from June to November 2004, monitoring the stress caused by the deficit irrigation scheme. The 0.065 nm FWHM Ocean Optics HR-2000 spectrometer (Ocean Optics, Dunedin, FL, USA) provided spectral measurements in the 680-770 nm range from top of the crowns in the diurnal series (Figure 6.2.2). The spectral measurements were made over selected tree crowns under the 3 different water stress treatments, measuring irradiance with a cosine corrector and crown radiance with a 7 m height pole attaching the fibre head at the end to collect radiance from a nadir view.

6.3. Experimental results and model simulation

Leaf water potential measurements collected from 11 trees over the summer showed large variations in water stress as function of the irrigation treatment (Figure 6.3.1). As expected, S1 and S2 trees with lower irrigation doses were more stressed than R trees with nominal irrigation. Consistently, both stomatal conductance and photosynthesis rates were greater for the low-stressed well watered treatment (R). The leaf chlorophyll fluorescence measurements collected diurnally from selected trees, and throughout the season, showed that steady-state Ft fluorescence values for the low-stressed trees (R) were higher than for the high-stressed treatment (S2, S1) (Figure 6.3.2). The relationships between Ft and leaf water potential throughout the season were in good agreement, showing a final recovery across treatments on both Ft and water potential after the first rainfalls.

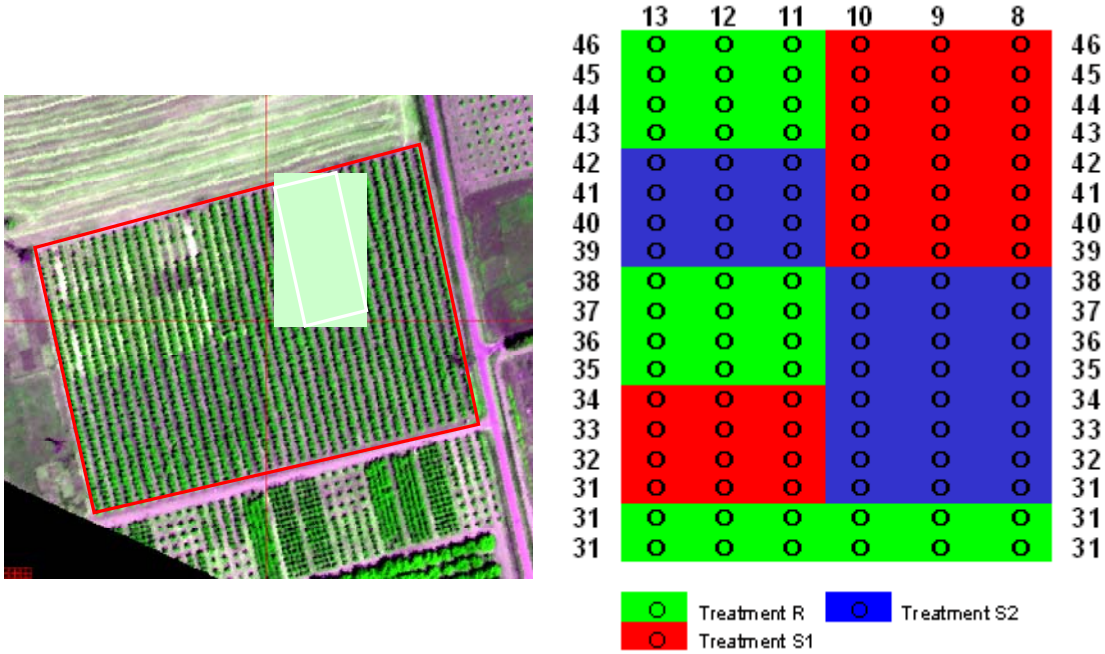

Figure 6.2.1. Airborne hyperspectral CASI image collected over the study area (left), showing the treatment blocks where deficit irrigation experiments were conducted (b).

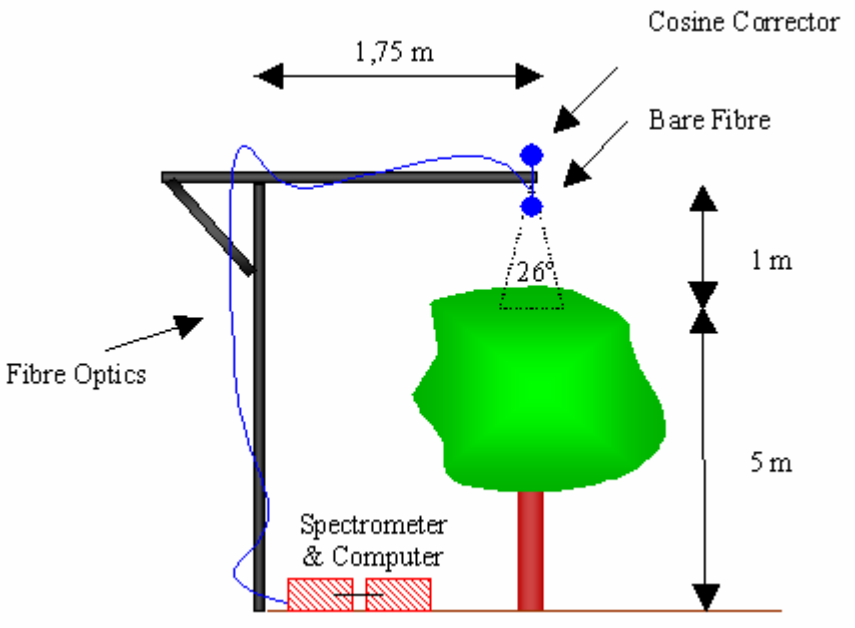

Figure 6.2.2. Schematic view of the experiment design for acquiring spectral measurements using the HR2000 high-resolution spectrometer.

Crown temperature measured with Apogee IRTS-P sensors from trees showed up to 4ºC differences between stressed and non-stressed trees, showing the larger daily temperature differences between 16.00 and 19.00 GMT. Relationships between temperature and water potential at the tree crown level were obtained throughout the season (r^2~0.7). The diurnal measurements of reflectance conducted with the Ocean Optics HR2000 spectrometer at 0.065 nm FWHM in the 680-770 nm range demonstrated that the fluorescence *in-filling* at the O_2-A band can be detected on the reflectance signal at the crown level, manifested in a sudden reflectance increment of the reflectance at 760 nm (Figure 6.3.3). The amplitude of the 760 nm peak, potentially associated with the emission of natural fluorescence, was compared with steady-state fluorescence measurements collected at the same time from the trees under different stress levels. The agreement obtained in diurnal trials between Ft and the O_2-A peak amplitude suggests that natural fluorescence can potentially be monitored using reflectance spectra. Nevertheless, the dependency of the emission peak on reflectance BRDF requires critical attention due to the known changes as a function of the viewing geometry and solar angle which accompany diurnal changes. The *FluorMODgui* radiative transfer model was used to simulate the effects of fluorescence on canopy reflectance, enabling the calculation of the 760 nm peak amplitude with and without fluorescence effects (Figure 6.3.3). The simulations show that the 760 nm peak observed on the experimental tree-level canopy reflectance is recreated with the physical model, disappearing when the canopy reflectance is simulated without fluorescence emission.

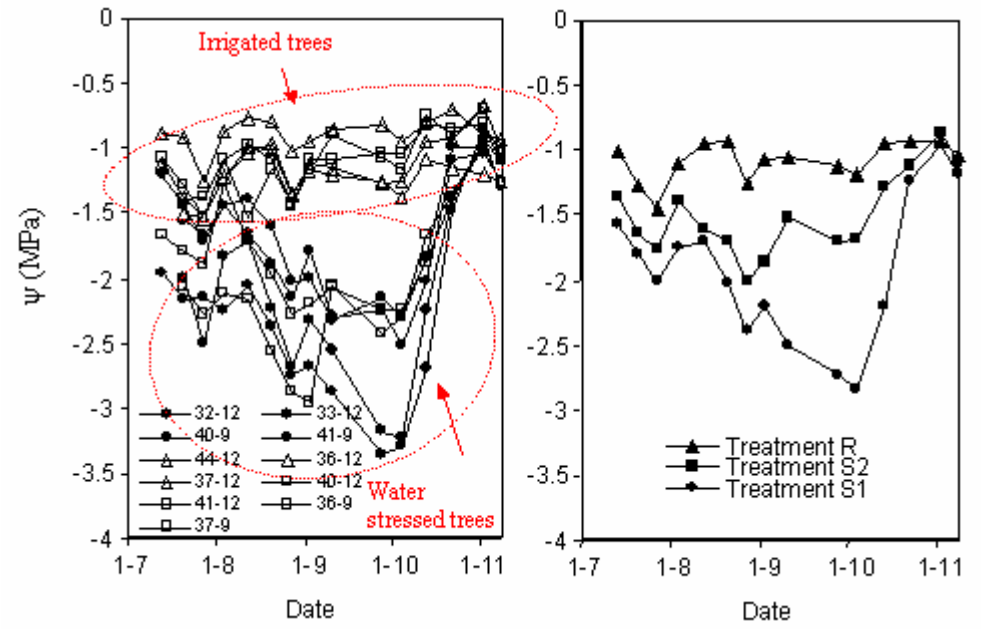

Figure 6.3.1. Measurements of leaf water potential collected from each tree over the summer (left) and averaged for each irrigation treatment (right).

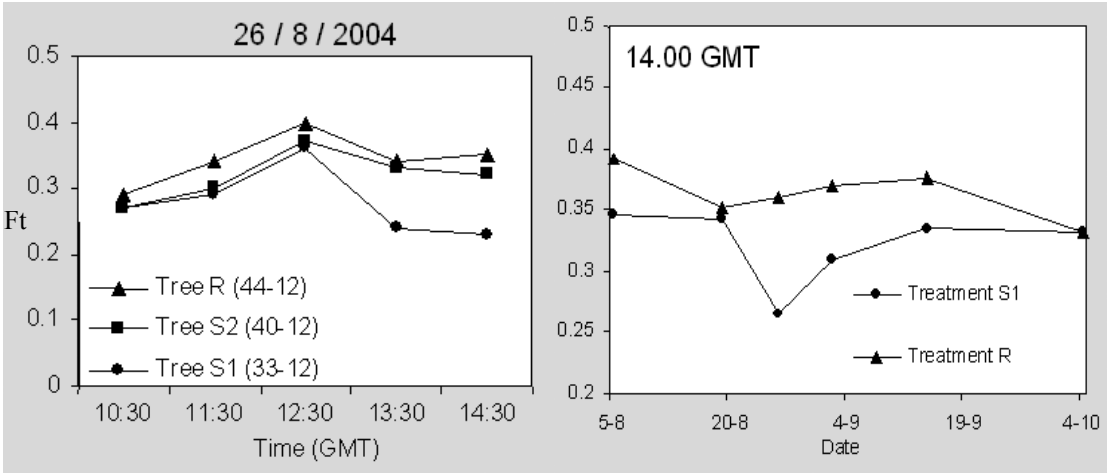

Figure 6.3.2. Steady-state natural leaf fluorescence collected with PAM-2100 from trees under different irrigation levels, showing the variation over the course of the day (left) and over the summer (right).

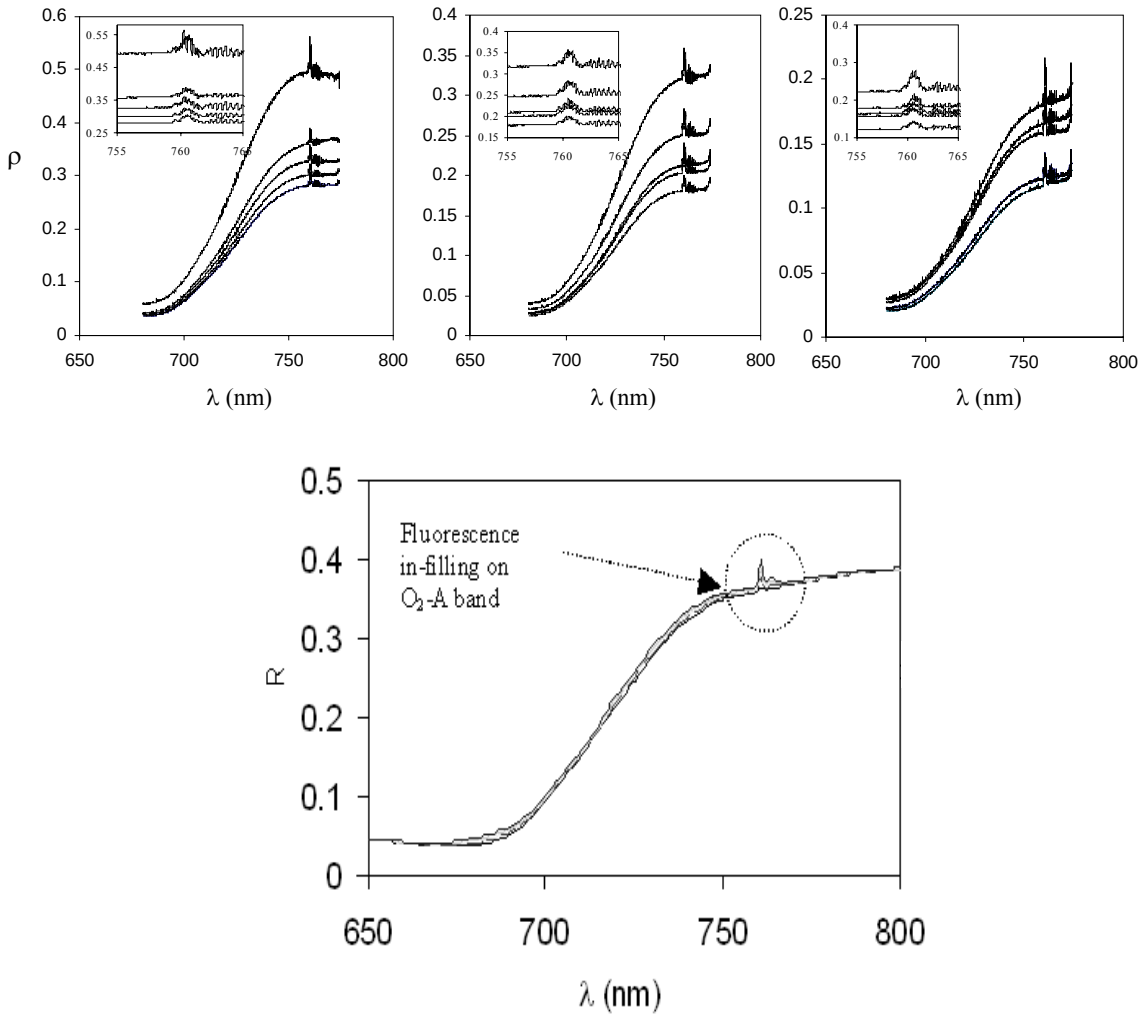

Figure 6.3.3. Crown reflectance acquired with the HR2000 spectrometer at 0.065 nm FWHM from trees under different stress levels (top), showing the peak at 760 nm due to fluorescence emission. The *FluorMODgui* model simulation recreated the same effect due to fluorescence emission (bottom).

6.4. Conclusions

Reflectance measurements collected with a high-spectral resolution spectrometer, and simulations conducted with the *FluorMODgui* model demonstrated that the observed fluorescence *in-filling* at 760 nm, detected as a sharp peak in the reflectance signature, is consistent with the modelled apparent canopy reflectance when fluorescence emission is added. These results obtained at canopy level for water stress monitoring are in agreement with leaf-level studies conducted by Meroni (2004) and Moya et al. (2004), showing that fluorescence emission can be detected at the leaf level and on a corn canopy using the O_2-A band under diuron herbicide treatment. The model demonstrates the effects of the fluorescence emission and the viewing geometry on the *in-filling* amplitude as simulated by the normal variation in a diurnal setting, showing small effects at the 760 nm band when canopy reflectance is simulated without fluorescence effects. This work suggests the potential application of spectral reflectance for monitoring natural chlorophyll fluorescence emission at the canopy level as an indicator of water stress.

7. CONCLUSIONS and RECOMMENDATIONS

Steady-state chlorophyll fluorescence is often a sensitive indicator of natural and stress-induced effects. The FluorMOD project set as its primary objective to simulate the effects of sun-induced fluorescence on unstressed vegetation through the development of an integrated leaf-canopy radiative transfer model incorporating biophysical inputs. A beta version of the model is now completed and is available for further testing and validation by the scientific community.

The components of the new model consist of a leaf model, *FluorMODleaf*, that simulates the effects of chlorophyll fluorescence, and a canopy model, *FluorSAIL*, that incorporates an excitation-fluorescence matrix computed externally by means of the leaf-level fluorescence model to simulate fluorescence effects on the canopy signature. Both models have been conveniently linked through a menu-driven graphic user interface *FluorMODgui*, which permits the leaf and canopy models to be run either individually or as an integrated unit.

This work represents a significant scientific advance in that it facilitates the transition of fluorescence-based analysis from a near-contact physiological technique to one amenable to remote, even satellite-based, approaches. By knowing what to expect in terms of a fluorescence contribution to hyperspectral signatures, it is possible to gauge the practicality and accuracy of instrumentation designed for use at remote scales. Thus, the model can help to guide the development of a new generation of sensors for fluorescence detection. Second, the project expands our understanding of the behaviour of the individual elements comprising remote hyperspectral signals, thereby supporting quantitative analysis of these signatures. To achieve this advance, the FluorMOD team bridges various scientific fields of endeavour – plant physiology, fluorescence instrumentation development, leaf & canopy biophysical modelling, and hyperspectral remote sensing & modelling, in a uniquely synergistic effort.

The *FluorMODleaf* model developed within this project simulates the chlorophyll fluorescence effects on leaf reflectance and transmittance, based on the widely used and validated PROSPECT leaf optical properties model. The new *FluorMODleaf* model is an adaptation of PROSPECT and is based on radiative transfer theory to accurately simulate the hemispherical reflectance and transmittance of various plant leaves, such as monocots, dicots or senescent leaves, over the solar spectrum. The fluorescence emission is introduced into PROSPECT, representing the simulated fluxes within the leaf as a network. The core of the model is the fluorescence emission elementary spectrum, a combination of Photosystem I (PS I) and Photosystem II (PS II) fluorescence spectra. Additional input parameters are the fluorescence quantum efficiency, the relative contribution of the two photosystems, stoichiometry of the PS II to PS I reaction centres, leaf temperature, and the light level. The upward and downward fluorescence spectrum can be described for different wavelengths of excitation.

The second component of *FluorMODgui*, the *FluorSAIL* canopy model, was developed to simulate the chlorophyll fluorescence effects on canopy reflectance using inputs from the *FluorMODleaf* model. *FluorSAIL* is based on the SAIL model, a widely used and validated canopy reflectance model. The excitation-fluorescence matrix computed by *FluorMODleaf* along with the internal radiation profiles simulated for solar and diffuse fluxes are used to calculate the radiance of each leaf. Numerical integration is used to predict the top-of-canopy radiance caused by contributions due to scattering and fluorescence. A PAR light-level fluorescence dependence is applied to individual leaves depending on their depth and

orientation with respect to the sun. In addition, distinction is made between sunlit and shaded leaves by employing the gap probability function of SAIL. The output of *FluorSAIL* can be used to obtain realistic top-of-canopy as well as and top-of-atmosphere radiance contributions associated with solar induced fluorescence. The new canopy fluorescence model allows the investigation of quite subtle interactions between atmospheric absorption on the one hand and the directional fluorescence and BRDF effects on the other. This is necessary for a correct interpretation of *in-situ* measurements and airborne or spaceborne hyperspectral radiance data obtained under passive illumination conditions.

The *FluorMODgui* V3.0 Graphic User Interface provides a seamless link between inputs and outputs required for running both *FluorMODleaf* and *FluorSAIL* models, facilitating consistent user interaction and enabling the setup of multiple runs to simulate diurnal effects under different viewing geometries. This graphic interface can be used as a tool for leaf and canopy model validation through the use of existing and future field datasets. This interface developed under the FluorMOD project can facilitate the testing of various remote sensing detection scenarios for future airborne and spaceborne fluorescence missions.

Initial testing of the new model has revealed that it is able to simulate the shape of the fluorescence signature in the red and far-red spectrum. Future sensitivity analyses will determine the accuracy of amplitude simulations. Possibly, scaling factors may be used to quantitatively amplify the fluorescence signal, given that it is quite low compared to reflectance or transmittance. Also, a finer discrimination among pigments in light-absorbing plant tissues may help to resolve amplitude aspects, because, while all pigments absorb light, only chlorophyll fluoresces in the red and far-red, yet the model currently treats the behaviour of chl a, chl b, and carotenoids uniformly, possibly leading to an error. One solution could be to include a spectrum of efficiency in the energy transfer that excites chlorophyll and produces fluorescence.

A canopy validation study conducted in the project for olive trees was designed to investigate whether diurnal variations in actual measured fluorescence would agree with the changes in reflectance at 760 nm, and also with the simulation of the model for the 760 band over the course of the day. These aspects were in agreement, although sun geometry also affected this peak. Therefore, caution is needed to carefully account for the influence of sun angle in future studies. It is also noted that if a scaling factor is to be used, it may be applied within the context of what is realistic for fluorescence quantum efficiency (considered as a maximum of 0.1 here); accordingly, resultant amplitudes for fluorescence may be small, which will be an important consideration for future spaceborne applications.

The up-to-date models, graphic interface version, and documentation can be obtained by interested collaborators from a dedicated web page at **http://www.ias.csic.es/fluormod**

RECOMMENDATIONS

Since validation by the scientific community is essential for providing inputs to future model improvements, it will be helpful if such validation activities are conducted in accordance with certain suggested guidelines.

Identification of potential sources of error
Given that many factors can influence the fluorescence signal, it is essential that efforts in testing and validation incorporate stringent attention to experimental factors, to ensure that they are standardized, accurate, and well-documented, in order to identify potential sources of disagreement between ground-truthing results and model predictions, and to identify errors in the model. These ongoing validation studies will supply important information for future improvements in *FluorMODleaf*, *FluorSAIL* and *FluorMODgui* graphic interface.

Who should conduct testing and validation
The need for stringent monitoring and control of experimental factors suggests that validation activities will need to be conducted in an orderly rollout, first to the scientific research community, then to more applied investigators, and finally, to operational users such as specialists in resource inventory monitoring, agriculture, and horticulture. It is also anticipated that members of the FluorMOD development team will serve as collaborators and resource personnel in validation project planning and execution.

Validation formats
An array of datasets can be used to test the accuracy and limits of the leaf and canopy models. These include existing datasets and those from new studies. Existing datasets that contain both ground-based and remote (e.g., from towers or airborne sensors) measures of two-band chlorophyll fluorescence would be needed, along with hyperspectral signatures obtained in temporal synchrony. A key aspect of existing and new datasets is that they should be able to address respective leaf-level and canopy-level accuracies of models. The recent LURE passive multidetector providing measurements at two wavelengths (687 and 760 nm), and analysis of hyperspectral signatures at sufficient spectral resolution are examples of fluorescence extraction approaches that might be appropriate for these activities. Selection of species for studies will necessarily be constrained to those with broad-leaf foliar structure, including many tree, shrub, and temperate crop species.

Provision of a feedback mechanism
Feedback of validation results to the FluorMOD development team will expectedly occur through the usual scientific mechanisms of publications, conference presentations, and professional interactions. In addition, the project website can serve as a venue for contact and information exchange, from which inquiries may be fielded to the appropriate model design team member(s).

8. REFERENCES

Agati G. (1998), Response of the in vivo chlorophyll fluorescence spectrum to environmental factors and laser excitation wavelength. *Pure and Applied Optics* 7:797-807.

Agati G., Cerovic Z.G., and Moya I. (2000), The effect of decreasing temperature up to chilling values on the in vivo F685/F735 chlorophyll fluorescence ratio in *Phaseolus vulgaris* and *Pisum sativum*: The role of the Photosystem I contribution to the 735 nm fluorescence band. *Photochemistry and Photobiology* 72(1):75-84.

Allen E. (1964), Fluorescent white dyes: Calculation of fluorescence from reflectivity values. *Journal of the Optical Society of America* 54(4):506-515.

Allen W.A., and Richardson A.J. (1968), Interaction of light with a plant canopy. *Journal of the Optical Society of America* 58(8):1023-1028.

Allen W.A., Gausman H.W., Richardson A.J., and Thomas J.R. (1969), Interaction of isotropic light with a compact leaf. *Journal of the Optical Society of America* 59(10):1376-1379.

Allen W.A., Gausman H.W., and Richardson A.J. (1970), Mean effective constants of cotton leaves. *Journal of the Optical Society of America* 60(4):542-547.

Allen W.A. (1973), Transmission of isotropic light across a dielectric surface in two and three dimensions. *Journal of the Optical Society of America* 63(6):664-666.

Allen W.A., Gausman H.W., and Richardson A.J. (1973), Willstätter-Stoll theory of leaf reflectance evaluation by ray tracing. *Applied Optics* 12(10):2448-2453.

Anderson J.M., and Boardman N.K. (1966), Fractionation of the photochemical system of photosynthesis. I. Chlorophyll contents and photochemical activities of particles isolated from spinach chloroplasts. *Biochimica et Biophysica Acta* 112:403-421.

Andrieu B., Baret F., Schellberg J., and Rinderle U. (1988), Estimation de spectres de feuilles à partir de mesures dans des bandes spectrales larges, in *Proceedings of the 4th International Colloquium on Spectral Signatures in Remote Sensing*, Aussois (France), ESA SP-287, pp. 351-356.

Baranoski G.V.B., and Rokne J.G. (1997), An algorithmic reflectance and transmittance model for plant tissue. *Computer Graphics Forum* 16(3):141-150.

Baranoski G.V.G., and Rokne J.G. (1999), A non-deterministic reconstruction approach for isotropic reflectances and transmittances. *Journal of Visualization and Computer Animation* 10:225-231.

Baret F., Andrieu B., and Guyot G. (1988), A simple model for leaf optical properties in visible and near infrared: application to the analysis of spectral shifts determinism, in *Applications of Chlorophyll Fluorescence* (Lichtenthaler H.K., ed.), Kluwer Academic Publishers, pp. 345-351.

Baret F., and Fourty T. (1997), Estimation of leaf water content and specific leaf weight from reflectance and transmittance measurements. *Agronomie* 17(9-10):455-464.

Bassi R., and Simpson D. (1987), Chlorophyll-protein complexes of barley Photosystem I. *European Journal of Biochemistry* 163(2):221-230.

Benford F. (1946), Radiation in diffuse medium. *Journal of the Optical Society of America* 36(9):524-554.

Berk A., Anderson G.P., Acharya P.K., Chetwynd J.H., Hoke M.L., Bernstein L.S., Shettle E.P., Matthew M.W., and Adler-Golden S.M. (1999), MODTRAN4 Version 2 User's Manual, AFRL, Space Vehicles Directorate, Hanscom AFB, MA 01731-3010.

Berthold D.A., Babcock G.T., and Yocum C.F. (1981), A highly resolved oxygen-evolving Photosystem II preparation from spinach thylakoids membranes. *FEBS Letter* 134:231-234

Boardman N.K., and Anderson J.M. (1964), Isolation from spinach chloroplasts of particles containing different proportions of chlorophyll a and b: their possible role in light reactions of photosynthesis. *Nature* 203:166-167.

Bonham J.S. (1986), Fluorescence and Kubelka-Munk theory. *Color Research and Applications* 11:223-230.

Brakke T.W., and Smith J.A. (1987), A ray tracing model for leaf bidirectional scattering studies, in *Proc. 7th Int. Geosci. and Remote Sens. Symp.* (IGARSS'87), Ann Arbor (MI), pp. 643-648.

Bréon F.-M., Maignan F., Leroy M., and Grant I. (2002), Analysis of hot spot directional signatures measured from space. *Journal of Geophysical Research* 107: D16,10.1029/2001JD001094.

Briantais J.M., Vernotte C., Krause G.H., and Weis E. (1986), Chlorophyll a fluorescence in higher plants: Chloroplasts and leaves, In *Light Emission by Plants and Bacteria* (Govindjee A.J. & Fork D.C., eds.), Academic Press, New York. pp. 539-583.

Bruggemann W. (1992), Low temperature limitations of photosynthesis in 3 tropical *Vigna* species – A chlorophyll fluorescence study. *Photosynthesis Research* 34(3):301-310.

Butler W.L., and Kitajima M. (1975), Energy transfer between PSII and PSI in chloroplasts. *Biochimica et Biophysica Acta* 396:72-85.

Butler W.L. (1978), Energy distribution in the photochemical apparatus of photosynthesis. *Annual Review of Plant Physiology* 29:345-378.

Camenen L., Goulas Y., Guyot G., Cerovic Z., Schmuck G., and Moya I. (1996), Estimation of the chlorophyll fluorescence lifetime of plant canopies: Validation of a deconvolution method based on the use of a 3-D canopy mockup*, Remote Sensing of Environment* 58:157-168.

Carter G.A., Theisen A.F., and Mitchell R.J. (1990), Chlorophyll fluorescence measured using the Fraunhofer line-depth principle and relationship to photosynthesis rate in the field. *Plant Cell and Environment* 13:79-83.

Carter G.A., Jones J.H., Mitchell R.J., and Brewer C.H. (1996), Detection of solar-excited chlorophyll a fluorescence and leaf photosynthetic capacity using a Fraunhofer Line Radiometer. *Remote Sensing of Environment* 55:89-92.

Cerovic Z.G., Samson G., Morales F., Tremblay N., and Moya I. (1999), Ultraviolet-induced fluorescence for plant monitoring: present state and prospects. *Agronomie* 19:543-578.

Chow W.S., Anderson J.A., and Hope A.B. (1988), Variable stoichiometries of photosystem II to photosystem I reaction centres. *Photosynthesis Research* 17:277-281.

Conel J.E., van den Bosch J., and Grove C.I. (1993), Application of a two-stream radiative transfer model for leaf lignin and cellulose concentrations from spectral reflectance measurements. Parts 1 & 2, in *Proceedings of the 4th Annual JPL Airborne Geoscience Workshop. Vol. 1. AVIRIS Workshop* (R.O. Green, Ed), 25-29 October 1993, Washington (DC), NASA-JPL Publication 93-26, pp. 39-51.

Croce R., Zucchelli G., Garlaschi F.M., Bassi R., and Jennings R.C. (1996), Excited state equilibration in the Photosystem I-Light-Harvesting I complex: P700 is almost isoenergetic with its antenna. *Biochemistry* 35:8572-8579.

Croce R., Dorra D., Holzwarth A.R., and Jennings R. (2000), Fluorescence decay and spectral evolution in intact Photosystem I of higher plants. *Biochemistry* 39:6341-6348.

Dahm D.J., and Dahm K.D. (1999), Representative layer theory for diffuse reflectance. *Applied Spectroscopy* 53(6):647-654.

D'Ambrosio N., Szabo K., and Lichtenthaler H.K. (1992), Increase of the chlorophyll fluorescence ratio F690/F735 during the autumnal chlorophyll breakdown. *Radiation and Environmental Biophysics* 31:31-62.

Dau H. (1994), Molecular mechanisms and quantitative models of variable photosystem II fluorescence. *Photochemistry and photobiology* 60(1):1-23.

Davies J.A., and McKay D.C. (1989), Evaluation of selected models for estimating solar radiation on horizontal surfaces. *Solar Energy* 43:153-168.

Dawson T.P., Curran P.J., and Plummer S.E. (1998), LIBERTY - Modelling the effects of leaf biochemical concentration on reflectance spectra. *Remote Sensing of Environment* 65:50-60.

DeEll, J., and Toivonen, P.M.A. (eds). 2003. *Practical Applications of Chlorophyll Fluorescence in Plant Biology*, Kluwer.

Dijkstra P. (1990), Cause and effect of differences in specific leaf area. In *Causes and Consequences of Variation in Growth Rate and Productivity of Higher Plants* (H. Lambers, M.L. Cambridge, H. Konings, and T.L. Pons, eds). Academic Publishing, The Hague (The Netherlands), pp. 125-140.

Dunahay T.G., Staehelin L.A., Seibert M., Ogilvie P.D., and Berg S.P. (1984), Structural, biochemical and biophysical characterization of four oxygen-evolving photosystem II from spinach. *Biochimica et Biophysica Acta* 764:179-193.

Duysens L.N.M., Amesz J., and Kamp B.M. (1961), Two photochemical systems in photosystems. *Nature* 190:510.

Durkin A.J., Jaikumar S., Ramanujam N., and Richards-Kortum R.R. (1994), Relation between fluorescence spectra of dilute and turbid samples. *Applied Optics* 33(3):414-423.

Emerson R. (1958), Yield of photosynthesis from simultaneous illumination with pairs of wavelengths. *Science* 127(3305):1059-1060.

Emmel P. (1998), Modèle de prédiction couleur appliqué à l'impression jet d'encre, PhD thesis, Ecole Polytechnique Fédérale de Lausanne, Suisse, 186 pp.

Emmel P., and Hersch (1998), Spectral colour prediction model for a transparent fluorescent ink on paper, In *Proceedings of the IS&T/SID 6th Color Imaging Conference: Color Science, Systems and Applications*, November 17-20, 1998, Scottsdale (Arizona, USA), pp. 116-122.

Emmel P. (2000), Nouvelle formulation du modèle de Kubelka et Munk avec applications aux encres fluorescentes, In *Actes de l'Ecole de Printemps 2000 - Le Pays d'Apt en Couleurs*, 14-18 mars 2000, Apt et Roussillon (France), pp. 87-96.

Evain S., Camenen, L., Moya, I. (2001), Three channels detector for remote sensing of chlorophyll fluorescence and reflectance from vegetation, In *Proceedings of the 8th International Symposium: Physical Measurements and Signatures in Remote Sensing*, CNES, Aussois (France), M. Leroy (Ed.), pp 395-400.

Evain S. (2002), Télédétection passive de la fluorescence des couverts végétaux [PhD Thesis], Université de Paris-Sud. Orsay- France.

Evain S., Ounis A., Baret F., Goulas Y., Louis J., Ducruet J-M., Cerovic Z.G., and Moya I. (2002), Passive vegetation fluorosensing using atmospheric oxygen absorption bands, In Recent Advances in Quantitative Remote Sensing, 16-20 September 2002, Valencia (Spain), J. Sobrino (Ed.).

Evans J.R., and Anderson J.M. (1987), Absolute absorption and relative fluorescence excitation spectra of the five major chlorophyll-protein complexes from spinach chloroplasts from spinach thylakoid membranes. *Biochimica et Biophysica Acta* 892:75-82.

Flexas J., Briantais J.-M., Cerovic Z., Medrano H., and Moya I. (2000), Steady-state and maximum chlorophyll fluorescence responses to water stress in grapevine leaves: A new remote sensing system. *Remote Sensing of Environment* 73:283-297.

Flexas J., Escalona J.M., Evain S., Gulias J., Moya I., Osmond C.B., and Medrano H. (2002), Steady-state chlorophyll fluorescence (Fs) measurements as a tool to follow variations of net CO_2 assimilation and stomatal conductance during water-stress in C_3 plants. *Physiologia Plantarum* 114(2):231-240.

Fourty Th., Baret F., Jacquemoud S., Schmuck G., and Verdebout J. (1996), Optical properties of dry plant leaves with explicite description of their biochemical composition: direct and inverse problems. *Remote Sensing of Environment* 56(2):104-117.

Fourty T., and Baret F. (1998), On spectral estimates of fresh leaf biochemistry. *International Journal of Remote Sensing* 19(7):1283-1297.

Franck F., Juneau P., and Popovic R. (2002), Resolution of the photosystem I and photosystem II contributions to chlorophyll fluorescence of intact leaves at room temperature. *Biochimica et Biophysica Acta* 1556:239-246.

Freedman A., Cavender-Bares J., Kebabian P.L., Bhaskar R., Scott H., Bazzaz F.A. (2002), Remote sensing of solar-excited fluorescence as a measure of photosynthetic rate. *Photosynthetica* 40(1):127-132.

French C.S. (1971), The distribution and action in photosynthesis of several forms of chlorophyll. *Proceedings of the National Academy of Sciences of the United States of America* 68(11):2893-2897.

Fukshansky L., and Kazarinova N. (1980), Extension of the Kubelka-Munk theory of light propagation in intensely scattering materials to fluorescent media. *Journal of the Optical Society of America* 70(9):1101-1111.

Fukshansky L., Fukshansky-Kazarinova N., and von Remisowsky A.M. (1991), Estimation of optical parameters in a living tissue by solving the inverse problem of the multiflux radiative transfer. *Applied Optics* 30(22):3145-3153.

Gabrys-Mizera H. (1976), Model consideration of the light conditions in non-cylindrical plant cells. *Photochemistry and Photobiology* 24:453-461.

Ganapol B., Johnson L., Hammer P., Hlavka C., and Peterson D. (1998), LEAFMOD: a new within-leaf radiative transfer model. *Remote Sensing of Environment* 6:182-193.

Gardner C.M., Jacques S.L., and Welch A.J. (1996), Fluorescence spectroscopy of tissue: Recovery of intrinsic fluorescence from measured fluorescence. *Applied Optics* 35(10):1780-1792.
Gitelson A.A., Buschmann C., and Lichtenthaler H.K. (1998), Leaf chlorophyll fluorescence corrected for reabsorption by means of absorption and reflectance measurements. *Journal of Plant Physiology* 152:283-296.
Govaerts Y.M., Jacquemoud S., Verstraete M.M., and Ustin S.L. (1996), Three-dimensional radiation transfer modeling in a dicotyledon leaf. *Applied Optics* 35(33):6585-6598.
Govaerts Y.M., and Verstraete M.M. (1998), Raytran: A Monte Carlo ray-tracing model to compute light scattering in three-dimensional heterogeneous media. *IEEE Transactions on Geoscience and Remote Sensing* 36(2):493-505.
Govindjee, and Yang L. (1966), Structure of red fluorescence band in chloroplasts. *The Journal of General Physiology* 49:763-780.
Govindjee (1995), Sixty-three years since Kautsky: chlorophyll a fluorescence. *Australian Journal of Plant Physiology* 22:131-160.
Gronwall T.H. (1926), Reflection of radiation from a finite number of equally spaced parallel planes. *Physical Review* 27:277-285.
Gueymard C. (1987), An isotropic solar irradiance model for tilted surfaces and 1st comparison with selected engineering algorithms. *Solar Energy* 38(5):367-386.
Haberlandt G. (1914), Optical sense-organs, in *Physiological Plant Anatomy*, Macmillan and Co. (London), pp. 613-631.
Havaux M., and Gruszecki W.I. (1993), Heat-induced and light-induced chlorophyll-a fluorescence fluorescence changes in potato leaves containing high or low-levels of the carotenoid zeaxanthin – Indications of a regulatory effect of zeaxanthin on thylakoid membrane fluidity. *Photochemistry and Photobiology* 58:607-614.
Haworth P., Watson J.L., and Arntzen C.J. (1983), The detection, isolation and characterization of a light-harvesting complex, which is specifically associated with Photosystem I. *Biochimica et Biophysica Acta* 724:151-158.
Hill R., and Bendall F. (1960), Function of the two cytochrome components in chloroplasts: a working hypothesis. *Nature* 186:136-137.
Hosgood B., Jacquemoud S., Andreoli G., Verdebout J., Pedrini G., and Schmuck G. (1995), *Leaf Optical Properties EXperiment 93 (LOPEX93)*. European Commission, Joint Research Centre, Institute for Remote Sensing Applications, Report EUR 16095 EN.
Ikegami I., and Katoh S. (1975), Enrichment of photosystem I reaction center chlorophyll from spinach chloroplasts. *Biochimica et Biophysica Acta* 376(6):588-592.
Ikegami I (1976), Fluorescence changes related in the primary photochemical reaction in the P-700-enriched particles isolated from spinach chloroplasts. *Biochimica et Biophysica Acta* 449:245-258.
Jacquemoud S., and Baret F. (1990), PROSPECT: a model of leaf optical properties spectra. *Remote Sensing of Environment* 34:75-91.
Jacquemoud S. (1992), *Utilisation de la haute résolution spectrale pour l'étude des couverts végétaux : développement d'un modèle de réflectance spectrale*. PhD Thesis, University of Paris – Denis Diderot, Paris (France), 164 pp.
Jacquemoud S., Ustin S.L., Verdebout J., Schmuck G., Andreoli G., and Hosgood B. (1996), Estimating leaf biochemistry using the PROSPECT leaf optical properties model. *Remote Sensing of Environment* 56(3):194-202.
Jacquemoud S., Bacour C., Poilve H., and Frangi J.-P. (2000), Comparison of four radiative transfer models to simulate plant canopies reflectance–Direct and inverse mode. *Remote Sensing of Environment* 74:471-481.
Jacquemoud S. (2004), Leaf optical properties, in *Reflection Properties of Vegetation and Soil, with a BRDF Data base* (von Shönermark M., Geiger B. & Röser H.P., eds), Wissenshaft & Technik Verlag (Berlin), 352 pp.
Judd D.B. (1942), Fresnel reflection of diffusely incident light. *Journal of Research of the National Bureau of Standards* 29:329-332.
Kebabian P.L., Theisen A.F., Kallelis S., and Freedman A. (1999), A passive two-band sensor for sunlight-excited plant fluorescence. *Review of Scientific Instruments* 70:4386-4393.

Kim M.S., Chappelle E.W., Corp L., and McMurtrey III J.E. (1993), The contribution of chlorophyll fluorescence to the reflectance spectra of green vegetation. *In Proceedings of the International Geoscience and Remote Sensing Symposium* (IGARSS '93), Volume 3, pp. 1321-1224.

Knoetzel J., Svendsen I., and Simpson D.J. (1992), Identification of the photosystem I antenna polypeptides in barley. Isolation of the three pigment-binding antenna complexes. *European Journal of Biochemistry* 206:209-215.

Kok B. (1961), Partial purification and determination of oxidation reduction potential of the photosynthetic chlorophyll complex absorbing at 700 nm. *Biochimica et Biophysica Acta* 48:527-533.

Kortüm G. (1969), *Reflectance spectroscopy*, Springer, 366 pp.

Krause G.H., and Weis E. (1984), Chlorophyll fluorescence as a tool in plant physiology. II. Interpretation of fluorescence signals. *Photosynthesis Research* 5:139-157.

Krause G.H., and Weiss E. (1988), The photosynthetic apparatus and chlorophyll fluorescence: An introduction. In *Applications of Chlorophyll Fluorescence* (Lichtenthaler H.K., ed.), Kluwer Academic Publisher, pp. 3-11.

Krause G.H., and Weis E. (1991), Chlorophyll fluorescence and photosynthesis: the basis. *Annual Review of Plant Physiology and Plant Molecular Biology* 42:313-349.

Kumar R., and Silva L. (1973), Light ray tracing through a leaf cross section. *Applied Optics* 12(12):2950-2954.

Lang M., and Lichtenthaler H.K. (1991), Changes in the blue-green and red fluorescence-emission spectra of beech leaves during the autumnal chlorophyll breakdown. *Journal of Plant Physiology* 138:550-553.

Lavorel J. (1963), Indications d'ordre spectroscopique sur l'hétérogénéité de la chlorophylle *in vivo*. *Colloques Internationaux du Centre National de la Recherche Scientifique* 119:161-176.

Lichtenthaler H.K. (1987), Chlorophyll fluorescence signatures of leaves during the autumnal chlorophyll breakdown. *Journal of Plant Physiology* 131:101-110.

Lichtenthaler H.K., and Rinderle U. (1988), The role of chlorophyll fluorescence in the detection of stress conditions in plants. *CRC Critical Reviews in Analytical Chemistry* 19 (suppl):529-585.

Louis J. (2004), *Télédétection et modélisation des signaux de fluorescence et de réflectance (PRI) des couverts végétaux*, PhD in Molecular biophysics, University of Paris 7 (Paris), 201 pp.

Ma Q., Ishimaru A., Phu P., and Kuga Y. (1990), Transmission, reflection, and depolarization of an optical wave for a single leaf. *IEEE Transactions on Geoscience and Remote Sensing* 28(5):865-872.

Maier S.W., Lüdeker W., and Günther K.P. (1999), SLOP: A revised version of the stochastic model for leaf optical properties. *Remote Sensing of Environment* 68(3):273-280.

Maier S.W. (2000), Modeling the Radiative Transfer in Leaves in the 300 nm to 2.5 µm Wavelength Region taking into Consideration Chlorophyll Fluorescence - The Leaf Model SLOPE. PhD Thesis - Technische Universität München (München), 124 pages.

Melamed M.T. (1963), Optical properties of powders. Part I. Optical absorption coefficients and the absolute value of the diffuse reflectance. *Journal of Applied Physics* 34:560–570.

Meroni M., (2004), High resolution leaf spectral signature for the detection of solar induced chlorophyll fluorescence, 2nd International Workshop on Remote Sensing of Vegetation Fluorescence, 17-19 Nov. 2004, Montreal, Canada.

Meziane D., and Shipley B. (1999), Interacting determinants of specific leaf area in 22 herbaceous species: effects of irradiance and nutrient availability. *Plant Cell and Environment* 22(5):447-459.

Mineucchi K., Takahashi K., Komatsu A., and Tatsumota H. (1999), Seasonal variation of laser induced fluorescence spectra in tree leaves. *Environmental Technology* 20:633-638.

Mohammed G.H., Binder W.D., and Gillies S.L. (1995), Chlorophyll fluorescence: A review of its practical forestry applications and instrumentation. *Scandinavian Journal of Forest Research* 10:383-410.

Mohammed G.H., Zarco-Tejada P., and Miller J.R. 2003, Applications of chlorophyll fluorescence in forestry and ecophysiology, chapter 3, in *Practical Applications of Chlorophyll Fluorescence in Plant Biology* (J.R. DeEll, ed), Kluwer, pp.79-124.

Moya I., Guyot G., and Goulas Y. (1992), Remotely sensed blue and red fluorescence emission for monitoring vegetation, *ISPRS International Society of Photogrammetry and Remote Sensing* 47:205-231.
Moya I., Camenen L., Latouche G., Mauxion C., Evain S., and Cerovic Z.G. (1998), An instrument for the measurement of sunlight excited plant fluorescence, in *Photosynthesis: Mechanisms and Effects* (G. Gorab, ed.), Kluwer Acad. Pub., Dordrecht, pp. 4265-4270.
Moya I., Camenen L., Evain S., Goulas Y., Cerovic Z.G., Latouche G., Flexas J., and Ounis A. (2004), A new instrument for passive remote sensing. 1. Measurements of sunlight-induced chlorophyll fluorescence. *Remote Sensing of Environment* 91:186-197.
Mukerji I., and Sauer K. (1993), Energy Transfer Dynamics of an Isolated Light Harvesting Complex of Photosystem I from Spinach: Time-resolved Fluorescence Measurements at 295K and 77K. *Biochimica et Biophysica Acta* 1142:311-320.
Mullet J.E., Burke J.J., and Arntzen J. (1980a), Chlorophyll proteins of photosystem I. *Plant Physiology* 65:814-822.
Mullet J.E., Burke J.J., and Arntzen J. (1980b), A developmental study of Photosystem I peripheral chlorophyll proteins. *Plant Physiology* 65:823-827.
Murakami A. (1997), Quantitative analysis of 77K fluorescence emission spectra in *Synechocystis* sp. PCC 6714 and *Chlamydomonas reinhardtii* with variable PS I / PS II stoichiometries. *Photosynthesis Research* 53:141-148.
Murata N., Nishimura M., and Takamiya A. (1966), Fluorescence of chlorophyll in photosynthetic systems III. Emission bands of chlorophyll a and the energy transfer between two pigment systems. *Biochimica et Biophysica Acta* 126:234-243.
Ogawa T., Obata F., and Shibata K. (1966), Two pigment proteins in spinach chloroplasts. *Biochimica et Biophysica Acta* 112:223-234.
Ogawa T., and Vernon L.P. (1970), Properties of partially purified photosynthetic reaction centers from *Scenedesmus* mutant 6E and *Anabaena variabilis* grown in the presence of diphenylamine. *Biochimica et Biophysica Acta* 197(2):292-301.
Olf H.G. (1988), Stokes's pile of plates revisited. *Journal of the Optical Society of America A* 5(10):1620-1625.
Olioso A., Méthy M., and Lacaze B. (1992), Simulation of canopy fluorescence as a function of canopy structure and leaf fluorescence. *Remote Sensing of Environment* 41:239-247.
Ounis A. (2001), Télédétection de la fluorescence des couverts végétaux induite par laser: Application des techniques de corrélation temporelle microseconde et nanoseconde [Ph.D. thesis], Université de Paris-Sud.
Ounis A, Cerovic ZG, Briantais J-M, and Moya I (2001), Dual excitation FLIDAR for the estimation of epidermal UV absorption in leaves and canopies. *Remote Sensing of Environment* 76:33-48.
Panou-Diamandi O., Uzunoglu N.K., Zacharakis G., Filippidis G., Papazoglou T., and Koutsouris D. (1998), A one layer tissue fluorescence model based on electromagnetic theory. *Journal of Electromagnetic Waves & Applications* 12(8):1101-1121.
Papageorgiou G. (1975), Chlorophyll fluorescence: an intrinsic probe of photosynthesis, in Bioenergetics of Photosynthesis (Govindjee, ed), Academic Press, New York.
Perez R., Seals R., Ineichen P., Stewart R., and Minicucci D. (1987), A new simplified version of the Perez diffuse irradiance model for tilted surfaces. *Solar Energy* 39(3):221-231.
Peterson R.B., Oja V., and Laisk A. (2001), Chlorophyll fluorescence at 680 and 730 nm and leaf photosynthesis. *Photosynthesis Research* 70:185-196.
Pfündel, E. (1998), Estimating the contribution of photosystem I to total leaf chlorophyll fluorescence. *Photosynthesis Research* 56:185-195.
Plascyk J.A. (1975), The MK II Fraunhofer line discriminator (FLD-II) for airborne and orbital remote sensing of solar-stimulated luminescence. *Optical Engineering* 14(4):339-346.
Prakash J.S.S., Baig M.A., Bhagwat A.S., and Mohanty P. (2003), Characterisation of senescence-induced changes in light harvesting complex II and photosystem I complex of thylakoids of *Cucumis sativus* cotyledons: Age induced association of LHCII with Photosystem I . *Journal of Plant Physiology* 160:175-184.

von Remisowsky A.M., McClendon J.H., and Fukshansky L. (1992), Estimation of the optical parameters and light gradients in leaves: Multi-flux *versus* two-flux treatment. *Photochemistry and Photobiology* 55(6):857-865.
Richards-Kortum R., Rava R.P., Fitzmaurice M., Tong L.L., Ratliff N.B., Kramer J.R., and Feld M.S. (1989), A one-layer model of laser-induced fluorescence for diagnosis of disease in human tissue: Applications to atherosclerosis. *IEEE Transactions on Biomedical Engineering*. 36(12):1222-1232.
Richter T., and Fukshansky L. (1996), Optics of a bifacial leaf: 1. A novel combined procedure for deriving the optical parameters. *Photochemistry and photobiology*. 63(4):507-516.
Roelofs T.A., Lee C.H., and Holzwarth A.R. (1992), A new approach to the characterization of the primary processes in photosystem II alpha- and beta-units. *Biophysical Journal*. 61:1147-1163.
Rosema A., Verhoef W., Schroote J., and Snel J.F.H. (1991), Simulating fluorescence light-canopy interaction in support of laser-induced fluorescence measurements. *Remote Sensing of Environment* 37:117-130.
Rosema A., Snel J.F.H., Zahn H., Buurmeijer W.F., and Van Hove L.W.A. (1998), The relation between laser-induced chlorophyll fluorescence and photosynthesis. *Remote Sensing of Environment* 65:143-154.
Sane P.V., and Park R.B. (1970), Purification of photosystem I reaction centers from spinach stroma lamella. *Biochemical & Biophysical Research Communication* 41:206-210.
Schanda R. (1986), *Physical Fundamentals of Remote Sensing*, Springer Verlag, 187 pp.
Schmuck G., and Moya I. (1994), Time-resolved chlorophyll fluorescence spectra of intact leaves. *Remote Sensing of Environment* 47(1):72-76.
Schreiber U., Bilger U., and Neubauer C. (1994), Chlorophyll fluorescence as a non-intrusive indicator for rapid assessment of in vivo photosynthesis. *Ecological Studies* 100: 49-70.
Shakespeare T., and Shakespeare J. (2003), A fluorescent extension to the Kubelka-Munk model. *Color Research and Applications* 28(1):4-14.
Shipley B., and Vu T.-H. (2002), Dry mater content as a measure of dry matter concentration in plants and their parts. *New Phytologist* 153:359-364.
Srivastava A., Greppin H., and Strasser R.J. (1995), The steady state chlorophyll *a* fluorescence exhibits *in vivo* an optimum as a function of light intensity which reflects the physiological state of the plant. *Plant Cell Physiology* 36(5):839-848.
Stern F. (1964), Transmission of isotropic radiation across an interface between two dielectrics. *Applied Optics* 3(1):111-113.
Stokes G.G. (1862), On the intensity of the light reflected from or transmitted through a pile of plates. *Proceedings of the Royal Society of London (Series B)* 11:545-556.
Strasser R.J., and Butler W.L. (1977), Fluorescence emission spectra of photosystem I, photosystem II and the light-harvesting chlorophyll a/b complex of higher plants. *Biochimica et Biophysica Acta* 462:307-313.
Subhash N., and Mohanan C.N. (1997), Curve-fit analysis of chlorophyll fluorescence spectra: Application to nutrient stress detection in sunflower. *Remote Sensing of Environment* 60:347-356.
Taiz L., and Zeiger, E. (1998), Plant Physiology, *Second Edition Sinauer Associates*: Sunderland, Massachusetts, 792 pp.
Terjung F. (1998), Reabsorption of chlorophyll fluorescence and its effects on the spectral distribution and the picosecond decay of higher plant leaves. *Zeitschrift für Naturforschung* C53: 924-926.
Theisen A.F., Rock B.N., and Eckert R.T. (1994), Detection of changes in steady-state chlorophyll fluorescence in *Pinus strobus* following short-term ozone exposure. *Journal of Plant Physiology* 144:410-419.
Trissl H.W., Hecks B., and Wulf K. (1993), Invariable trapping times in photosystem I upon excitation of minor long-wavelength-absorbing pigments. *Photochemistry and Photobiology* 57(1):108-112.
Tucker C.J., and Garratt M.W. (1977), Leaf optical properties as a stochastic process. *Applied Optics* 16(3):635-642.
Tuckerman L.B. (1947), On the intensity of the light reflected from or transmitted through a pile of plates. *Journal of the Optical Society of America* 37(10):818-825.
Ustin S.L., Jacquemoud S., and Govaerts Y.M. (2001), Simulation of photon transport in a three-dimensional leaf: Implication for photosynthesis. *Plant Cell and Environment* 24:1095-1103.

Ustin S.L., Jacquemoud S., Zarco-Tejada P.J., and Asner G.P. (2004), Remote sensing of the environment: state of the science and new directions, in *Manual of Remote Sensing. Volume 4: Remote Sensing for Natural Resource Management and Environmental Monitoring* (S.L. Ustin, ed), John Wiley & Sons, 848 pp.

Valentini R., Cecchi G., Mazzinghi P., Mugnozza G.S., Agati G., Bazzani M., Angelis P. de, Fusi F., Matteucci G., Raimondi V., and Scarascia-Mugnozza G. (1994), Remote sensing of chlorophyll a fluorescence of vegetation canopies: 2. Physiological significance of fluorescence signal in response to environmental stresses. *Remote Sensing of Environment* 47:29-35.

Van Dorssen R.J., Plijter J.J., Dekker J.P., Den Ouden A., Amesz J., and Van Gorkom H.J. (1987), Spectroscopic properties of chloroplast grana membranes and of the core of photosystem II. *Biochimica et Biophysica Acta* 809:134-143.

Verhoef W. (1984), Light-scattering by leaf layers with application to canopy reflectance modeling – the SAIL model. *Remote Sensing of Environment* 16:125-141.

Verhoef W. (1998), Theory of radiative transfer models applied in optical remote sensing of vegetation canopies, PhD Thesis, Wageningen Agricultural University, 310 pp.

Verhoef W., and Bach H. (2003), Simulation of hyperspectral and directional radiance images using coupled biophysical and atmospheric radiative transfer models. *Remote Sensing of Environment* 87:23-41.

Vernon L.P., Shaw E.R., and Ke B. (1966), A photochemically active particle derived from chloroplasts by the action of the detergent Triton X-100. *The Journal of Biological Chemistry* 241(17):4101-4109.

Welch A.J., Gardner C., Richards-Kortum R., Chan E., Criswell G., Pfefer J., and Warren S. (1997), Propagation of fluorescent light. *Lasers in Surgery and Medicine* 21:166-178.

Wessels J.S.C. (1966), Isolation of a chloroplast fragment fraction with NADPH+-photoreducing activity dependent on plastocyanin and independent cytochrome f . *Biochimica et Biophysica Acta* 126:581-583.

Wong D., and Govindjee (1979), Antagonistic effects of mono-and divalent cations on polarization of chlorophyll fluorescence in thylakoids and changes in excitation energy transfer. *FEBS Letters* 97:373-379.

Wu J., Feld M.S., and Rava R.P. (1993), Analytical model for extracting intrinsic fluorescence in turbid media. *Applied Optics*. 32(19):3585-3595.

Yamada N., and Fujimura S. (1991), Nondestructive measurement of chlorophyll pigment content in plant leaves from three-color reflectance and transmittance. *Applied Optics* 30(27):3964-3973.

Yamamoto Y., and Ke B. (1980), Regulation of excitation energy distribution in photosystem-II fragments by magnesium ions. *Biochimica et Biophysica Acta* 592: 296-302.

Yeh P. (1988), *Optical waves in layered media*. John Wiley & Sons, 406 pp.

Zarco-Tejada P.J., Miller J.R., Mohammed G.H., Noland T.L. (2000a), Chlorophyll fluorescence effects on vegetation apparent reflectance: I. Leaf-level measurements and model simulation. *Remote Sensing of Environment* 74(3):582-595.

Zarco-Tejada P.J., Miller J.R., Mohammed G.H., Noland T.L., and Sampson P.H. (2000b), Chlorophyll fluorescence effects on vegetation apparent reflectance: II. Laboratory and airborne canopy-level measurements with hyperspectral data. *Remote Sensing of Environment* 74(3):596-608.

Zarco-Tejada P.J., Miller J.R., Mohammed G.H., Noland T.L., and Sampson P.H. (2001), Estimation of chlorophyll fluorescence under natural illumination from hyperspectral data. *International Journal of Applied Earth Observation and Geoinformation*, Special Issue on Applications of Imaging Spectroscopy, 3:321-327.

Zarco-Tejada P.J., Pushnik J.C., Dobrowski S., and Ustin S.L. (2003), Steady-state Chlorophyll a fluorescence detection from canopy derivative reflectance and double-peak effects. *Remote Sensing of Environment* 84:283-294.

Zarco-Tejada P.J., Pérez-Priego O., Sepulcre-Cantó G., Miller J.R., and Fereres E. (2005), Chlorophyll Fluorescence Detection with a High-Spectral Resolution Spectrometer through in-filling of the O2-A band as function of Water Stress in Olive Trees, 2nd International Workshop on Remote Sensing of Vegetation Fluorescence, 17-19 Nov. 2004, Montreal, Canada.

Zucchelli G., Jennings R.C., and Garlaschi F.M. (1992), Independent fluorescence emission of the chlorophyll spectral forms in higher plant photosystem II. *Biochimica et Biophysica Acta* 1099:163-169.

9. GLOSSARY and ABBREVIATIONS

4SAIL: Recent version of the SAIL model which is numerically robust and provides more outputs related to internal fluxes, absorbed flux and thermal emissivity applications.

ABM: Algorithmic BDF Model.

Anti-Stokes fluorescence: Fluorescence emitted at a shorter wavelength than that of excitation.

b: A parameter relating PAR with the rate constant for light energy dissipation, range 0-1.

Beer-Lambert Law: Exponential light extinction law for absorbing media, excluding scattering.

BRF: Bi-directional canopy Reflectance Factor. The canopy reflectance measured in the field by using an ideal white Lambertian horizontal surface as a reference panel.

BRDF (sr-1): Bi-directional Reflectance Distribution Function, 2-dimensional distribution (in zenith and azimuth) of the reflected radiance from a surface for collimated incident radiation from a given direction, relative to the incident irradiance.

C_{ab} ($\mu g/cm^2$): Chlorophyll a+b content, range 5-100 in *FluorMODleaf*.

Chl F: Normalized chlorophyll fluorescence.

CF: Chlorophyll fluorescence. Red and far-red light emitted by the photosystems of green vegetation upon absorption of photosynthetically active radiation.

C_m (μg): Dry matter content, range 0.002-0.02 in *FluorMODleaf*.

C_w (cm): Water equivalent thickness, an indicator of leaf water content, range 0-0.5 in *FluorMODleaf*.

D.A.R.T.: Discrete Anisotropic Radiative Transfert, sophisticated 3D canopy radiative transfer model based on a finite element method.

Eigenvalue: Mathematical term expressing how a square matrix transforms a particular vector (called eigenvector) into a multiple of itself (i.e., a vector with identical direction, but different length). The eigenvalue is equal to the length ratio of both vectors.

Electron transport resistance: Resistance occurring in the photosynthetic electron transport chain of a photosystem, which affects overall photosynthetic rate.

Esun ($Wm^{-2}\mu m^{-1}$): Solar irradiance on the ground.

Esky ($Wm^{-2}\mu m^{-1}$): Sky irradiance on the ground.

Etot ($Wm^{-2}\mu m^{-1}$): Total irradiance.

ext_solar_rad ($mW\ cm^{-2}\mu m^{-1}sr^{-1}$): Extraterrestrial radiance of a white Lambertian horizontal panel.

FdN: Downward fluorescence matrix corresponding to excitation wavelengths in the 400-750 nm range and fluorescence emission in the 640-850 nm range.

FLSAIL: Canopy fluorescence model based on SAIL, intended for simulating laser-induced fluorescence.

Fluorescence lifetime: the decay time of the emission after the excitation has been stopped.

Fi: Fluorescence quantum efficiency or quantum yield: Fluorescence emission per unit of light absorbed, range 0 (no fluorescence) to 0.1 (10% fluorescence) in *FluorMODleaf*.

fluoleaf: Output from *FluorMODleaf* model of solar induced fluorescence, 640-850 nm at 1 nm resolution.

FluorMODgui: Graphic user interface that links the leaf fluorescence model *FluorMODleaf* to the canopy fluorescence model *FluorSAIL*.

FluorMODleaf: Leaf fluorescence model based on an adaptation of PROSPECT.

FluorSAIL: Integrated model of canopy fluorescence under natural light conditions, based on 4SAIL, and providing also radiance spectra on ground level and above the atmosphere.

flurad ($Wm^{-2}\mu m^{-1}sr^{-1}$): Fluorescence radiance on the ground level.

Fraunhofer line: Sharp spectral line in which solar incident radiation is nearly absent due to light absorption in the solar atmosphere.

FRT: Fluorescence–Reflectance–Transmittance model.

FuN: Upward fluorescence matrix corresponding to excitation wavelengths in the 400-750 nm range and fluorescence emission in the 640-850 nm range.

FWHM: Full Width Half Maximum, term expressing the width of a spectral interval by referring to the wavelength range over which the response function is greater than 50% of the maximum response.

Gap probability: The probability of free line of sight through a canopy layer.

h: Hot spot parameter: empirical constant controlling the width of the so-called hot spot, a region of higher reflectance around the retro-direction.; in SAIL models taken as equal to the ratio of leaf width and canopy height. Range 0.01-1 for input to *FluorSAIL*.

Heat dissipation constant: A value denoting the degree of absorbed light energy converted to heat in the light conversion reactions of photosynthetic tissues.

Hot spot parameter: Empirical constant controlling the width of the so-called hot spot, a region of higher reflectance around the retro-direction.; in SAIL models taken as equal to the ratio of leaf width and canopy height.

Kubelka-Munk model: Generic two-stream radiative transfer model for diffuse hemispherical fluxes (upward and downward).

Lambertian: When radiance is independent of viewing direction, or perfectly isotropic.

LAI (canopy): Canopy leaf area index, equal to the total one-sided leaf area per unit ground area, range 0-8 for input to *FluorSAIL*

$LIDF_a$ and **$LIDF_b$:** Leaf Inclination Distribution Functions: Distribution of leaf slope, regardless of leaf azimuth. For inputs to *FluorSAIL*: Spherical (a= –0.35, b= –0.15); Planophile (a=1, b=0); Erectophile (a= –1, b=0); Plagiophile (a=0, b= –1); Extremophile (a=0, b=1); Uniform (a=0, b=0).

LEAFMOD: Leaf Experimental Absorptivity Feasibility Model.

LIBERTY: Leaf Incorporating Biochemistry Exhibiting Reflectance and Transmittance Yields model.

LOPEX: Leaf Optical Properties Experiment.

MODTRAN4: State-of-the-art atmospheric radiative transfer model.

N: Internal structure parameter, range 1-3 in *FluorMODleaf*.

N-flux models: Kubelka-Munk models.

PAR: Photosynthetically active radiation, wavelength range 400-700 nm.

PAR_b: See b.

PAR_{re}: See r_e.

PSI: Photosystem I. One of two photosystems involved in light energy conversions in plant photosynthetic tissues, with peak light absorption at 700 nm.

PSII: Photosystem II. One of two photosystems involved in light energy conversions in plant photosynthetic tissues, with peak light absorption at 680 nm.

PROSPECT model: Leaf optical Properties Spectra model.

Raa (or Raz): Relative azimuth angle, in degrees, range 0-180 for input to *FluorSAIL*.

Rayleigh scattering: Where the wavelength is much larger than the particle size.

RAYTRAN: Monte Carlo Ray Tracing model.

Rdo: Directional reflectance factor for diffuse incident flux.

r_e: PAR-related constant denoting electron transport resistance, range 0-1.

refrad ($Wm^{-2}\mu m^{-1}sr^{-1}$): Reference radiance (without fluorescence) on ground level.
refref: Reference reflectance factor on the ground (without fluorescence).
refSAIL: Reference reflectance factor computed analytically with 4SAIL model.
refSAIL/refref: Ratio SAIL/*FluorSAIL* for reference reflectance factor.
reftot: Total reflectance factor on the ground (with fluorescence).
Relative azimuth: Viewing azimuth angle relative to the sun's azimuth (the sun's position in the horizontal plane relative to local North).
rho_dd: Spherical albedo.
rho_so: Atmospheric path reflectance.
RN: Leaf reflectance without fluorescence.
RNF: Leaf reflectance with fluorescence.
Rso: Bi-directional reflectance factor for direct solar flux.
S: Species temperature dependence in *FluorMODleaf*: 1:broad bean; 2:bean; 3:ficus; 4:tomato; 5:pea
SAIL model: Scattering by Arbitrarily Inclined Leaves canopy reflectance model.
SLOP model: Stochastic model for Leaf Optical Properties.
soilspectrum: Spectral soil reflectance.
Stochastic models: Probabilistic models.
Stoichiometry (Sto): With respect to photosystems, the ratio of PSII to PSI reaction centres. High light: Sto~2; low light: Sto~1.1.
tau_oo: Direct transmittance in view direction.
tau_sd: Diffuse transmittance for sunlight.
tau_do: Diffuse transmittance in view direction.
tau_ss: Direct transmittance in sun direction.
T (ºC): Temperature.
TN: Leaf transmittance without fluorescence.
TN: Leaf transmittance with fluorescence.
TOA: Top of atmosphere.
TOAref_bare ($Wm^{-2}\mu m^{-1}sr^{-1}$): Reference top-of-atmosphere radiance for bare soil surroundings.
TOAtot_bare ($Wm^{-2}\mu m^{-1}sr^{-1}$): Total top-of-atmosphere radiance for bare soil surroundings.
TOAref_same ($Wm^{-2}\mu m^{-1}sr^{-1}$): Reference top-of-atmosphere radiance for surroundings same as target.
TOAtot_same ($Wm^{-2}\mu m^{-1}sr^{-1}$): Total top-of-atmosphere radiance for surroundings same as target.
TOC: Top of canopy.
totrad ($Wm^{-2}\mu m^{-1}sr^{-1}$): Total radiance on ground level.
Vza: Viewing zenith angle, in degrees, range 0-85 for input to *FluorSAIL*.

10. APPENDICES

APPENDIX 10.1. Presentations, reports, publications from FluorMOD project

Miller J.R., Berger M., Alonso L., Cerovic Z., Goulas Y., Jacquemoud S., Louis J., Mohammed G., Moya I., Pedrós R., Moreno J., Verhoef W., and Zarco-Tejada P.J. (2004), Progress on the Development of an Integrated Canopy Fluorescence Model, 2003 International Geoscience and Remote Sensing Symposium, IGARSS'03, pp. 601-603 Vol.1, ISBN 0-7803-7929-2 - 0-7803-7930-6, Toulouse (France).

Miller, J. et al., (2004), Overview of FluorMOD: A Project to Develop an Integrated Leaf-Canopy Fluorescence Simulation Model, 2nd International Workshop on Remote Sensing of Vegetation Fluorescence, 17-19 Nov. 2004, Montreal (Canada.).

Pedrós R., Jacquemoud S., Goulas Y., Louis J., and Moya I. (2004), A new leaf fluorescence model, 2nd International Workshop on Remote Sensing of Vegetation Fluorescence, 17-19 Nov. 2004, Montreal (Canada).

Pedrós R., Jacquemoud S., Goulas Y., Louis J., and Moya I. (2005), A new leaf fluorescence model, 2nd International Workshop on Remote Sensing of Vegetation Fluorescence, 17-19 Nov. 2004, Montreal (Canada).

Verhoef, W. (2004), Extension of SAIL to model solar-induced canopy fluorescence spectra, 2nd International Workshop on Remote Sensing of Vegetation Fluorescence, 17-19 Nov. 2004, Montreal (Canada).

Verhoef W. (2005), Extension of SAIL to model solar-induced canopy fluorescence spectra, 2nd International Workshop on Remote Sensing of Vegetation Fluorescence, 17-19 Nov. 2004, Montreal (Canada).

Zarco-Tejada P.J., Pérez-Priego O., Sepulcre-Cantó G., Miller J.R., and Fereres E., (2005), Chlorophyll Fluorescence Detection with a High-Spectral Resolution Spectrometer through in-filling of the O2-A band as function of Water Stress in Olive Trees, 2nd International Workshop on Remote Sensing of Vegetation Fluorescence, 17-19 Nov. 2004, Montreal (Canada).

Zarco-Tejada P.J., Miller J.R., Pedrós R., Verhoef W., and Berger M. (2004), *FluorMODgui*: A Graphic User Interface for the Spectral Simulation of Leaf and Canopy Fluorescence Effects, 2nd International Workshop on Remote Sensing of Vegetation Fluorescence, 17-19 Nov. 2004, Montreal (Canada).

Zarco-Tejada P.J., Miller J.R., Pedrós R., Verhoef W., and Berger M., *FluorMODgui V3.0*: A Graphic User Interface for the Spectral Simulation of Leaf and Canopy Fluorescence. Submitted to *Computers & Geosciences*, January 2005.

APPENDIX 10.2. FluorMOD project team meetings

Meeting and Purpose	Date	Location
1: Kickoff meeting	3 October 2002	ESTEC, The Netherlands
2: Progress	4-5 December 2002	U.Paris/LURE, France
3: Progress	22 May 2003	ESTEC, The Netherlands
4: Mid-term review	31 October 2003	ESTEC, The Netherlands
5: Progress	17 February 2004	U.Valencia, Spain
6: Progress	8 July 2004	U.Valencia, Spain
7: Progress	16 November 2004	Montreal, Canada
8: Final meeting	17 March 2005	ESTEC, The Netherlands

APPENDIX 10.3. Project Tasks and Scientist Responsibilities

Project Task	Description
Task 1	**Review of existing vegetation fluorescence models, selection of appropriate models**
1.1	Review of passive leaf fluorescence science
1.2	Review of leaf fluorescence models
1.3	Review of canopy fluorescence models
1.4	Proposed leaf-canopy fluorescence modelling approach
Deliverables	*Report appropriate radiative transfer leaf and canopy models to be used in this study*
Task 2	**Analysis of leaf fluorescence model: model advancement**
2.1	Development and coding of leaf fluorescence model
2.2	Development of measurement protocols for laboratory & field experiments to assess leaf fluorescence model performance
2.3	Assessments of leaf fluorescence model
Deliverables	*Software coded leaf-fluorescence model* *Model validation / improvement report as appropriate*
Task 3	**Development of an integrated leaf-canopy fluorescence model**
3.1	Development and coding of fluorescence radiative transfer (RT) model, with coupled leaf fluorescence model (software development)
3.2	Coupling of high resolution atmospheric and FRT models
3.3	Performance of simulations for scenarios identified in Task 1.4
Deliverables	*Software coded leaf-canopy fluorescence/reflectance model* *Model validation / improvement report as appropriate*
Task 4	**Model validation using campaign and comparison with indirect retrieval methods**
4.1	Review of indirect fluorescence retrieval methods developed for hyperspectral data cubes
4.2	Evaluation of model performance for new field experiments
4.3	Evaluation of model performance with appropriate existing hyperspectral datasets
4.4	Fluorescence retrieval tests with above datasets
Deliverables	*Report on model validation, for simulated/measured fluorescence signal level over canopies under different viewing conditions*
Task 5	**Reporting on project conclusions and recommendations**
Deliverables	*Electronic copies of reports of presentations at meetings by sub-contractors, Mid-term and Final Project reports, delivered to ESTEC*

Task	Responsible Scientist	YG	SJ	JM	PZ	JRM	GM	WV
Task 1	Review of existing models							
1.1	YG	*					*	
1.2	SJ	*	*		*	*	*	*
1.3	WV	*	*	*	*	*		*
1.4	JM	*	*	*		*		*
Task 2	Development of leaf model							
2.1	SJ	*	*		*			*
2.2	YG	*	*		*	*	*	
2.3	SJ	*	*		*	*	*	
Task 3	Development of canopy model							
3.1	WV	*	*	*	*	*		*
3.2	WV			*	*	*		*
3.3	WV			*	*	*		*
Task 4	Model validation							
4.1	JM			*	*	*		
4.2	YG	*		*	*			
4.3	JM	*	*	*	*			*
4.4	JM	*		*	*			
Task 5	Reporting							
5	JRM	*	*	*	*	*	*	*

GM: Gina Mohammed
JM: Jose Moreno
JRM: John Miller
PZ: Pablo Zarco-Tejada
SJ: Stephane Jacquemoud
WV: Wout Verhoef
YG: Yves Goulas